GRID SIZE EFFECTS WITH SMEARED CRACKING IN FINITE ELEMENT ANALYSIS OF REINFORCED CONCRETE

by

Robert H. Dodds

David Darwin

Jerry L. Smith

Linda D. Leibengood

A Report on Research Sponsored By

THE NATIONAL SCIENCE FOUNDATION

Research Grant

PFR 79-24696

UNIVERSITY OF KANSAS

LAWRENCE, KANSAS

August 1982

50272-101

REPORT DOCUMENTATION PAGE	1. REPORT NO. NSF/CEE-82034	2.	3. Recipient's Accession No.

4. Title and Subtitle

Grid Size Effects With Smeared Cracking In Finite Element Analysis of Reinforced Concrete

5. Report Date

6.

7. Author(s)

R. H. Dodds, D. Darwin, J. Smith, L. Leibengood

8. Performing Organization Rept. No.

SM Report No. 6

9. Performing Organization Name and Address

University of Kansas Center for Research, Inc.
2291 Irving Hill Drive, West Campus
Lawrence, Kansas 66045

10. Project/Task/Work Unit No.

11. Contract(C) or Grant(G) No.

(C)

(G) NSF PFR 79-24696

12. Sponsoring Organization Name and Address

National Science Foundation
Washington D.C. 20550

13. Type of Report & Period Covered

14.

15. Supplementary Notes

16. Abstract (Limit: 200 words)

The effects of modeling parameters on the response of finite element representations of reinforced concrete members are examined. Convergence of load-deflection curves and cracking patterns is studied. Nonlinear behavior is limited to cracking of the concrete and yielding of the reinforcement. The "smeared" crack representation is governed by a limiting tensile stress criterion. Concrete is treated as linear elastic in compression. Reinforcement has a bilinear stress-strain curve. Constant strain bar elements and rectangular isoparametric elements model the steel and the concrete, respectively. Analyses are performed for flexural members with span-to-depth ratios of 12-1, 5-1 and 2-1, under both a uniformly distributed load and a concentrated load at midspan, using a minimum of three variations in grid refinement. Load-deflection curves exhibit convergence with grid refinement. Concrete tensile strength has a negligible influence on response for the members studied. Load increment size affects the response only in unstable regions of the load-deflection curve and does not affect the stiffness or the post-yield response.

17. Document Analysis a. Descriptors

cracking (fracturing), cracking patterns, concrete (reinforced), finite elements, load-deflection, structural engineering.

b. Identifiers/Open-Ended Terms

c. COSATI Field/Group

18. Availability Statement	19. Security Class (This Report)	21. No. of Pages
Release Unlimited	Unlimited	
	20. Security Class (This Page) Unlimited	22. Price

(See ANSI-Z39.18) *See Instructions on Reverse*

OPTIONAL FORM 272 (4-77)
(Formerly NTIS-35)
Department of Commerce

ACKNOWLEDGMENTS

The initial phase of this work was performed by Mr. Jerry Smith in partial fulfillment of the requirements for the Master of Science degree. Ms. Linda Leibengood conducted the final computer analyses and prepared the figures.

This research was supported by the National Science Foundation under NSF Grant PFR 79-24696. Additional support was provided by the University of Kansas General Research Allocation 3842-20-0038.

Numerical computations were performed on the Harris 500 computer system operated by the Computer Aided Engineering Laboratory at the University of Kansas.

TABLE OF CONTENTS

LIST OF TABLES

LIST OF FIGURES

LIST OF FIGURES (continued)

LIST OF FIGURES (continued)

LIST OF FIGURES (continued)

CHAPTER 1

INTRODUCTION

1.1 General

The finite element method has been widely adopted for predicting the response of structures loaded into the nonlinear region. Successful application of this analysis tool requires the synthesis of element types, material constitutive relationships, and solution methods into a modeling scheme that incorporates the important nonlinear effects occurring in the actual structure. Structural analysts must also balance the level of modeling detail with the computational effort required for numerical solution. Overly detailed models, while capable of accurately predicting nonlinear response, may be too expensive to implement.

Reinforced concrete structures pose unique modeling problems due to the number, type, and interaction of effects that contribute to nonlinear response. Analysis procedures for structures such as shear walls and beams must include nonlinearity arising from a number of sources. These are: 1) yielding and strain hardening of reinforcement, 2) degeneration of bond between concrete and reinforcement, 3) nonlinear response of concrete subjected to compression, and 4) cracking of concrete in tension.

The response of a reinforced concrete structure (or member) can be examined at either the microscopic or the macroscopic level. Microscopic analysis predicts the detailed stress distribution near

cracks, bond stresses, and the propagation of individual cracks under loading. A macroscopic analysis provides the strength and overall deformation characteristics of the structure expressed in terms of load-deflection curves and generalized cracking patterns. Modeling procedures for the prediction of microscopic response may be unnecessarily complex for macroscopic analysis and may not be justified due to the large computational effort. A shear wall, for example, may develop hundreds of cracks under loading; the detailed consideration of each individual crack is clearly impractical and may be unnecessary for a strength and deformation analysis. In contrast, the propagation of a single crack in a large unreinforced concrete structure, such as a gravity dam, may have disasterous consequences. A microscopic analysis is both warranted and feasible for this type of structure, i.e., one for which the propagation of a single crack dominates the response.

Recent microscopic response studies by Bazant and Cedolin (4,5) have raised a serious question regarding the general applicability of cracking models based on a simple limiting tensile stress criterion. Tensile panels containing a predefined crack (Mode I) were analyzed using a blunt band crack representation. The material stiffness normal to the crack plane and the shear stiffness were reduced to zero for elements within a one element wide crack band. The load required to propagate the predefined crack for plain concrete was shown to be strongly dependent on the refinement of the finite element grid when the limiting tensile strength criterion was used. Uniform refinement of the element grid produced a sharper crack tip and rapidly increased the computed tensile stress in the element nearest to the crack tip. Predic-

tion of crack extension using the computed tensile stress was thus shown to be highly dependent upon the finite element grid selected. However, the energy release rate, G, associated with extension of the blunt crack converged to a constant value with mesh refinement and was therefore recommended as a more appropriate parameter to govern crack extension. Similar computations for a reinforced panel predicted a constant energy release rate but only following the introduction of a bond slip model for the reinforcement traversing the crack plane.

Extrapolated to the analysis of common reinforced concrete structures that develop numerous cracks, these microscopic studies imply that load-deflection curves generated using a limited tensile stress cracking criterion will not converge with increasing mesh refinement. For such structures, cracks are most commonly incorporated in element grids with either a "discrete" or a "smeared" representation. The discrete crack model allows element edges to uncouple thereby introducing a geometric discontinuity, with a strain concentration ahead of each crack tip. The magnitude of the computed strain (stress) concentration naturally depends on the degree of mesh refinement. In the limit of mesh refinement, the discrete crack representation and the blunt band crack representation are identical. The same sensitivity to mesh refinement exhibited by the blunt band model should also be expected with the discrete crack model. With the widely used "smeared" crack representation, simple pointwise stress discontinuities within elements simulate the loss of stiffness due to crack formation. Strain fields within the elements and displacements across element boundaries remain continuous, irrespective of grid refinement. For this reason,

the smeared representation may be considered a macroscopic damage model for cracked concrete.

The smeared crack representation and limiting tensile stress criterion have been used extensively for the analysis of beams, plates, shells, shear walls, etc. Good correlations with experimental load-deflection curves and crack patterns have been reported. This appears to contradict implications of the microscopic crack extension studies. The level of finite element mesh refinement used for beam, plate, and shell models was generally based on engineering judgement within the constraints of computer program capacity and funds available for the analysis. Bazant and Cedolin (4) suggest that the correct predictions of structural response in those studies were obtained by the fortuitous selection of element dimensions relative to the aggregate size and concrete tensile strength, and that more refined meshes would have predicted divergent load-deflection curves. Clearly, grid refinement has some effect on computed results as for all finite element analyses. Yet, it is not obvious how grid refinement affects the computed response when cracks are represented using the smeared model.

In view of these questions and with the continued widespread use of smeared crack-tensile stress models, this study was conducted to investigate the effect of a number of finite element modeling parameters, including grid refinement, on the macroscopic, nonlinear response of reinforced concrete structures.

1.2 Previous Work

This section provides a brief summary of the major approaches that are used to incorporate cracking in the finite element analysis of reinforced concrete. Cracking models must address two problems: 1) material constitutive relationships that predict the formation and possibly propagation of a crack, and 2) representation within the element mesh of the discontinuity introduced by the crack. Predictive methods for crack formation have traditionally been based on a limiting tensile stress or strain criterion and are collectively termed stress controlled models. More recently, procedures to predict the propagation of an existing crack have been developed following the principles of linear elastic fracture mechanics.

Two methods are commonly employed to accommodate the crack in a finite element grid. In the first method, termed "discrete cracking", the boundaries between elements are permitted to separate, while preserving geometric continuity within the elements. In the second method, termed "smeared cracking", element boundaries remain geometrically continuous during deformation, with cracks introduced by eliminating the material stiffness normal to the cracks at sampling points within elements. The smeared crack representation therefore does not introduce a direct geometric discontinuity in the mesh -- only a stress discontinuity.

The following sections describe the use of smeared and discrete crack representations in conjunction with the stress controlled and fracture mechanics based constitutive models. More detailed discus-

sions can be found in Ref. (33).

1.2.1 Stress Controlled Models

The first finite element model for reinforced concrete was developed by Ngo and Scordelis (25) to study local bond, concrete and steel stresses along predefined cracks in beams (Fig. 1.1). Two nodes were defined at each mesh point on element boundaries along the path of each crack. A crack was formed by allowing separation of the nodal points (Fig. 1.2). Ngo, Scordelis and Franklin (26) later used linkage elements along the cracks to simulate aggregate interlock (Fig. 1.3). Constant strain triangle elements were used to model the concrete in these early studies.

Nilson (24) eliminated the necessity to predefine crack locations. An automated process was developed to introduce cracks between elements. When the average tensile stress at the interface of two adjacent elements exceeded the modulus of rupture, common nodes were disconnected, thus introducing a crack. This scheme, in effect, propagated the crack (either new or existing) by one element dimension and created some degree of strain (and thus stress) concentration at the crack tip. For elements at the exterior of the mesh, only common outside nodes were disconnected. For interior cracks all common nodes were separated (Fig. 1.4).

Mufti, et al., (21,22) further improved the discrete cracking model by initially incorporating two separate nodes at each element connection point. The nodes were connected with a linkage element having stiffness parallel and perpendicular to the crack. All possible crack

locations were thus predefined. The stiffness of a linkage element perpendicular to the crack was gradually decreased to zero as the tensile stress exceeded the cracking strength. The linkage elements parallel to a crack were used to simulate aggregate interlock. Al-Mahaidi (1) conducted a similar investigation but with two or four nodes connected by linkage elements at one point. The four nodes allowed cracking in two perpendicular directions (Fig. 1.5).

Despite their apparent simplicity, the discrete cracking models have not been widely employed in analysis. Two major drawbacks have existed for this approach: 1) crack paths are constrained to follow predefined element boundaries, and 2) the solution procedure may be inefficient. Each time a crack forms, a new node must be introduced to uncouple the nodal degrees of freedom. This changes the mesh topology and thus necessitates a regeneration of the structure stiffness and triangulation. Addition of nodal points to model numerous cracks also increases the bandwidth of the global stiffness matrix, thereby quadratically increasing solution time. Recently, some progress has been made in equation solving techniques that reduce these objections to discrete cracking (30).

To help overcome early objections associated with the discrete crack model, Rashid (27) introduced the "smeared crack model", in which cracked concrete is represented as a linearly elastic, orthotropic material. When the principal tensile stress (or strain) at a material sampling point within an element exceeds the tensile strength, a crack is formed by reducing the modulus of elasticity to zero in the direction of the principal stress. The tensile stress carried prior to cracking

is then redistributed to surrounding elements. Subsequent stress changes are related to strain increments in the cracked coordinate system by the following constitutive matrix:

$$\begin{Bmatrix} d\sigma_1 \\ d\sigma_2 \\ d\tau_{12} \end{Bmatrix} = \begin{bmatrix} 0 & 0 & 0 \\ 0 & E & 0 \\ 0 & 0 & 0 \end{bmatrix} \begin{Bmatrix} d\varepsilon_1 \\ d\varepsilon_2 \\ d\gamma_{12} \end{Bmatrix} \tag{1.1}$$

in which E is Young's modulus for concrete. σ_1, σ_2, ε_1, and ε_2 are the principal stresses and strains in the cracked coordinate system (direction 1 is perpendicular to the crack plane). The shear modulus is reduced to zero upon crack formation in this early model.

Whereas the discrete crack model represents a single crack with fixed direction, determined by element orientation, the orthotropic constitutive relationship simulates many closely spaced (or smeared) cracks near the sampling point, oriented perpendicular to the principal tensile stress (Fig. 1.6). A consequence of incorporating the crack in this manner is that no real geometric discontinuity develops in the finite element grid as it does for the discrete crack representation. Strain fields within the finite elements remain continuous functions of the spatial coordinates.

The smeared model was used successfully by several investigators (7,8,19,34). However, the absence of shear stiffness along the crack interface sometimes led to ill-conditioned stiffness matrices once large areas of the structure cracked (17,31). To eliminate these problems, later investigators (2,3,10,11,16,32) reinserted the shear modulus, G, with a reduction factor, β (assigned a value between zero

and one). In this case, the incremental, orthotropic constitutive matrix becomes:

$$\begin{Bmatrix} d\sigma_1 \\ d\sigma_2 \\ d\tau_{12} \end{Bmatrix} = \begin{bmatrix} 0 & 0 & 0 \\ 0 & E & 0 \\ 0 & 0 & \beta G \end{bmatrix} \begin{Bmatrix} d\varepsilon_1 \\ d\varepsilon_2 \\ d\gamma_{12} \end{Bmatrix} \tag{1.2}$$

Retention of a non-zero shear modulus, G, effectively places springs parallel to the crack and simulates aggregate interlock and dowel action. Fortunately, the particular choice of β is not critical (16,17). A value of 0.4 is normally adopted. The inclusion of some shear stiffness alleviates the stiffness ill-conditioning problems and improves the computed crack patterns.

Eq. (1.1) and (1.2) predict subsequent stress changes once a crack forms. Techniques are also required to reduce the existing tensile stress at crack formation. In the simplest of these, the tensile stress normal to the crack is immediately reduced to zero. In other methods, collectively termed "tension stiffening" (15,17,30,35), the tensile stress is gradually reduced to zero through a descending branch of the tensile stress-strain curve. Tension stiffening has improved both numerical stability of the solution process and comparisons with experimental results (15), but has not been universally adopted.

The smeared crack model offers two major advantages compared with the discrete crack representation. First, no redefinition of the element mesh topology is required during analysis. Significant reductions in computational effort are therefore realized. Secondly, the smeared model eliminates the bias of predetermined crack orientations

inherent in most discrete representations.

1.2.2 Fracture Mechanics Models

Because concrete in tension responds in a brittle manner, considerable effort has been made to derive constitutive models based on linear elastic fracture mechanics. These models predict the direction in which a crack propagates and the load increase required to extend the crack. Fracture mechanics models are applied as follows. With a known crack geometry, a finite element analysis is performed to determine the rate of energy release, G, that would occur for an increase in crack length. When the energy release rate exceeds a critical value, G_c , the crack extends until G is again below the critical value, i.e., the structure reaches another equilibrium configuration for the same applied loading. During crack extension, the stresses in the previously uncracked material are redistributed to the reinforcement and to the concrete ahead of the crack. The major parameter in this process is the critical value of the energy release rate. G_c is assumed to be a material property of concrete that is independent of the crack length, loading, structure dimensions, etc.

Rostam and Bysckov (28), and Salah El-Din and El-Adawy Nassef (29) effectively combined the discrete crack representation with fracture mechanics constitutive models to compute moment versus crack length relationships for singly reinforced beams. Crack propagation for these Mode I (tension) type problems was modeled by incrementally releasing constraints applied to nodes along the crack front. These studies used constant strain triangle elements, not singularity type elements, to

model the crack tip. Modeer (20) has also used the discrete crack approach with constant strain triangles, but with crack propagation controlled by a crack opening displacement (COD) criterion. Both reinforced and unreinforced beams were considered with a stress controlled criterion to initiate cracks. These studies considered members containing only one crack and did not attempt to accurately model the strain singularity ahead of the crack tip. More recently, Saouma (30) developed a procedure to follow the propagation of combined Mode I and Mode II (shear) cracks in beams and shear panels. An automated computer procedure was devised to construct new element meshes (containing special singularity elements) each time one or more cracks extended. Crack propagation occurred when G reached a critical value, with the crack extending in the direction of maximum calculated G. Specialized solution algorithms were also developed to minimize the impact of new nodes and elements incorporated in the mesh. Saouma's work is notable as combined Mode I (tension) and Mode II (shear) cracks were allowed, without the necessity to predefine crack paths.

A combination of the computationally more efficient smeared crack representation and a fracture mechanics constitutive model is presented by Bazant and Cedolin (4,5). A single crack is modeled by a one element wide "band" of quadrilaterals composed of constant strain triangles. When the energy release rate (computed using a scheme to account for reinforcement bond slip) exceeds the critical value, the tensile and shear stiffness in the crack tip element is reduced to zero, thus affecting a crack extension equal to the dimension of one element. Bazant and Cedolin (4) showed that the computed energy release rate con-

verges to a constant value with increasing mesh refinement, while corresponding stress estimates at the crack tip increase without bound. Therefore, they argue that the stress controlled constitutive model is not objective, since the degree of mesh refinement employed near the tip directly controls the predicted tensile stress.

1.3 Objective and Scope

This report examines the effects of finite element modeling parameters on the nonlinear strength and deformation response of reinforced concrete members due to cracking. Convergence properties of the macroscopic measures of response, including load-deflection curves and general cracking patterns, are of primary interest. Acceptable finite element models must generate convergent load-deflection curves for increasing grid refinement.

Nonlinearity is limited to cracking of the concrete and yielding of the reinforcement. Crack formation is governed by a limiting tensile stress criterion. A "smeared" representation is used to incorporate cracks in the finite element mesh. Since the major emphasis of the study concerns nonlinearity due to cracking, the concrete is treated as a linear elastic material in compression. While this assumption simplifies the parametric study of cracking, it precludes the comparison of computed solutions with experimental results. The reinforcement stress-strain curve is linear elastic with linear strain hardening after yield. Constant strain bar elements are used to model the reinforcement.

Finite element analyses are performed for slender, moderate, and deep beams, with respective span-to-depth ratios of 12 to 1, 5 to 1, and 2 to 1. Each beam is analyzed for a uniformly distributed load and a midspan, concentrated load using a minimum of three variations in grid refinement. Both the four node (linear) and eight node (quadratic) isoparametric elements are employed to model concrete portions of the members.

Additional analyses are conducted for the shear critical deep beam (2:1 aspect ratio) to assess the influence of concrete tensile strength and loading increment size on the solutions. Separate analyses of the deep beam are also performed to study the effect of numerical integration order for models constructed with the quadratic element.

CHAPTER 2

NUMERICAL PROCEDURES

2.1 General

This chapter describes the major components of the analytical model and the solution procedures adopted in this study. Items specifically addressed include: 1) material constitutive relationships selected to model concrete and reinforcement, 2) finite element formulations for modeling concrete and reinforcement, and 3) relevant aspects of the iterative process used to solve the resulting nonlinear equilibrium equations. The formulations and procedures described are incorporated in the POLO-FINITE (12,13,18) system, which was used to obtain the numerical results presented in Chapter 3.

2.2 Nonlinear Material Models

2.2.1 Concrete

Cracking under tensile stress is the only nonlinear behavior of concrete modeled. A "crack" is formed when the computed tensile stress exceeds the tensile strength, f'_t. Cracks are incorporated in the finite element mesh using the smeared representation. Concrete is assumed to respond linearly for all levels of compressive stress.

Prior to cracking, concrete is modeled as a linearly elastic, isotropic material in a state of plane stress. The incremental stress-strain relationship prior to any cracking is:

$$\begin{Bmatrix} d\sigma_x \\ d\sigma_y \\ d\tau_{xy} \end{Bmatrix} = \frac{E}{1 - \nu^2} \begin{bmatrix} 1 & \nu & 0 \\ \nu & 1 & 0 \\ 0 & 0 & (1 - \nu)/2 \end{bmatrix} \begin{Bmatrix} d\varepsilon_x \\ d\varepsilon_y \\ d\gamma_{xy} \end{Bmatrix} \quad (2.1)$$

Initially, all stress-strain sampling points are assumed to be uncracked. At each loading stage, strain increments are converted to elastic stress increments using Eq. (2.1). The accumulated total stresses are rotated to principal axes, and the maximum tensile stress is compared to the tensile strength of the concrete. If the computed stress exceeds the tensile strength, a crack is introduced by setting the total stress to zero in the corresponding direction. Concrete at the point is thereafter modeled as an elastic, orthotropic material with material directions fixed parallel and normal to the crack. The incremental stress-strain relationship becomes:

$$\begin{Bmatrix} d\sigma_1 \\ d\sigma_2 \\ d\tau_{12} \end{Bmatrix} = \begin{bmatrix} \alpha E & 0 & 0 \\ 0 & E & 0 \\ 0 & 0 & \beta G \end{bmatrix} \begin{Bmatrix} d\varepsilon_1 \\ d\varepsilon_2 \\ d\gamma_{12} \end{Bmatrix} \quad (2.2)$$

in which subscripts 1 and 2 refer to material axes (direction 1 is normal to the first crack). The shear modulus, G, = 0.5E/(1+ν). All subsequent stress computations are performed by transforming strain increments to the 1-2 material directions and then applying Eq. (2.2). The resultant stress increments are added to previous stresses in the 1-2 system, followed by a rotation of the new total stresses to the global coordinate axes. The normal stiffness reduction factor, α, is a numerical device that may improve the stability of the equilibrium equa-

tions by retaining a very small stiffness normal to the crack. Unless otherwise noted, a zero value for α is employed in this study. When used, typical values of α range from 10^{-3} to 10^{-6}. Retention of a non-zero shear stress-strain term in Eq. (2.2) simulates aggregate interlock by allowing the concrete to develop additional shear stress along the crack. A constant value of 0.4 for the shear stiffness reduction factor, β, is used in this study. No attempt is made to gradually reduce β with increasing crack width. No provisions are included to model crack closure.

Eq. (2.2) implies that no Poisson effect exists between stress increments in the 1-2 material directions once a crack forms. However, at the instant of crack formation, the stress σ_2 parallel to the crack contains a Poisson coupling term with direction 1 due to the isotropic constitutive relationship in effect prior to cracking. The loss of Poisson coupling at the instant of cracking lets the concrete "rebound" along direction 2. Stress σ_2 changes by the amount $-\nu\varepsilon_1 E/(1-\nu^2)$. This effect may be included or neglected in the cracking material model. When included, σ_2 becomes simply $E\varepsilon_2$ immediately after cracking. A number of preliminary analyses were conducted to determine the effects of Poisson coupling. Computed load-deflection curves and general crack patterns with and without "rebound" showed no detectable differences. This result might be anticipated considering the very small value of ε_1 when the tensile stress exceeds f'_t. The "rebound" effect was neglected in this study.

If the total stress σ_2 exceeds the tensile strength of the concrete, a second crack is introduced perpendicular to the first crack. When two cracks are present, the incremental stress-strain relation becomes:

$$\begin{Bmatrix} d\sigma_1 \\ d\sigma_2 \\ d\tau_{12} \end{Bmatrix} = \begin{bmatrix} \alpha E & 0 & 0 \\ 0 & \alpha E & 0 \\ 0 & 0 & \beta G \end{bmatrix} \begin{Bmatrix} d\varepsilon_1 \\ d\varepsilon_2 \\ d\gamma_{12} \end{Bmatrix} \tag{2.3}$$

The ability to transfer shear along both cracks is retained through the β factor. Formation of a second crack is generally associated with cyclically applied loads, although it is theoretically possible for a second crack to form under monotonic loading if sufficient load redistribution occurs.

2.2.2 Reinforcement

The reinforcement is modeled as a material in a state of uniaxial stress. A simple bilinear stress-strain law is used (described in Ch. 3).

2.3 Finite Elements

2.3.1 Bar Elements for Reinforcement

Two techniques are commonly employed to model the reinforcement. In the first method, a "smeared" composite material matrix is generated by adding the constitutive matrix for the reinforcement to

that of the concrete in volumetric proportions. A single, 2-D finite element may then model both the concrete and the reinforcement. This approach is particularly convenient when the reinforcement is not parallel to the element edges.

In the second approach, termed the "discrete" model, separate finite elements are utilized for the concrete and the reinforcement. Simple constant strain bar elements are adequate to represent the reinforcement. These elements have two nodes, each with a single axial degree of freedom (Fig. 2.1). The discrete reinforcement model is adopted in this study due to its simplicity and availability in the computer code.

2.3.2 Isoparametric Elements

Numerically integrated finite elements, based on the isoparametric formulation, are used to represent the concrete. Isoparametric elements have several advantages compared to simple constant strain triangular elements. Substantially more accurate solutions are obtained with fewer elements, thus reducing input and computational effort. Isoparametric elements generally distribute residual forces occurring in nonlinear analysis over a larger portion of the model. This may reduce the number of corrective iterations required. The Gauss points in isoparametric elements have proven to be optimal locations for the calculation of strains and stresses. For 2-D linear analysis, Nayak (23) presents computational evidence indicating that a linear displacement (4 node) isoparametric element is approximately equivalent to eight constant strain triangles. Similarly, the quadratic displacement (8

node) isoparametric element is approximately equivalent to sixteen triangular elements.

Both the four node and eight node isoparametric elements (Fig. 2.2 and 2.3) are used in this investigation. Complete details of the element formulation are given in Ref. (37).

Isoparametric element stiffnesses are calculated using the standard Gauss numerical integration procedure. A four point (2x2) Gauss quadrature rule (Fig. 2.4) exactly integrates the four node element stiffness in linear analysis. Both the four point and nine point (3x3, Fig. 2.5) integration rules are considered for the eight node element. The four point rule comprises "reduced" integration for the eight node element. Reduced integration saves considerable computational effort compared to the 3x3 rule and has been extensively employed in nonlinear plasticity analyses (23). The 3x3 rule exactly integrates the eight node element stiffness in linear analysis.

2.4 Solution Procedures

When cracking of the concrete and yielding of the reinforcement are considered, the finite element method produces a nonlinear set of equilibrium equations. However, the load path dependent nature of cracking precludes generation of the equation coefficients for an arbitrarily specified load level. Therefore, structural response is computed by applying the total load in a sequence of incremental load steps. Within each step, the nonlinear equilibrium equations are linearized using a tangent stiffness approach. These equations are solved to determine approximate increments of the nodal displacements.

Residual or "unbalanced" forces develop since the linearized displacement increments do not satisfy the nonlinear equilibrium equations. The true equilibrium configuration at each load step is found by iteratively correcting the displacements with small changes arising from application of the residual forces. The procedure continues until residual force components vanish within some prescribed tolerance. Although the solution method is incremental, the iterative process employed in this study considers total equilibrium conditions for the structure to compute residual forces. No errors accumulate from one step to the next with this solution method.

Variations of this solution procedure, known as the Newton-Raphson method, are widely used for nonlinear finite element analysis. Fig. 2.6 illustrates the basic process for a single degree of freedom system. With the Newton-Raphson method, the analyst has several options to control the solution process. In this investigation, the incremental (tangent) stiffness is updated before each load step and before each equilibrium iteration. Frequent updating of the tangent stiffness produces a more accurate distribution of residual forces, accelerates the convergence rate, and reduces the number of iterations required for a load step. Cedolin and dei Poli (6) studied the solution convergence rates for various modifications of the Newton-Raphson method applied to cracking problems. Stiffness updating before each iteration was found to yield the best convergence rate, and in some cases, the use of any other scheme resulted in a non-convergent or very slowly convergent solution.

The following outline summarizes the major computational phases necessary to analyze the structure for each load step.

1) Compute the incremental equivalent nodal loads, $\{\Delta P\}$, corresponding to the increment of applied load defined for the step. Set the residual nodal loads equal to the applied load increment, $\{R\} = \{\Delta P\}$, for the first iteration of a load step.

2) Update the total nodal loads applied to the structure through the current step, $\{P_{NEW}\} = \{P_{OLD}\} + \{\Delta P\}$, to reflect the new loading increment.

3) Generate the incremental (tangent) constitutive relation, $[D_T]$, for all concrete and reinforcement elements using the current stresses, strains, and loading history.

4) Using the updated $[D_T]$ matrices, recompute the stiffness matrices for newly cracked elements and assemble the new structure tangent stiffness matrix, $[K_T]$. Triangulate the new tangent stiffness.

5) Solve for the increment of nodal displacements using the triangulated stiffness. $\{\Delta U\} = [K_T]^{-1}\{R\}$. Update the total nodal displacements, $\{U_{NEW}\} = \{U_{OLD}\} + \{\Delta U\}$.

6) Compute increments of strain at Gauss points within each element. Update the total strains at each Gauss point.

7) Update stresses at each Gauss point given previous strains, stresses, and loading history (number of cracks and crack angles). New total stresses at each Gauss point result from these computations.

8) Evaluate the nodal forces required to maintain each element in its deformed configuration, $\{IF\}$. These are given by $\{IF\} = \int_V [B]^T\{\sigma\}\, dv$. Assemble these into a nodal vector for the structure,

$\{IF_S\}$.

9) Compute the structure residual nodal load vector as $\{R\} = \{P_{NEW}\} - \{IF_S\}$.

10) Apply convergence tests to determine the level of residual loads remaining. If the convergence tests are satisfied, go to (1) and begin processing the next load step; otherwise go to (3) and begin the next iteration.

The two convergence tests used to terminate the iterative solution process are:

$$\left\|\{R\}\right\| < 0.03 * \left\|\{\Delta P\}\right\| \tag{2.4}$$

$$\text{MAX} \left|\{R_i\}\right| < 0.02 * \left\|\{\Delta P\}\right\| \tag{2.5}$$

where $\{R\}$ is the residual load vector and $\{\Delta P\}$ is the applied incremental load vector. The first test, Eq. (2.4), compares Euclidean norms (square root of the sum of the squares) of the residual load and applied load vectors and represents an average measure of equilibrium. The second test, Eq. (2.5), detects any highly localized residual loads that could be missed by a vector norm computation. Both tests must be satisfied for acceptance of a solution. These convergence tests force the equilibrium iterations to continue until no further cracks develop for the applied load increment.

CHAPTER 3

RESULTS AND DISCUSSION

3.1 General

A parametric study of nonlinear simple beam responses was conducted using the solution and modeling procedures described in the previous chapter. Three span-to-depth ratios of 12:1, 5:1, and 2:1 were considered. These span-to-depth ratios cover beam responses ranging from those dominated primarily by flexure (12:1) to those controlled by shear (2:1). In subsequent discussions, these geometries are referred to as the slender beam (12:1), the moderate beam (5:1), and the deep beam (2:1). Analyses were conducted for a uniformly distributed load applied across the top surface of the beam and for a single concentrated load applied on the top surface at midspan.

Analyses were also performed to assess the influence of smeared cracks on the stiffness characteristics and convergence properties of the four and eight node isoparametric elements. Difficulties arising from the development of zero-energy modes in cracked eight node elements were explored. Additional analyses were conducted to investigate the effect of loading increment size on the path dependent formation of cracks.

This chapter presents a detailed description of the problems selected for the parametric study, the numerical results obtained, and a discussion of the findings.

3.2 Beam Properties and Modeling Details

All beams analyzed were 7 inches thick, 15 inches deep and simply supported at each end. Span lengths of 180, 75, and 30 inches for the slender, moderate, and deep beams provided the span-to-depth ratios desired. A concrete elastic modulus of 3,600 ksi and a reinforcing steel modulus of 29,000 ksi were used. A reinforcing steel yield point of 60 ksi was selected, with linear strain hardening at a slope of 5% of the elastic modulus (Fig. 3.1). All beams were singly reinforced with a reinforcing ratio of 1.5% (1.6 sq.in.). No shear reinforcement was provided. A limiting tensile strength (f_t') of 400 psi was used to predict cracking in the model. Several analyses were also performed for the deep beam to assess the influence of tensile strength on the response of shear critical members. A 10 psi tensile strength was employed to approximate a zero strength condition for these analyses (a tensile strength of zero leads to numerical difficulties in the finite element solution, as extensive cracking occurs at a very small load). Tables 3.1 and 3.2 summarize the beam dimensions and material properties.

To eliminate possible effects of the finite element shape, square elements were used whenever the geometry permitted. In those few cases which required rectangular elements to be used, the rectangular elements were placed immediately above the simple support.

The slender and moderate beams were analyzed using 1, 2, and 5 elements through the 15 in. depth. For the deep beam, grids were analyzed with up to 20 elements through the depth.

Early in this study, it was found that placement of concrete elements below the reinforcement (modeled with bar elements) produced numerical problems during solution when the normal stiffness reduction factor, α in Eq. 2.3, was assigned a zero value. In the high moment regions, elements below the reinforcement develop a near vertical crack at each Gauss integration point. When a perfectly vertical crack develops at each point in an element, a complete loss of stiffness occurs in the horizontal direction. In solutions for the beam problems, exactly vertical cracks do not form in an element due to small shear stresses present below the bar elements. However, the single precision arithmetic (48 bit word) employed for the computations was insufficient to detect these small differences in crack orientation, and a singular or near singular stiffness resulted at the adjacent bottom nodes. The situation was remedied by eliminating the layer of concrete elements below the reinforcement, which produced a very slight decrease in the initial cracking loads. Alternatively, a very small value for the normal stiffness reduction factor could have been retained to prevent the numerical problems.

When connected, the eight node isoparametric element and the two node constant strain bar element do not maintain interelement displacement compatibility. Models in this study were constructed with two rod elements for each eight node element at the level of the reinforcement, i.e., a bar element connected a corner and a mid-side node. To determine the error introduced by the displacement incompatibility, several analyses were performed for the deep beam meshes. Models were constructed with a single bar element connecting the quadratic element

corner nodes. The mid-side node displacements of the quadratic element were constrained to be the average of the adjacent corner node displacements, thus re-establishing displacement compatibility with the bar element. Comparison of solutions with and without displacement compatibility revealed negligible differences in the load-deflection curves.

Uniformly distributed loads were modeled using energy equivalent forces applied to the nodes along the top surface. The concentrated loading was modeled by a single force applied to the midspan top surface node. Symmetry of the loads and constraints about mid-span permitted the use of only one half of the beam in the finite element models. Horizontal constraints imposed on all midspan nodes enforced the symmetry boundary condition. The simple support was modeled by a vertical constraint imposed at the bottom edge node.

A deflection measure was developed to minimize the effect of localized deformation at the simple support and under the concentrated load. For the purpose of comparison, deflections were computed by subtracting the mid-depth deflection over the support from the mid-depth deflection at center span. These values are termed "mid-depth deflections" on all load-deflection curves. If a node did not fall at mid-depth, the average displacement for the two nodes on each side of mid-depth was used.

Loads were applied to the finite element models in a sequence of increments or steps. Initially, load step sizes were estimated using theoretical predictions of the loads corresponding to first cracking and yielding. During subsequent analyses, load step sizes were selected to

provide an adequate description of the load-deflection curves. Variable size load increments were used in each case to obtain a better resolution of the load-deflection curves near loading levels at which extensive cracking or yielding occurred. Load-displacement curves presented in this chapter show the individual load steps for each analysis. Section 3.5 examines the sensitivity of computed displacements and cracking patterns to the selected load increment size.

The qualitative load-deflection response for all beams is illustrated in Fig. 3.2. Four distinct regions may be identified in this figure. For discussion, these regions are denoted: 1) elastic precracking, 2) cracking prior to yield of the reinforcement, 3) rounded knee that develops at initial yielding, and 4) post-reinforcement yield and strain hardening with little additional cracking. The unlimited strain hardening, coupled with the elastic model for concrete in compression, permits the load to increase almost linearly with displacement once significant yielding occurs. Therefore, no limit loads are attainable with this model.

3.3 Numerical Examples

3.3.1 Slender Beam

Analyses were conducted for the slender beam (12:1 span-to-depth ratio) considering both distributed and concentrated loading for 1, 2, and 5 elements through the depth. A 2 x 2 integration order was used for both the linear and quadratic elements. Load-deflection curves and crack patterns for the uniform load case are shown in Figs. 3.3-3.7.

The linear element grids become more flexible as the number of elements through the depth increases; the quadratic element grids, however, become progressively stiffer with grid refinement. As will be discussed in Section 3.4, this unusual trend can be traced to the development of zero energy deformation modes in cracked quadratic elements that are evaluated with a reduced (2x2) integration order. The computed load-displacement responses for both element types rapidly converge to a common solution, as shown in Fig. 3.7, and appear to provide an upper and lower bound strength prediction.

Several analyses were performed using fully (3x3) integrated quadratic element grids. Load-deflection curves were found to coincide exactly with those for the four node element and are therefore not shown on the figures.

The quadratic element solution for one element through the depth (Fig. 3.4) shows the greatest departure from the other five solutions obtained for this problem. This solution predicts initial yielding of the reinforcement at approximately 80% of the load obtained in other solutions. Similar behavior is also observed for the concentrated load case (Fig. 3.9). The coarse grid is stiffer than the finer grids before cracking; but once cracks develop, the region affected is larger than for the finer grids which results in a significant loss of stiffness. The stiffness loss apparently increases the strain in the reinforcement, which causes the lower yield load.

The extensive vertical cracks in the uniformly loaded beam (Figs. 3.5 and 3.6) clearly indicate the flexural nature of the response. Crack orientations in the linear element grids are erratic

until a grid with five elements through the depth is used. The inability of the linear element to accurately model the shear stress distribution leads to the alternating crack directions. The eight node element, even for the coarse grid, produces realistic crack orientations due to the improved shear stress representation. Fine grids for both element types show the influence of the simple support reaction. The region of inclined cracks due to high shear stress extends approximately twice the beam depth from the support.

The extent of cracking through the beam depth is an important aspect of the crack patterns. For the linear element, coarse grids (1 element through the depth) develop cracks at all Gauss points, whereas the intermediate and fine grids have one or more layers of completely uncracked points above mid-depth. In the coarse grids, both the shear force and the compression force of the couple providing the internal resisting moment must be transferred by a completely cracked, and thus more flexible, element.

Crack patterns for the fine meshes (5 through the depth) exhibit gaps near the neutral axis-- several uncracked or partially cracked elements are surrounded by totally uncracked elements. The appearance of "gaps" in the cracking pattern has been termed "strain localization" by other investigators (5). Almost no partial cracking occurs within linear elements (Fig. 3.5). All Gauss points within an element are either cracked or uncracked, with the resulting longitudinal saw-tooth crack pattern near the neutral axis. In contrast, many quadratic elements have only one or two cracked Gauss points (Fig. 3.6). This difference may be attributed to the mid-side node of the quadratic

element which provides considerably more freedom for deformation once cracks form. The displacements of a mid-side node relative to those of the corresponding corner nodes and the linear strain variation within the element permit a crack at one Gauss point to "relieve" stresses at adjacent points in the same element. Linear elements, with their simpler strain variation, are unable to relieve other points in an element when one point cracks. They do relieve adjacent elements through the normal discontinuity of strains across element boundaries, as indicated by the gaps in crack patterns. A similar situation can occur for the quadratic element, in which full or partial cracking in one element completely relieves an adjacent element. The absence of partially cracked and/or completely relieved elements (gaps) for the coarse and intermediate grids indicates that the stress relief effect diminishes rapidly with distance from a cracked Gauss point.

Load-deflection curves and cracking patterns for the same grids subjected to a concentrated load are shown in Figs. 3.8-3.12. As for the uniform load case, the four node element grids converge from the stiff side, whereas the eight node element grids converge from the flexible side. Fine grids for both element types converge to a common solution, as shown in Fig. 3.12.

3.3.2 Moderate Beam

Analyses were performed for the moderate beam (5:1 span-to-depth ratio), considering models with 1, 2, and 5 linear and quadratic elements through the depth. The response of beams within this range of span-to-depth ratio is controlled by shear and flexure over approx-

imately equal portions of the length.

Load-deflection curves and crack patterns for the distributed and concentrated load models are shown in Figs. 3.13-3.17 and 3.18-3.22, respectively. Linear element grids decrease in stiffness, while the quadratic element grids (again using 2x2 integration) first increase and then decrease in stiffness with grid refinement. After the reinforcement yields, the trends become similar to those observed for the slender beams, with the linear element grids continuing to decrease in stiffness while the quadratic element grids increase in stiffness. Convergence of load-deflection curves to a common solution with increased grid refinement is shown in Fig. 3.17.

The crack patterns for the uniform load (Figs. 3.15 and 3.16) clearly distinguish those regions controlled by flexure and those controlled by shear. Extensive diagonal cracks inclined at approximately 45 degrees, indicate the high shear, low flexure stresses near the support. Linear element coarse and intermediate grids again do not predict realistic crack patterns. The alternating crack directions within an element become much less noticeable for the fine grid. The quadratic elements produce reasonable crack patterns for all three levels of grid refinement. Gaps observed in cracking patterns for the slender beam solutions occur infrequently for the moderate beam. It can be argued that, due to the more complex stress field within the moderate beam, a grid with five elements through the depth does not reflect the same degree of grid refinement as it does for the slender beam. Considering the ratio of element size to span length, the fine grid for the moderate beam is actually less refined than it is for the slender beam.

The trends evident for the concentrated load case (Figs. 3.18-3.22) closely follow those for the uniform load case. Fine element grids for both element types appear to be converging to a common solution (Fig. 3.22). However, the rate of convergence is not as rapid as for the uniform load case.

3.3.3 Deep Beam

Analyses were performed for the deep beam (2:1 span-to-depth ratio) subjected to a distributed load and a concentrated load. Due to the high stress gradients present in the deep beam, finer grids were employed than for the slender and moderate beams. Up to 20 linear elements and 10 quadratic elements were used through the depth for the deep beam analyses. Load-deflection curves and cracking patterns are given in Figs. 3.23-3.36. The response of beams with this span-to-depth ratio is controlled almost entirely by shear, especially for the concentrated load case. Consequently, diagonal tension cracks oriented at near 45 degrees develop along a line connecting the simple support and the beam top surface at mid-span (see, for example, Fig. 3.34). Only small regions near the bottom edge and at mid-span develop flexural cracks.

Load-deflection curves for the linear element (Figs. 3.23 and 3.29) follow the same trend of increased flexibility with grid refinement observed for the slender and moderate beams. For the distributed load, quadratic element load-deflection curves, generated using reduced integration, also indicate increasing flexibility with grid refinement (Fig. 3.24). Under a concentrated load, the quadratic element load-deflection curves (Fig. 3.30) show, at first, increased flexibility,

then increased stiffness with additional grid refinement. This trend is due in part to the formation of a horizontal crack (labelled "A") just below mid-depth of the 5x5 grid, as shown in Fig. 3.31. Nodes above crack "A" displace upward (positive) rather than downward. When used to calculate the mid-depth deflection, the positive displacement over the support increases, rather than decreases, the mid-depth deflection at a given load. The 2x2 element grid does not develop a similar horizontal crack and thus appears much stiffer (edge nodes displace downward). The 10x10 grid has several nearly horizontal cracks near mid-depth as shown in Fig. 3.31, and yet nodes on the leftmost edge displace downward*.

The linear element grids, shown in Fig. 3.34, also exhibit horizontal cracks near mid-depth above the simple support; but all nodes on the edge displace downward. When solved with full (3x3) rather than reduced integration, quadratic element grids exhibit the same trend in load-deflection curves (increased flexibility with grid refinement, Fig. 3.33) and the same trend in the cracking patterns (horizontal cracks above support, Fig. 3.35) as the linear element grids. The response sensitivity to the formation of a horizontal crack above the support and the reversal of trends in load-deflection curves obtained for the quadratic element with reduced integration cast doubt on the element's integrity when smeared cracks are present. These problems prompted a detailed study of the stiffness characteristics of isoparametric elements containing smeared cracks (see Section 3.4).

---

* If only the absolute deflection at mid-span is considered, the quadratic element load-deflection curves (Fig. 3.32) for the concentrated load case show much better agreement. The 5x5 and 10x10 grids yield very similar curves; however, the 10x10 grid remains slightly stiffer.

Full (3x3) integration for the quadratic element was tried for each loading type in an attempt to obtain load-deflection curves with monotonic convergence. The results shown in Figs. 3.25 and 3.33 indicate that the desired monotonic behavior is obtained with full integration. Full (3x3) integration was then adopted to generate the quadratic element results described in the remainder of this section.

Load-deflection curves and crack patterns for the distributed load case are shown in Fig. 3.23 and 3.25-3.28. Coarse element grids did not demonstrate satisfactory convergence. Thus, linear element grids up to 15x15 and quadratic element grids up to 10x10 were analyzed to obtain convergence. As observed for the slender and moderate beams, the linear element grids decrease in stiffness with increasing grid refinement. Solutions for the 10x10 and 15x15 linear element grids are essentially identical (Fig. 3.23). Prior to yielding of the reinforcement, the response is insensitive to grid refinement. As observed for the slender and moderate beams, gaps in the linear element grid cracking patterns are present and indicate stress relief in adjacent elements due to cracking. Fig. 3.25 shows the quadratic element (3x3 integration) load-deflection curves for the distributed load. Small differences between the solutions occur prior to yielding of the reinforcement. Increased grid refinement slightly lowers the load required to yield the reinforcement. Load-deflection curves for the 5x5 and 10x10 quadratic element grids are essentially the same, indicating convergence. Gaps in the quadratic element cracking patterns are also obtained (Fig. 3.27).

Linear and quadratic element load-deflection curves, compared in Fig. 3.28, exhibit convergence toward a common solution, as obtained for the slender and moderate beams. The linear element 15x15 grid solution closely parallels the 10x10 grid solution for the quadratic element. The 10x10 quadratic element grid has 33% more nodes than the 15x15 linear grid and becomes slightly more flexible between the 4 and 6 kip/in load levels.

Load-deflection curves and crack patterns for the concentrated load case (Figs. 3.29 and 3.33-3.35) follow the same general trends observed for the distributed load case. The crack patterns (Figs. 3.34 and 3.35) exhibit regions of flexural cracks similar to those obtained for the distributed load case. Gaps in the cracking patterns are not nearly as common as for the distributed load case. These figures also reveal that complete "through depth" cracking occurs at a small percentage of the load required to yield the reinforcement. Even after all elements through the depth are cracked, the beam has considerable strength remaining due to the shear capacity of the cracked concrete. To insure that a fully converged solution had been obtained, a 20x20 grid analysis was performed using the linear element. As shown in Fig. 3.29, the 15x15 and 20x20 grid load-deflection curves are nearly identical over the entire loading range.

Fig. 3.36 compares the linear and quadratic element load-deflection curves for the concentrated load case. Differences in the two curves develop between the 20 and 40 kip loading levels. Above the 80 kip load level the stiffnesses are very similar; the average slope of the linear load-deflection curve is just slightly larger than the

quadratic element curve slope. Moreover, the loads at which the reinforcement yields are identical. The displacement jumps between the 20 and 40 kip load levels for the quadratic element and between the 40 and 80 kip load levels for the linear element occur as the structural system changes from a beam to a tied arch due to the very extensive shear cracking. Section 3.5 demonstrates that the exact load at which the shear cracking occurs is sensitive to the element type, grid refinement, and load increment size. It is also shown that the four load increments used here to reach the 80 kip load level are not sufficient for the linear element to adequately predict the displacement shift due to the transition.

3.4 Stiffness Characteristics of Cracked Elements

For the deep beam, the quadratic element with reduced integration produces load-deflection curves that have oscillating, rather than monotonic, convergence characteristics with increased grid refinement (Fig. 3.30). This behavior was at first attributed solely to the development of specific horizontal cracks above the support, as discussed in Section 3.3.3. However, upon closer study, the basic stiffness characteristics of quadratic elements containing smeared cracks are also found to affect the response.

In the slender and moderate beam solutions, load-deflection curves for the quadratic element with reduced integration exhibit monotonically increasing stiffness with grid refinement, irrespective of the load case and deflection measure. When the same problems are analyzed with the fully integrated quadratic element, the load-

deflection curves show increased flexibility with grid refinement, as expected for most finite element solutions. These observations raise questions about the stiffness characteristics of quadratic elements containing smeared cracks, particularly "shear" cracks, as observed in the deep beam. This section presents the results of numerical tests devised to study the stiffness characteristics of cracked isoparametric elements.

3.4.1 Elements With Parallel Cracks

To study the behavior of a cracked element in shear, a simple test problem was devised, as illustrated in Fig. 3.37. The problem consists of a square, unreinforced single element fixed at one end and loaded in shear. The material constitutive matrix at each integration point represents a smeared crack oriented at 45 degrees with the horizontal. The normal stiffness reduction factor, α, is assigned a value of zero. Table 3.3 lists the tip displacements computed for the linear element, the quadratic element with reduced integration, and the quadratic element with full integration. Values are normalized relative to the deflection at node 4 of the linear element (Fig. 3.37). Both the linear element and fully integrated quadratic element produce finite displacement values, as required for a non-zero value of the shear stiffness reduction factor, β. The quadratic element with reduced integration, however, produces extremely large displacements, indicative of a singular stiffness matrix. The fully integrated quadratic element, while not singular, is noticeably more flexible than the linear element. The large difference between top and bottom node deflection for the

quadratic element clearly demonstrates the additional freedom of deformation introduced by the mid-side node.

To further explore the singularity that occurred with reduced integration, an eigenvalue analysis was performed on the stiffness matrix for the elements of the test problem. Eigenvalues of a stiffness matrix are proportional to the strain energy generated when an element is deformed in the shape of the corresponding eigenvector. Rigid body motion (two translations and a rotation for these 2-D elements) generates no strain energy and thus is associated with a zero eigenvalue. Table 3.4 lists the number of zero and non-zero stiffness matrix eigenvalues for the uncracked and cracked elements (all cracks at 45^{o} as shown in Fig. 3.37). The same number of zero eigenvalues is also obtained for each case shown in the table for a rectangular element (2:1 aspect ratio). The uncracked linear and fully integrated quadratic elements have the three required zero eigenvalues to represent rigid body motion. The uncracked quadratic element with reduced integration has four zero eigenvalues, indicating the existence of an additional deformation mode that causes no strain at the 2x2 Gauss point locations. The additional "zero energy mode" was discovered soon after reduced integration came into widespread use. In most analyses, reduced integration dramatically improves the element performance. A discussion of zero-energy modes and reduced integration can be found in most recent finite element texts (37).

Of interest here is the number of additional zero energy modes that occur when all integration points are cracked at similar angles. As shown in Table 3.4, the linear element in the test problem has one

additional zero eigenvalue for a total of four; the fully integrated quadratic element has three additional zero eigenvalues for a total of six. The reduced quadratic element, however, has four additional zero eigenvalues for a total of eight. From this analysis, it is now clear why the quadratic element with reduced integration fails in the simple shear test problem. Removal of the constrained degrees of freedom (at nodes 1-3) from the stiffness matrix of the quadratic element in Fig. 3.37 leaves a 10x10 set of equations with a rank of eight, two less than the number of equations. Constraints applied to the boundary nodes eliminate only six of the zero energy modes. The shear loading activates one, or a combination, of the two remaining zero energy modes for the cracked element resulting in an unstable structure. The constrained stiffness matrices for the linear and fully integrated quadratic elements, however, possess sufficient rank to remain positive definite and thus are stable.

3.4.2 Elements With Differing Crack Orientation

The particular case discussed above for an element containing parallel cracks represents the most severe condition for element stiffness degradation. In most analyses, this condition rarely occurs due to the load redistribution process. Cracks with varying orientations generally form at the Gauss points. This should have the effect of increasing the element stiffness relative to parallel crack configurations. To study this effect, additional eigenvalue analyses were performed. A randomly oriented smeared crack was imposed at each Gauss point of an element. The element stiffness matrix was computed, and the

eigenvalues extracted. Results of these computations are summarized in Table 3.5.

Both the linear element and the fully integrated quadratic element have no zero energy deformation modes in excess of the three required for rigid body motion. The remaining non-zero eigenvalues for these elements are smaller in magnitude than those for the uncracked elements. The quadratic element with reduced integration, however, has eight zero energy modes irrespective of the crack orientations. Moreover, the formation of a crack at each Gauss point in this element introduces a zero energy deformation mode, i.e., an element with one cracked Gauss point has a total of five zero energy modes of deformation. The same number of zero energy modes was also obtained for each case shown in Table 3.5 with a rectangular element (2:1 aspect ratio).

For the linear element, altering the orientation of just one of four initially parallel cracks eliminates the single excess zero energy mode. In a fully integrated quadratic element, the three zero energy modes are eliminated by varying the orientation of just three (of nine) initially parallel cracks.

3.4.3 Effects of the Normal Stiffness Reduction Factor

The normal stiffness reduction factor, α, is often used simply to avoid placing a zero on the diagonal of the material constitutive matrix. The exact role of a non-zero α in the solution process has not been studied previously. It is generally known that small values do not drastically alter the nodal displacements. The eigenvalue analyses conducted as part of this study have defined the role of the

stiffness reduction factor. It suppresses the formation of zero energy deformation modes in cracked elements. Consider, for example, an element with dimensions of 1x1x1. The zero eigenvalues in excess of the three associated with rigid body motion become simply α times Young's modulus, E.

The test problem in Fig. 3.37 was solved for $\alpha=10^{-3}$ and 10^{-5} to assess the sensitivity of the computed displacements to a range of α values. Results for these two cases and for $\alpha=0$ are listed in Table 3.6. The four node element results show little effect for this range of α, with only a 4% displacement reduction occuring for the relatively large α value of 10^{-3}. The quadratic element displacements show a much larger effect for both full and reduced integration cases. The 50% displacement reduction for the fully integrated element suggests that $\alpha=10^{-3}$ is too large.

For the reduced integration case, any small positive value of α is sufficient to render the stiffness matrix positive definite. The computed displacements appear to vary inversely with the prescribed value of α ; the artificial stiffness normal to the crack provides the primary load resisting mechanism. These numerical results suggest that the use of a normal stiffness reduction factor is a questionable technique and may in some instances disguise undesirable element behavior.

3.4.4 Significance of Stiffness Test Results

The test problem and eigenvalue analyses provide a basis to explain the trends in load-deflection curves obtained using the quadratic element. When the structure geometry and loading are such that cracked elements must resist the applied loading, then the structure stiffness degradation is unpredictable if the cracked elements have zero energy modes. Zero energy modes in cracked elements that are not required to resist the applied loads (due to redistribution among other elements) do not appear to adversely affect the structure stiffness.

For beams analyzed with the linear and the fully integrated quadratic elements, load-deflection curves show an increased flexibility with grid refinement. This trend is observed in most finite element analyses. A set of four cracks for the linear element, and seven cracks for the quadratic element, with precisely the same orientation is required to introduce the first zero energy mode. Non-uniform strain fields and the redistribution of loads among elements prevent this from occurring.

The quadratic element with reduced integration exhibits two different trends in the convergence of load-deflection curves with grid refinement. Load-deflection curves for the slender beam indicate a stiffness increase with grid refinement; for the deep beam, load-deflection curves show a general flexibility increase with grid refinement. The moderate beam behavior lies between that for the slender and deep beam; grid refinement at first increases the flexibility but further refinement increases the stiffness.

Results of the element stiffness study point to the formation of zero energy modes as the source of the different convergence trends. Once a crack forms at a Gauss point, regardless of the crack orientation, an additional zero energy mode is obtained in the quadratic element with reduced integration. The type of convergence observed in the load-deflection curves depends directly on whether or not cracked elements provide the internal resisting forces. In the slender beam, for example, the load transfer mechanism is bending, with the internal moment provided by compression in elements at the top surface and tension in the reinforcement. The coarse grid has a single element through the depth which is subjected to both tension and compression. Tension cracks along the bottom row of Gauss points (Fig. 3.11) introduce zero energy modes that decrease the element stiffness in compression. As a consequence, the load-deflection curve is more flexible and a much lower yield load is predicted (Fig. 3.9). The intermediate and fine grids have completely uncracked elements available near the top surface that provide the compression force and shear transfer. These grids are therefore stiffer than the coarse grid. Just above the yield load, cracks develop in the top row of elements for the intermediate grid. The top row of elements in the fine grid does not crack after yielding. The fine grid is therefore stiffer after the reinforcement yields. The presence of fully cracked elements with zero energy modes along the bottom surface in the fine and intermediate grids has no effect on the load-deflection curves.

In contrast to the slender beam, the primary load transfer mechanism for the deep beam is shear, which must be resisted by the concrete. Virtually all elements develop shear cracks, including those near the top surface, independent of the grid refinement. Only cracked elements, usually with eight zero energy modes each (four Gauss points cracked), are available to resist the shear force. Grid refinement simply increases the flexibility for this case.

3.5 Effects of Load Increment Size on Load-Deflection Curves

The formation of cracks is generally considered to be a loading path dependent phenomenon. Bazant and Cedolin (5) suggest that the load increment size used in a finite element analysis significantly affects the computed response. They adjust load increment sizes as the solution progresses such that a single element (composed of 4 triangles) cracks for each increment of external load. However, during iterations to distribute residual loads, any number of additional cracks may form as necessary to reach the equilibrium configuration.

There are two major problems with this solution method. The first problem concerns the practicality of cracking a single Gauss point (or element as the case may be) with each external load increment. When considering grids of isoparametric elements, the number of sampling points is generally large compared to grids of quadralateral elements formed from triangles. In the 20x20 grid of linear elements, for example, there are 1600 Gauss points at which a crack may form. An extraordinarily large number of load increments is required to reach a fully cracked state using this procedure, which may render the analysis

economically infeasible. Furthermore, most finite element codes do not support automatic determination of load increment sizes based upon projected stress increments. Load increment sizes are usually specified directly by the analyst as a multiplier applied to a loading pattern.

The second problem with the procedure followed by Bazant and Cedolin is the inconsistency between allowing formation of only one crack for an external load increment and permitting any number of cracks to form during an equilibrium iteration at fixed external load. A more consistent approach is to successively scale the residual load vector to permit the formation of only one crack per iteration. Chen (9) has adopted this solution strategy for relatively coarse grids of constant strain triangle elements. However, with the large number of sampling points in isoparametric element grids, this solution strategy may not be feasible..

To gain some insight into the sensitivity of load-deflection curves to load increment size, the deep beam (shear panel) with the concentrated load at mid-span was subjected to additional study. A 15x15 grid of linear elements was used for the load increment size study. Cracking patterns for the load increment sizes used to generate the load-deflection curves in Fig. 3.29 revealed that essentially all cracks formed below the 80 kip load level. The effects of load increment size on crack formation could therefore be determined by considering the load level from first cracking (24 kips) through 80 kips. The loading range was divided into 8, 15, 29, and 83 equal size load steps. This contrasts to four steps used to reach the 80 kip load level for this grid in prior analyses (Fig. 3.29). For the 83 load steps, only one or two

Gauss points cracked in the first iteration of each step (which corresponds to the application of the external load increment). The solution procedure thus became that recommended by Bazant and Cedolin. As a final check, the 20x20 linear element grid was also analyzed using 83 load steps to detect any combined load step-grid size effects.

Fig. 3.38 shows load-deflection curves generated for the varying numbers of load steps with the 15x15 grid. For 8 or more load steps, the response up to the 80 kip load level consists of four distinct regions: (1) linear elastic below 24 kips, (2) flexural cracking below approximately 0.006 in. of deflection, (3) a transition region in which the structural behavior changes from a beam to a tied arch, as indicated by the displacement jump, and (4) additional minor shear cracking once the tied arch configuration is attained. Fig. 3.39 compares the 15x15 and 20x20 grid load-deflection curves that were generated using 83 load steps. The two curves are identical with the exception of the beam to tied arch transition, which occurs at different load levels. The cracking patterns for the 15x15 grid (Fig. 3.40) clearly illustrate the transition behavior. For the first 50 load steps, primarily flexure cracks formed below a diagonal line connecting the simple support and the load point at mid-span. During load step 51 (P=49 kips), extensive diagonal shear cracks formed during the equilibrium iterations, although only one Gauss point cracked in the first iteration of the load step. The development of extensive diagonal shear cracks characterizes the transition in structural behavior from a beam to a tied arch. The tied arch has only about 65% of the stiffness of the beam. These cracking patterns also reveal more distinct gaps

than those generated with the larger load increments (Fig. 3.34). A large load increment in the early stages of loading may cause the stresses to be overestimated and thus lead to excessive cracking.

The curves in Figs. 3.38 and 3.39 demonstrate the sensitivity of the beam to tied arch transition to both load step size and grid refinement. For the 15x15 grid, the use of smaller load steps increases the load at which the transition initiates. Increasing the grid refinement lowers it. The slope of the load-displacement curve for the 20x20 grid during the transition is very nearly zero, which indicates an unstable structure. This behavior is analagous to snap-through buckling in shells when driven by applied loads rather than applied displacements. The "snap-through" behavior observed for the deep beam transition occurs when, for a very small load increase, the level of cracking rapidly increases until the stable tied arch configuration is attained. This clearly indicates that the transition behavior in the deep beam is fracture sensitive. Fracture mechanics techniques are required to predict accurately the transition response, if this is the purpose of the analysis.

These results demonstrate equally as well that the macroscopic stiffness and strength of the structure are insensitive to the load step sizes used in the finite element computations. This is expected since structural behavior before the transition (a beam) and after (a tied arch) is not dependent upon the load that initiates the transition, but rather the current extent of the cracking. The exact load to initiate the transition plays a minor role in the response of this particular member. The transition behavior does not affect the stiffness of the

tied arch configuration or the load necessary to yield the reinforcement. It does, however, produce the load-deflection curve jump observed in Figs. 3.38 and 3.39. The magnitude of the displacement jump is nearly identical for the range of load steps considered (8 to 83). The load-deflection curves agree very well after the transition, both in slope and absolute position. The four load steps used to reach the 80 kip load level in earlier analyses (Figs. 3.33 and 3.36) are clearly inadequate to sense the displacement shift during the transition. This example emphasizes the importance of proper load increment selection. The nonlinear analysis of reinforced concrete structures must consider different combinations of grid refinement and load increment size.

In other types of structures, for which there is not an alternative equilibrium configuration, the transition load may indeed constitute the "failure" load. Unreinforced structures and certain structures with very low reinforcement ratios would be included in this category. A fracture mechanics based analysis may then be necessary to accurately predict the transition load. The stress controlled-smeared crack model and the solution algorithms employed in this study will predict an unstable structure if another equilibrium configuration does not exist. The stress controlled model thus serves as a good indicator of its own adequacy, and will indicate when a fracture mechanics analyses is required.

The effect of element type is illustrated in Figs. 3.41a and b, which compare the load-deflection curves for the 10x10 grid of eight node elements with the 15x15 grid of four node elements for 4, 8 and 29 load increments. While both models attain stable configurations fol-

lowing the beam to tied arch transition, it is clear that the models differ in both the stiffness following the transition and the transition load itself. The 10x10 grid of quadratic elements remains more flexible than the 15x15 grid of linear elements (see also Fig. 3.36). This difference may be traced to the lower stiffness exhibited by the cracked, fully integrated eight node element, observed in Section 3.4. These results suggest that the effects of element type remain an open question and require additional study.

3.6 Effects of Concrete Tensile Strength

The deep beam was selected to study the effect of concrete tensile strength on response. Diagonal tension stresses in "shear panels" of this type usually cause large areas to crack and may lead to a considerable loss of stiffness. The effect of concrete tensile strength should be more pronounced for such a structure than for a slender beam which is controlled by flexure. Of the problems considered, the deep beam with the concentrated load at mid-span provides the most severe diagonal tension.

Load-deflection curves obtained in Section 3.5 for a tensile strength of 400 psi represent an upper bound solution. To obtain a lower bound solution, the 15x15 linear element grid was analyzed using a tensile strength of 10 psi. Load-deflection curves for the 400 and 10 psi tensile strengths are given in Fig. 3.42. The tensile strength directly controls the load at which initial cracking occurs. The crack patterns that are obtained with a 10 psi tensile strength closely resemble those in Fig. 3.40, only they occur at 1/40 of the load. These

results clearly demonstrate the negligible influence of f'_t on the overall response.

3.7 Concluding Remarks

This chapter presents the results of a large number of numerical studies designed to evaluate the response characteristics of a limiting tensile strength-smeared crack model for nonlinear analyses of reinforced concrete structures. Questions raised by recent investigations concerning this modeling approach have been addressed. The specific concerns include:

1) Do load-deflection curves converge with grid refinement? If yes, in what manner, and what governs the type of convergence?
2) Are numerical or response problems introduced when the tensile stress is immediately reduced to zero upon crack formation?
3) What is the impact of load increment size on the response, i.e., how path dependent is the response?
4) What are the effects of concrete tensile strength on response?

Each of these questions was studied from the viewpoint of the macroscopic response, as measured by the overall load-deflection curves and cracking patterns. It must be emphasized that for the types of problems considered in this study, the flexure reinforcement enabled the members to reach stable equilibrium configurations following extensive crack formation. Consequently, the "limit" strength of each structure was only partially determined by the degree of cracking. A stable equilibrium configuration, either a beam or tied arch, was attained for

each member, even after very significant cracking occurred. Large changes in structural stiffness due to the softening effect of cracking were generally limited to early portions of the load deflection-curves (up to one-half the load to yield the reinforcement).

This study indicates that load-deflection curves do exhibit convergence toward a common solution with grid refinement. The rate of convergence depends on the geometry, type of loading, and element type. The shear dominated deep beam solutions converge more slowly and require finer grids than do those for the flexure controlled members. The linear and fully integrated quadratic element load-deflection curves show monotonically increased flexibility with grid refinement, very similar to the response obtained in ordinary linear analyses. Convergence characteristics of load-deflection curves generated using quadratic elements with reduced integration are problem dependent and vary based on whether or not cracked elements must resist the applied load. These elements contain one additional zero energy deformation mode for each cracked Gauss point, which may considerably increase the structure flexibility unless adjacent elements suppress the zero energy modes. In the coarse grids (1 element through depth) for flexure dominated problems, cracked elements must resist the shear and compressive forces. Adjacent elements are not available to suppress the zero energy modes. Consequently, grid refinement leads to increased stiffness as uncracked elements above the mid-depth become available to resist the load. For the deep beam problem, cracking occurs completely through the depth for all grids, thus requiring that the cracked elements resist the load. Grid refinement simply increases the flexibility

for this case. The linear and fully integrated quadratic elements do not develop zero energy modes, except when all Gauss points within an element crack at precisely the same orientation.

It has been suggested that immediately reducing the tensile stress to zero upon crack formation may lead to solution instability as grids are refined. No such difficulties are experienced in analyzing the beam and shear panel structures considered in this study. From a qualitative viewpoint, it may be argued that the impact of crack formation at a Gauss point is determined by the cracked element size and the sizes of the adjacent elements. The residual load magnitude imposed on adjacent elements is governed by the cracked element size; the influence of the residual load applied to the nodes of adjacent elements depends upon their size-- larger elements are influenced less. In this study, element grids are uniformly refined, which probably minimizes any effects of this type.

Below a certain magnitude, load increment size is found to have no influence on the overall stiffness and strength predictions for the deep beam considered. The load increment size does affect the load at which the beam to tied arch transition occurs for this type of member. Fracture mechanics based analyses are recommended when accurate prediction of the transition load is the goal of the analysis. For the deep beam studied, the transition behavior is a very minor aspect of the overall structural response. The transition load constitutes only 10-15% of the load required to yield the reinforcement. The load increment study also shows that a reasonable number of load steps is required to predict the displacement jump that occurs during the transition.

Analyses with a range of load increment sizes may be necessary if a major transition is structural behavior is suspected.

The concrete tensile strength controls the initial cracking load and the rate at which cracking penetrates through the depth. Neither of these responses appears to have a significant impact on the overall load-deflection curve. Once a stable, fully cracked configuration is attained, the response is independent of the tensile strength.

CHAPTER 4

SUMMARY AND CONCLUSIONS

4.1 Summary

A parametric study has been conducted to examine the influence of finite element modeling parameters on the predicted nonlinear response of reinforced concrete members. Nonlinear effects were limited to cracking of the concrete and yielding of the reinforcement. The investigation focused on the sensitivity of macroscopic response to the finite element modeling parameters. In this study, macroscopic response was characterized by load-deflection curves and general trends in the cracking patterns.

Three classes of problems were considered in the study; namely, 1) long, shallow beams with flexure dominated response, 2) moderate length beams influenced by both flexure and shear, and 3) deep beams (shear panels) in which shear dominated the response. Span-to-depth ratios of 12:1, 5:1, and 2:1 were selected for analysis to represent the three problem classes. The beams were singly reinforced and simply supported. Each beam was analyzed for a uniformly distributed load applied across the top surface and for a concentrated load applied at mid-span.

The finite element modeling parameters studied were: the element type (order of displacement approximation), the element grid refinement, the order of Gauss numerical integration, the concrete tensile strength, f'_t, and the load increment size.

The concrete was modeled as a linear material in compression. Cracks were introduced in the finite element grid using a "smeared" representation that simulates a crack by a stress discontinuity within the continuous strain field of an element. Cracks were formed when the principal tensile stress exceeded a limiting value for the material. The tensile stress was immediately reduced to zero upon crack formation.

Flexural reinforcement was modeled using constant strain, discrete bar elements. The stress-strain curve for the reinforcement followed a simple bilinear, strain hardening approximation.

Concrete portions of the beams were modeled with four node, linear displacement and eight node, quadratic displacement isoparametric elements. The nonlinear response was computed incrementally using the Newton-Raphson procedure with corrective equilibrium iterations. The structural tangent stiffness was recomputed before each iteration to assure accurate distribution of the residual loads and to maximize the convergence rate.

4.2 Conclusions

Results of the finite element parametric study presented in this report support the following conclusions.

1. Load-deflection curves for the reinforced concrete members considered in this study exhibit general convergence toward a common solution with increased grid refinement. Flexure controlled members converge more rapidly than do shear controlled members.

2. The type of convergence, whether from the stiff or the flexible side, depends on the geometry, loading, element type, and numerical integration order (for the quadratic element).
3. For the member geometries and load cases considered, changes in structural stiffness due to cracking are generally complete at loads less than one-half the load required to yield the reinforcement. Each member reaches a stable, cracked configuration early in the loading process and experiences only minor crack development under additional loading. No difficulties were experienced in continuing the analysis beyond yielding of the reinforcement.
4. Detailed analyses for a flexure reinforced deep beam show that below a certain magnitude, the load increment size does not affect the macroscopic stiffness or strength (yield load) predictions. For a specific grid refinement, the load increment size does influence the load at which the transition in structural behavior from a beam to a tied arch occurs. With the use of large load increments, the analysis may not detect the existence of such a transition.
5. Concrete tensile strength has only a minor effect on the overall load-deflection curve for the flexure reinforced deep beam. The tensile strength controls the initial cracking load and the loading at which the stable cracked configuration is attained.
6. Cracking patterns for the slender and moderate beams are sensitive to the element type and grid refinement. Coarse grids of linear elements exhibit alternating crack directions within each

element due to the poor shear stress representation. Even for coarse grids, the quadratic element, with its higher order strain variation, produces more realistic crack patterns that do not show large differences in crack angles within an element.

7. Crack patterns for the slender and deep beam fine grids show partially and completely uncracked elements adjacent to fully cracked elements. This behavior is attributed to "stress relief" of neighboring Gauss points that occurs when a point cracks. Other investigators have referred to this phenomenon as "strain localization".

8. For the flexure reinforced deep beam studied, considerably finer element grids (more elements through the depth) are required to eliminate grid size effects in the response. A 15x15 grid of linear elements is found to be adequate.

9. Eigenvalue analyses of cracked element stiffness matrices reveal that the linear and the fully integrated quadratic elements have one and three additional zero energy modes, respectively, when all Gauss points are cracked and the cracks are parallel. A similarly cracked quadratic element with reduced integration has four additional zero energy modes. Thus, eight of the sixteen deformation modes produce no strain at the 2x2 Gauss points.

10. Further, eigenvalue analysis studies show that the four node element and the fully integrated quadratic element develop no spurious zero energy modes when cracks at the Gauss points have slightly different orientations, as occurs in most analyses. The quadratic element with reduced integration has an additional

spurious zero energy mode for each cracked Gauss point, regardless of the crack orientation.

11. The development of zero energy deformation modes in the quadratic element with reduced integration causes unpredictable response when cracked elements are required to resist the applied load (e.g. for a coarse mesh in flexure problems and in all grids for a deep beam or shear panel).

12. Because of response variations with the reduced quadratic element, it is not recommended for general use. The linear element and the fully (3x3) integrated quadratic element are both recommended for general use. Load-deflection curves exhibiting monotonic convergence from the stiff side with grid refinement can be expected.

13. The stress controlled-smeared crack modeling scheme is suitable for macroscopic strength and deformation analyses of members in which the "limit" strength is not governed solely by cracking. Clearly, unreinforced and very lightly reinforced members require analysis using fracture mechanics procedures.

14. The stress controlled-smeared crack representation adequately models the general softening effect that results from cracking in common reinforced concrete members. Such members invariably achieve stable equilibrium configurations following extensive crack formation when load is transferred to the reinforcement. The failure of the solution procedure adopted in this study to reach the stable cracked configuration would strongly indicate the need for a fracture mechanics investigation.

4.3 Recommendations for Further Study

A number of areas remain to be examined for the analytical prediction of cracking behavior in reinforced concrete structures. These are briefly outlined below.

1. The effect of tension stiffening, i.e., the gradual decrease of stress to zero after cracking, was not considered. Various schemes have been proposed to represent the descending branch of the tensile stress strain curve but few, if any, studies have been conducted to determine the interaction with grid refinement.
2. All beams in this study had a reinforcing ratio of 1.5%, which approaches the upper bound permitted in design codes. The effect of lower reinforcement ratios, perhaps the minimum allowed, should be examined.
3. None of the beams analyzed had stirrups for shear reinforcement. It is not clear what affect various amounts of shear reinforcement would have on the convegence properties of the solution. Shear reinforcement would contribute significantly to the response of the deep beam (shear panel).
4. A simple nonlinear model for biaxial compression incorporated in the finite element model would permit meaningful comparisons with experimental data. It would also enable investigation of the descending branch of the overall load-deflection curve, e.g., stability behavior.

5. The use of a "smeared" representation for the reinforcing steel should be considered. The discrete bar element approach, while quite simple, restricts reinforcement to the interelement boundaries.

6. The difference in stiffness between a fully cracked, four node element and a fully cracked, eight node element requires further study. The use of a nine node, Lagrangian element should also be examined to assess any effects due to the non-uniform shear strain variation that occurs over the eight node element.

REFERENCES

1. Al-Mahaidi, "Nonlinear Finite Element Analysis of Reinforced Concrete Deep Members," thesis presented to Cornell University, Ithaca, N.Y., in 1979, in partial fulfillment of the requirements for the degree of Doctor of Philosophy.

2. Bashur, F.K., and Darwin, D., "Nonlinear Model for Reinforced Concrete Slabs," CRINC Report SL-76-03, University of Kansas Center for Research, Lawrence, Ks., Dec. 1976.

3. Bashur, F.K., and Darwin, D., "Nonlinear Model for Reinforced Concrete Slabs," Journal of the Structural Division, ASCE, Vol. 104, No. ST1, Jan. 1978, pp. 157-170.

4. Bazant, Z.P., and Cedolin, L., "Blunt Crack Band Propagation in Finite Element Analysis, Journal of the Engineering Mechanics Division, ASCE, Vol. 105, No. EM2, Apr. 1979, pp. 297-315.

5. Bazant, Z.P., and Cedolin, L., "Fracture Mechanics of Reinforced Concrete," Journal of the Engineering Mechanics Division, ASCE, Vol. 106, No. EM6, Dec. 1980, pp. 1287-1306. (Discussion by Darwin and Dodds, Vol. 108, No. EM2, Apr. 1982, pp. 464-466. Closure, Vol. 108, No. EM2, Apr. 1982, pp. 466-471.)

6. Cedolin, L., and dei Poli, S., "Finite Element Studies of Shear Critical R/C Beams," Journal of the Engineering Mechanics Division, ASCE, Vol. 103, No. EM3, June 1977, pp. 395-410.

7. Cervanka, V., "Inelastic Finite Element Analysis of Reinforced Concrete Panels Under In-plane Loads," thesis presented to the University of Colorado, Boulder, Colorado, in 1970, in partial fulfillment of the requirements for the degree of Doctor of Philosophy.

8. Cervanka, V, and Gerstle, K.H., "Inelastic Analysis of Reinforced Concrete Panels Part I:Theory," International Association of Bridge and Structural Engineers Publications, Vol. 31-11, 1971, pp. 31-45, "Part II:Experimental Verification and Application," Vol. 32-11, 1972, pp. 25-39.

9. Chen, W.F., Plasticity In Reinforced Concrete, McGraw-Hill Co., 1982.

10. Darwin, D., and Pecknold, D.A., "Inelastic Model for Cyclic Biaxial Loading of Reinforced Concrete," Civil Engineering Studies SRS No. 409, UIUC, Urbana, Ill., July 1974.

11. Darwin, D., and Pecknold, D.A., "Analysis of RC Shear Panels Under Cyclic Loading," Journal of the Structural Division, ASCE, Vol. 102, No. ST2, Feb. 1976, pp. 355-369.

12. Dodds, R.H., and Lopez, L.A., "A Generalized Software System for Non-Linear Analysis," Advances in Engineering Software, Vol. 2, No. 4, 1980, pp. 161-168.

13. Dodds, R.H., Lopez, L.A., Pecknold, D.A., "Numerical and Software Requirements for General Nonlinear Finite Element Analysis," Civil Engineering Studies SRS No. 454, UIUC, Urbana, Ill., Sept. 1978.

14. Franklin, H.A., "Nonlinear Analysis of Reinforced Concrete Frames and Panels," thesis presented to the University of California at Berkeley, in 1970, in partial fulfillment of requirements for the degree of Doctor of Philosophy.

15. Gilbert, R.I., and Warner, R.F., "Nonlinear Analysis of Reinforced Concrete Slabs with Tension Stiffening," UNICIV Report No. R-167, University of New South Wales, Kensington, N.S.W., Austrailia, Jan. 1977.

16. Hand, F.R., Pecknold, D.A., and Schnobrich, W.C., "Nonlinear Layered Analysis of RC Plates and Shells," Journal of the Structural Division, ASCE, Vol. 99, No. ST7, July 1973, pp. 1491-1505.

17. Lin, C.S., and Scordelis, A.C., "Nonlinear Analysis of RC Shells of General Form," Journal of the Structural Division, ASCE, Vol. 101, No. ST3, March 1975, pp. 523-528.

18. Lopez, L.A., Dodds, R.H., Rehak, and Urzua, J., "POLO-FINITE: A Structural Mechanics System for Linear and Nonlinear Analysis," Issued as a technical report by: Civil Engineering Laboratory, Univ. of Ill. at Urbana-Champaign, and Department of Civil Engineering, Univ. of Ks., Lawrence, Ks, 1980.

19. Mikkola, M.J., and Schnobrich, W.C., "Material Behavior Characteristics for Reinforced Concrete Shells Stressed Beyond the Elastic Range," Civil Engineering Studies SRS No. 367, UIUC, Urbana, Ill., Aug. 1970.

20. Modeer, M., "A Fracture Mechanics Approach to Failure Analysis of Concrete Materials," Report TVBM-1001, Division of Building Materials, University of Lund, Sweden, 1979.

21. Mufti, A.A., Mirza, M.S., McCutcheon, J.O., and Houde, J., "A Study of the Behavior of Reinforced Concrete Elements," Structural Concrete Series No. 70-5, McGill University, 1970.

22. Mufti, A.A., Mirza, M.S., McCutcheon, J.O., and Houde, J., "A Study of the Nonlinear Behavior of Structural Concrete Elements," Proceedings, The Speciality Conference on Finite Element Methods in Civil Engineering, Montreal, Canada, June 1972.

23. Nayak, G.C., "Plasticity and Large Deformation Problems by the Finite Element Method," unpublished Ph. D. thesis, University of Wales, Swansea, 1971.

24. Nilson, A.H., "Nonlinear Analysis of Reinforced Concrete by the Finite Element Method," Journal of the American Concrete Institute, Vol. 65, No. 9, Sept. 1968, pp. 757-776.

25. Ngo, D., and Scordelis, A.C., "Finite Element Analysis of Reinforced Concrete Beams," Journal of the American Concrete Institute, Vol. 64, No. 14, Mar. 1967, pp. 152-163.

26. Ngo, D., Scordelis, A.C., and Franklin, H.A., "Finite Element Study of Reinforced Concrete Beams with Diagonal Tension Cracks," UC-SESM Report No. 70-19, University of California at Berkeley, Dec. 1970.

27. Rashid, Y.R., "Analysis of Prestressed Concrete Pressure Vessels," Nuclear Engineering and Design, Vol. 7, No. 4, Apr. 1968, pp. 334-344.

28. Rostam, S., and Bysckov, E., "Cracks in Concrete Structures," Report No. I15, Structural Research Laboratory, Technical University of Denmark, 1971.

29. Salah El-Din, A.S., and El-Adawy Nassef, M.M., "A Modified Approach for Estimating the Cracking Moment of Reinforced Concrete Beams," Journal of the American Concrete Institute, Vol. 72, No. 7, 1975, pp. 356-360.

30. Saouma, V., "Automated Nonlinear Finite Element Analysis of Reinforced Concrete: A Fracture Mechanics Approach," thesis presented to Cornell University, Ithaca, NY, in 1980, in partial fulfillment of the requirements for the degree of Doctor of Philosophy.

31. Schnobrich, W,C., et. al., Discussion of "Nonlinear Stress Analysis of Reinforced Concrete," by Valliappan and Doolan, Journal of the Structural Division, ASCE, Vol. 98, No. ST10, Oct. 1972, pp.2327-2328.

32. Suidan, M., and Schnobrich, W.C., "Finite Element Analysis of Reinforced Concrete," Journal of the Structural Division, ASCE, Vol. 99, No. ST10, Oct. 1973, pp. 2109-2122.

33. Task Committee on Finite Element Analysis of Reinforced Concrete Structures, State-of-the-Art Report on Finite Element Analysis of Reinforced Concrete, American Society of Civil Engineers, New York, N.Y., 1982, 545 pp.

34. Valliappan, S., and Doolan, T.F., "Nonlinear Stress Analysis of Reinforced Concrete Structures," Journal of the Structural Division, ASCE, Vol. 98, No. ST4, Apr. 1972, pp. 885-898.

35. Vangreunen, J., "Nonlinear Geometric, Material and Time Dependent Analysis of Reinforced Concrete and Prestressed Concrete Slabs and Panels," UC-SESM Report No. 79-3, University of California at Berkeley, Oct. 1979.

36. Yuzugullu, O., and Schnobrich, W.C., "A Numerical Procedure for the Determination of the Behavior of a Shear Wall Frame System," Journal of the American Concrete Institute, Vol. 70, No. 7, July 1973, pp. 474-479.

37. Zienkiewicz, O.C., The Finite Element Method 3rd Edition, McGraw-Hill, London, 1977.

Table 3.1
BEAM DIMENSIONS

Beam**	Span-to-Depth Ratio	Length* (in.)	Depth* (in.)	Thickness* (in.)
Slender	12:1	180	15	7
Moderate	5:1	75	15	7
Deep	2:1	30	15	7

*1 in. = 2.54 cm

**All beams have 1.5% reinforcement (1.6 sq. in.)

Table 3.2
MATERIAL PROPERTIES

Property	Symbol	Assumed Value
STEEL		
Young's Modulus	E_s	29,000 ksi (200 GPa)
Strain Hardening Modulus	E_T	$0.05E_s$ = 1,450 ksi (10 GPa)
Yield Stress	σ_y	60 ksi (414 MPa)
CONCRETE		
Young's Modulus	E_c	3,600 ksi (24.8 GPa)
Cracking Stress	σ_{cr}	400 psi (2.76 MPa)
Poisson's Ratio	ν	0.2
Shear Modulus Reduction Factor	β	0.4

Table 3.3
CRACKED SHEAR PANEL STIFFNESS TEST

Element	Normalized Tip Deflection		
	Top	Middle	Bottom
4 Node	1.0	- -	2.47
8 Node (3x3)	1.35	2.03	7.72
8 Node (2x2)	$>10^{10}$	$>10^{10}$	$>10^{10}$

Table 3.4
ELEMENT STIFFNESS EIGENVALUE ANALYSIS (All Parallel Cracks)

	Integration Order	Total DOF	Number of Zero Eigenvalues	Number of Non-Zero Eigenvalues	Rank of Constrained Stiffness Fig. 3.37
Linear, Uncracked	2 x 2	8	3	5	4
Linear, Cracked	2 x 2	8	4	4	4
Quadratic, Uncracked	3 x 3	16	3	13	10
Quadratic, Cracked	3 x 3	16	6	10	10
Quadratic, Uncracked	2 x 2	16	4	12	10
Quadratic, Cracked	2 x 2	16	8	8	8

Table 3.5
ELEMENT STIFFNESS EIGENVALUE ANALYSIS (Randomly Oriented Cracks)

Element	Integrated Order	Total DOF	Number of Zero Eigenvalues
Linear, Uncracked	2 x 2	8	3
Linear, Cracked	2 x 2	8	3
Quadratic, Uncracked	3 x 3	16	3
Quadratic, Cracked	3 x 3	16	3
Quadratic, Uncracked	2 x 2	16	4
Quadratic, Cracked	2 x 2	16	8

Table 3.6
EFFECTS OF NORMAL STIFFNESS REDUCTION FACTOR

	Normalized Tip Deflection (See Fig. 3.35)					
	$\alpha = 0$		$\alpha = 10^{-5}$		$\alpha = 10^{-3}$	
	Top	Bottom	Top	Bottom	Top	Bottom
4 Node	1.0	2.47	1.0	2.47	0.976	2.37
8 Node (3x3)	1.35	7.72	1.34	7.63	0.85	3.72
8 Node (2x2)	$>10^{10}$	$>10^{10}$	310	1301	3.26	13.18

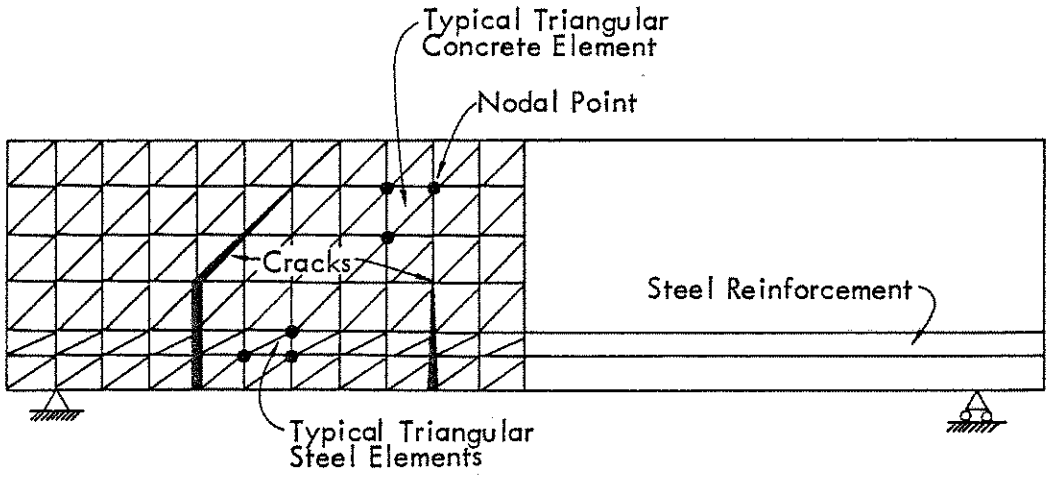

Fig. 1.1 - Finite Element Model for Reinforced Concrete Beam, Ngo and Scordelis (25).

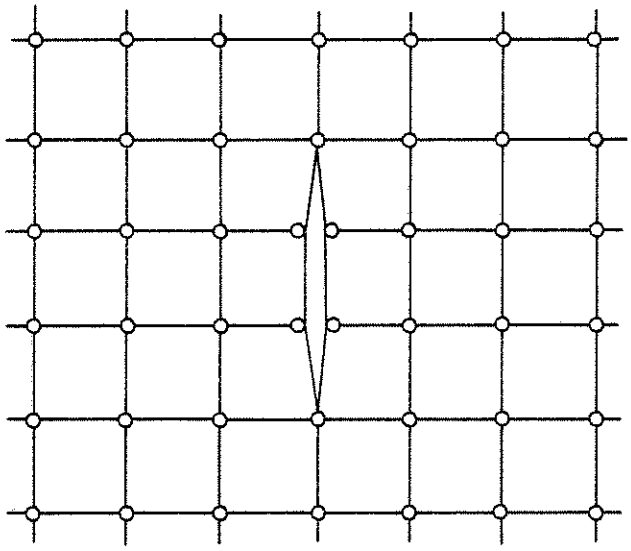

Fig. 1.2 - Discrete Representation of a Single Crack, Ngo and Scordelis (25).

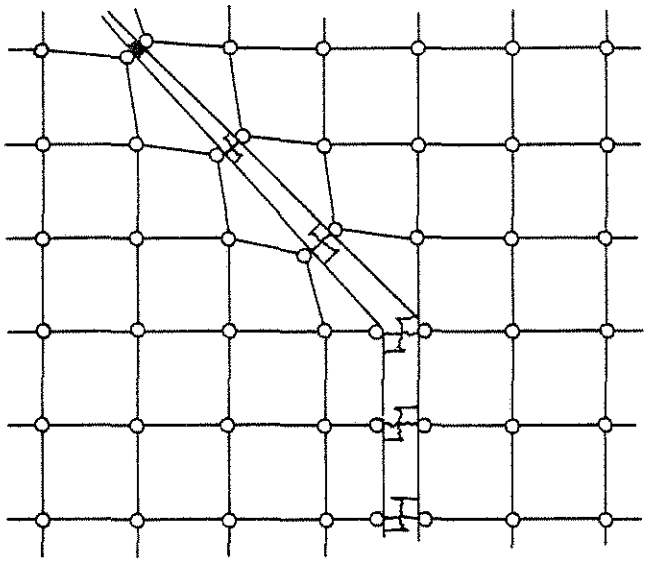

Fig. 1.3 - Discrete Crack Representation with Spring Elements to Model Aggregate Interlock, Ngo, Scordelis, and Franklin (26).

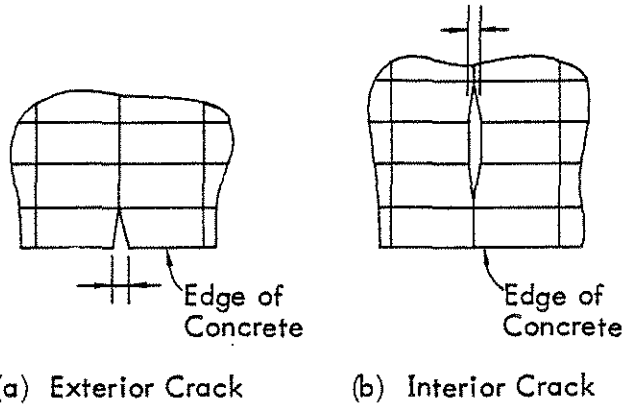

Fig. 1.4 - Discrete Crack Representation at Interior and Exterior Grid Points, Nilson (24).

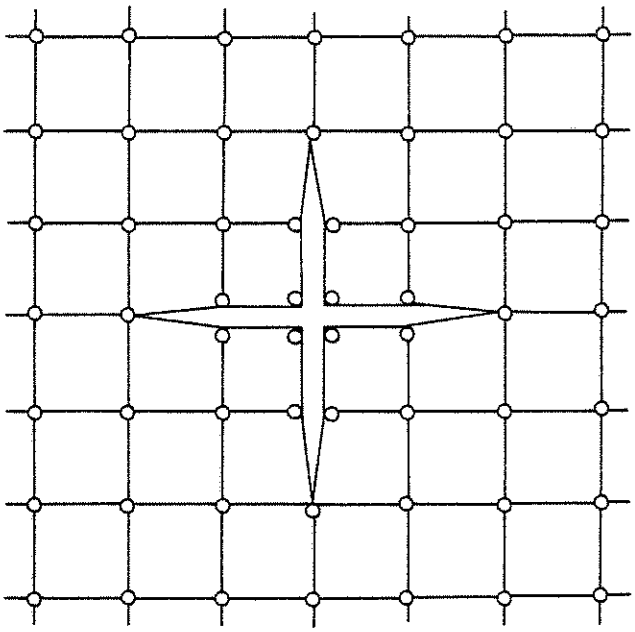

Fig. 1.5 - Discrete Representation of Two Cracks, Al-Mahaidi (1).

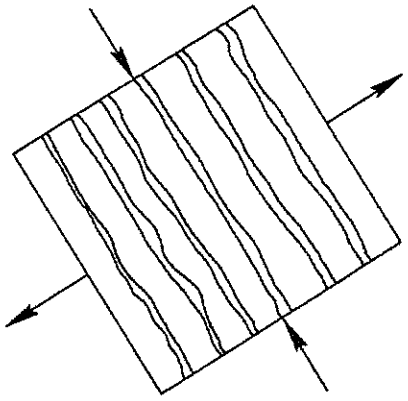

Fig. 1.6 - Interpretation of the Smeared Crack Model.

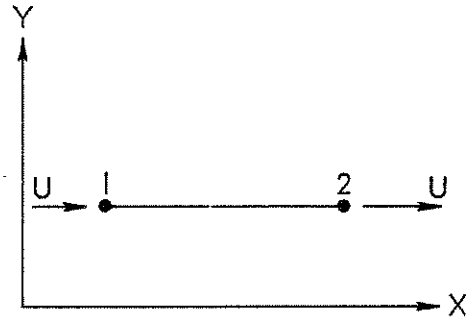

Fig. 2.1 - Bar Element for Reinforcement

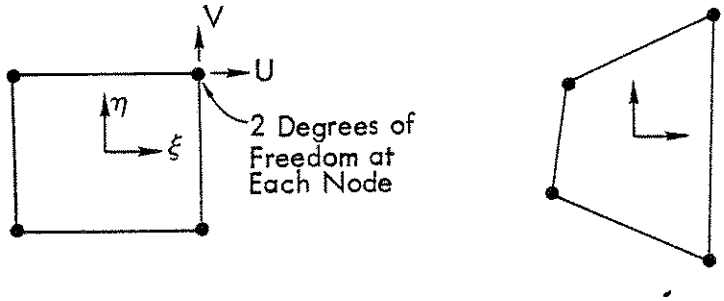

Fig. 2.2 - Linear, Four Node, Isoparametric Elemènt.

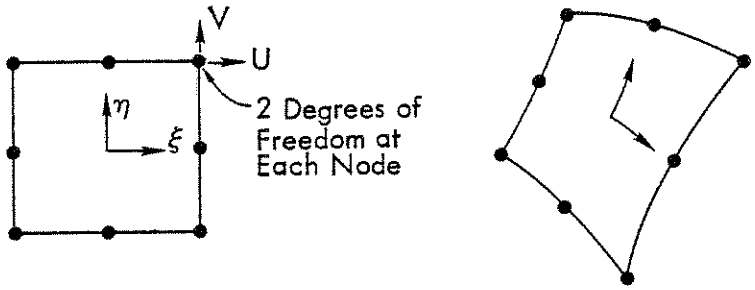

Fig. 2.3 - Quadratic, Eight Node, Isoparametric Element.

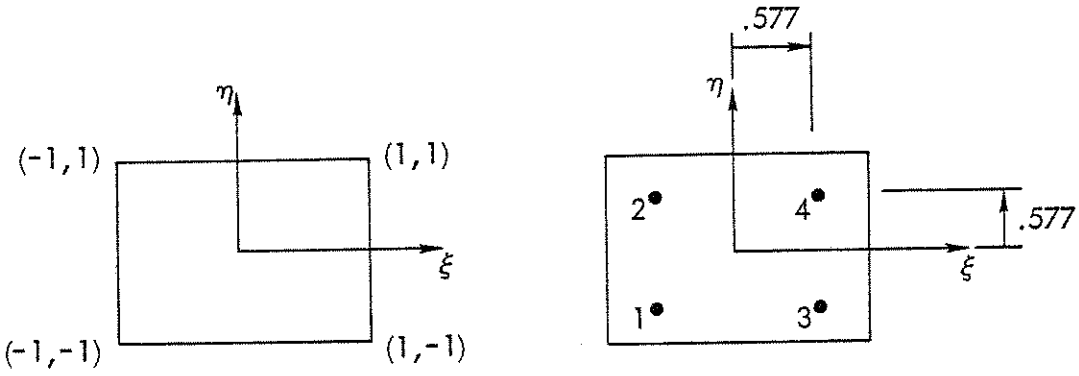

Fig. 2.4 - Gauss Point Location for 2x2 Integration in Isoparametric Coordinates.

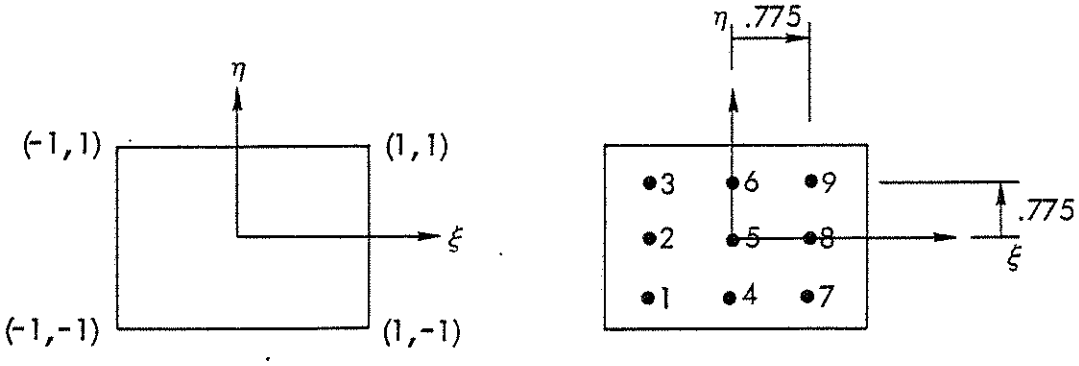

Fig. 2.5 - Gauss Point Location for 3x3 Integration in Isoparametric Coordinates.

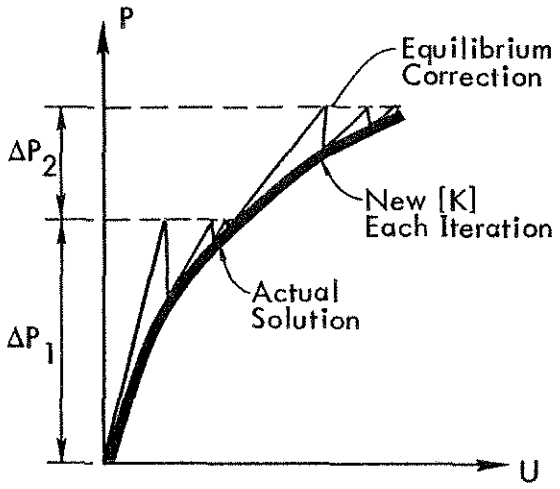

Fig. 2.6 - Single Degree of Freedom Representation of the Newton-Raphson Solution Procedure.

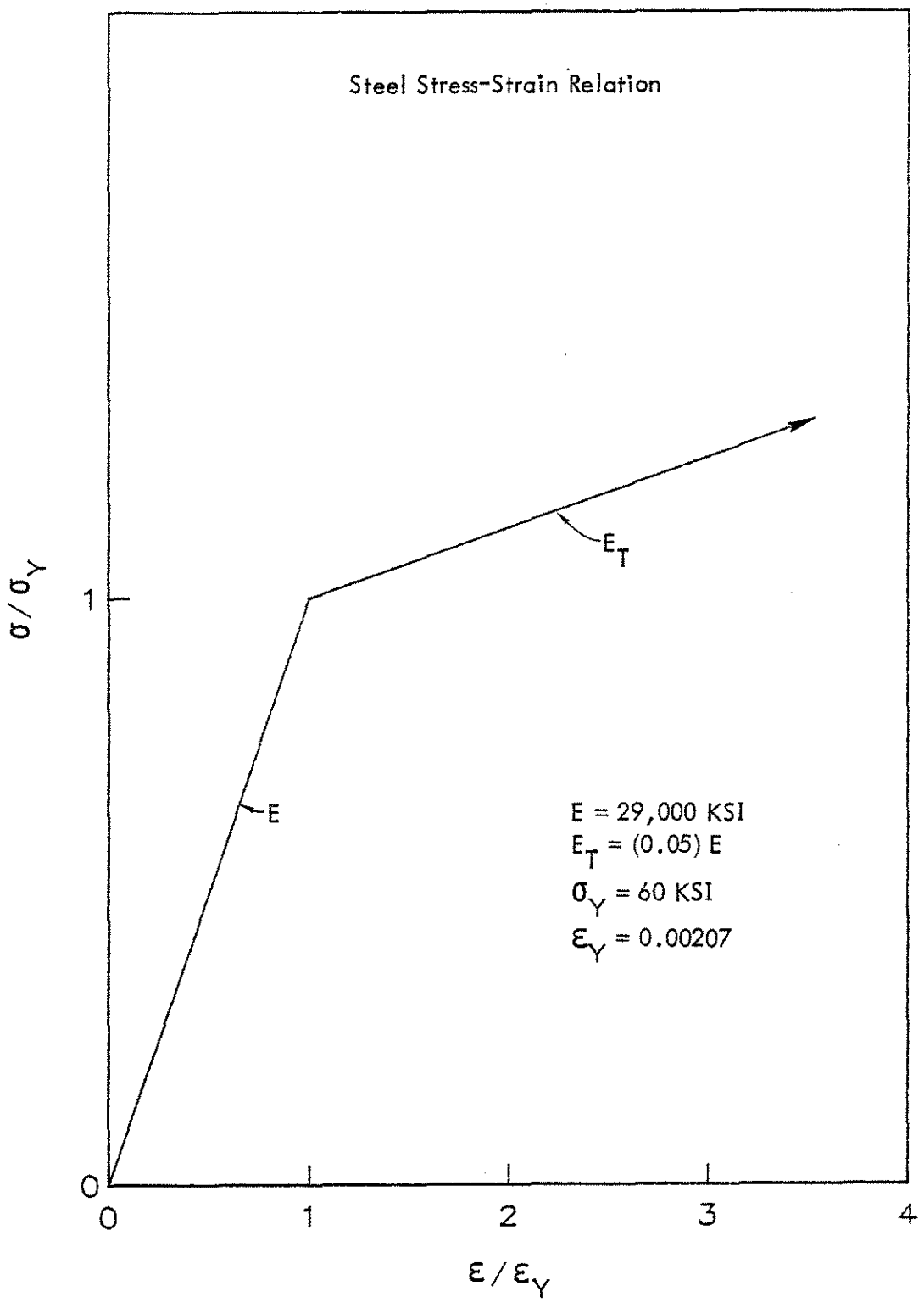

Fig. 3.1 - Uniaxial Stress-Strain Curve for Reinforcing Steel.

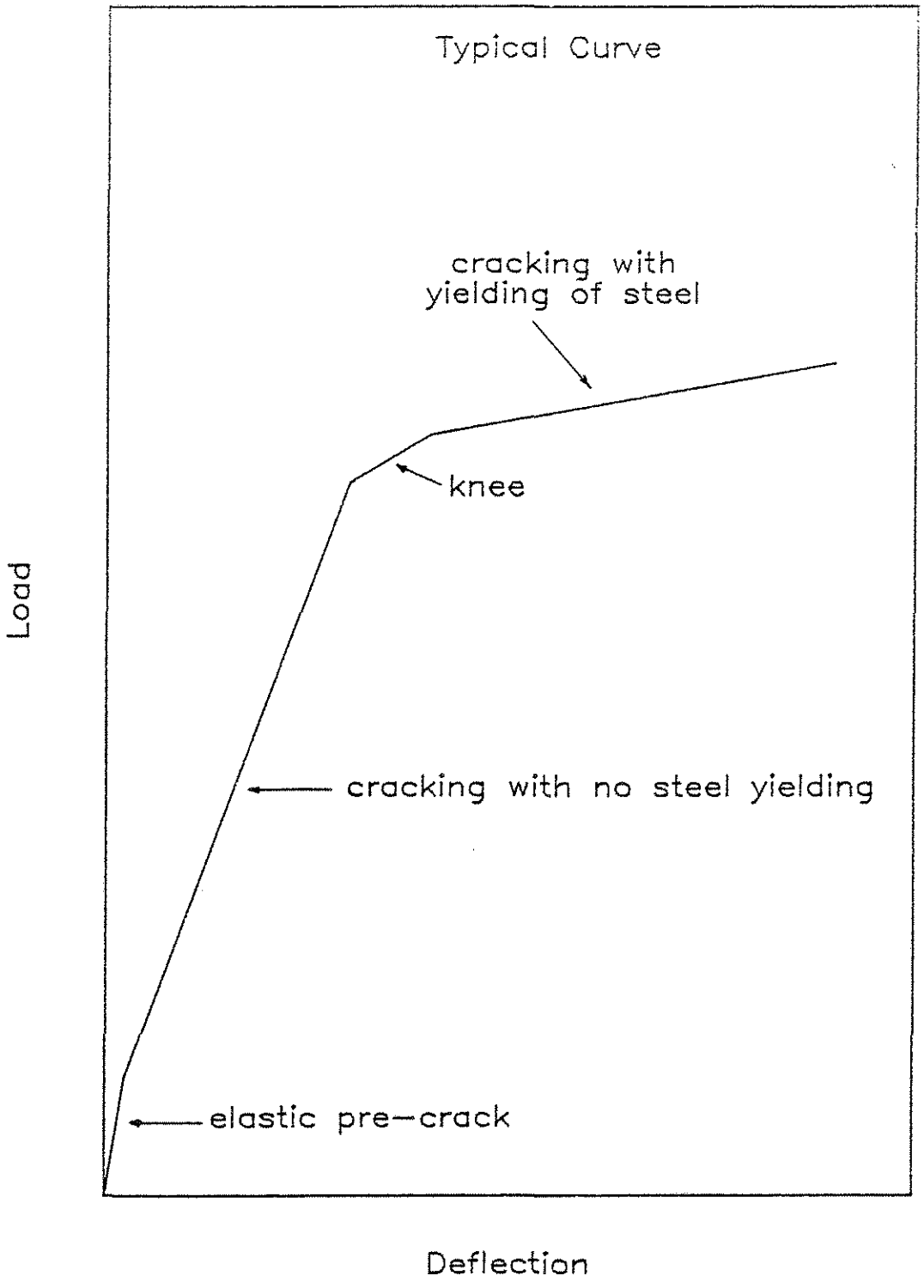

Fig. 3.2 - Qualitative Load-Deflection Response for All Span-to-Depth Ratios.

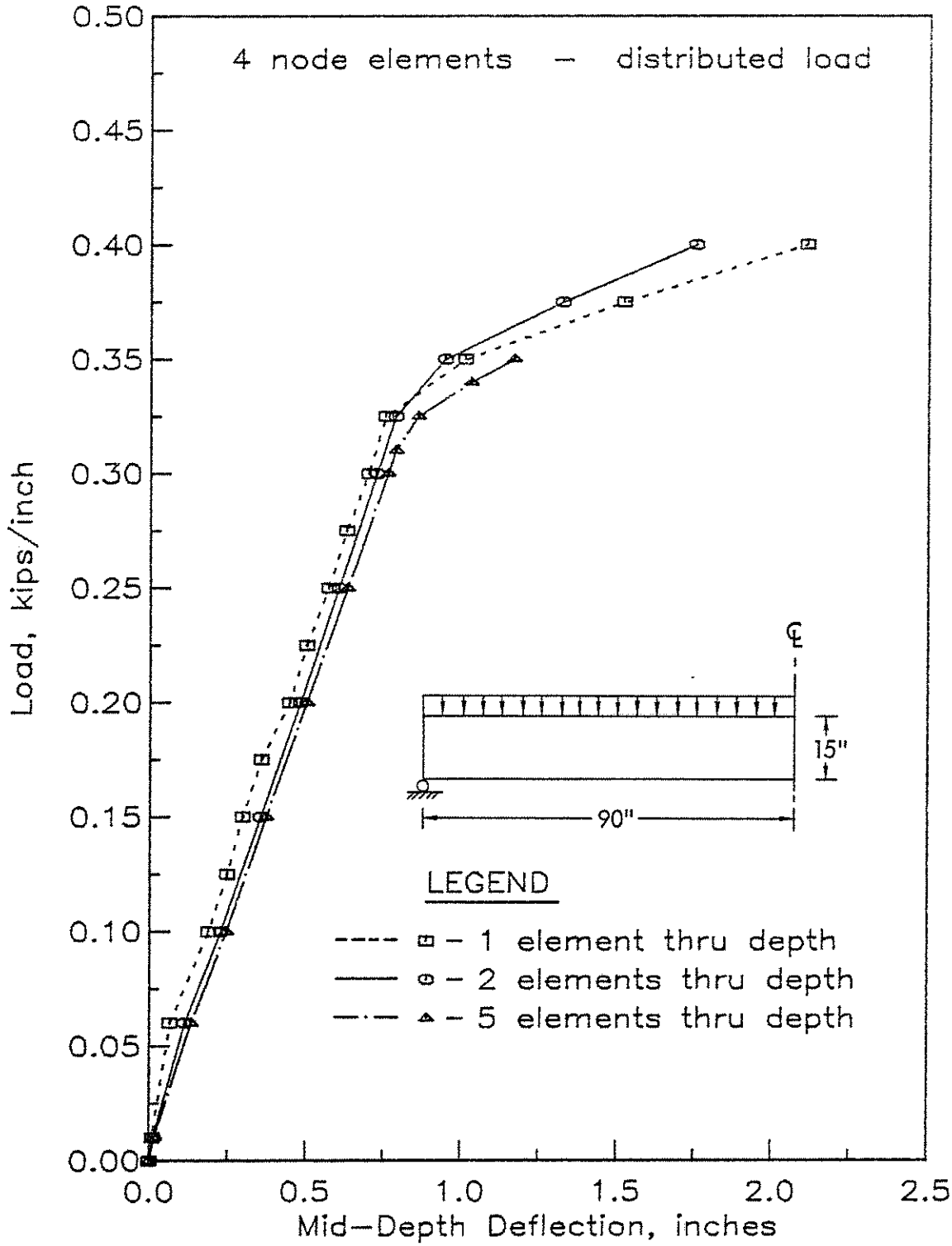

Fig. 3.3 - Load-Deflection Curves for Slender Beam, Distributed Load, Linear Elements.

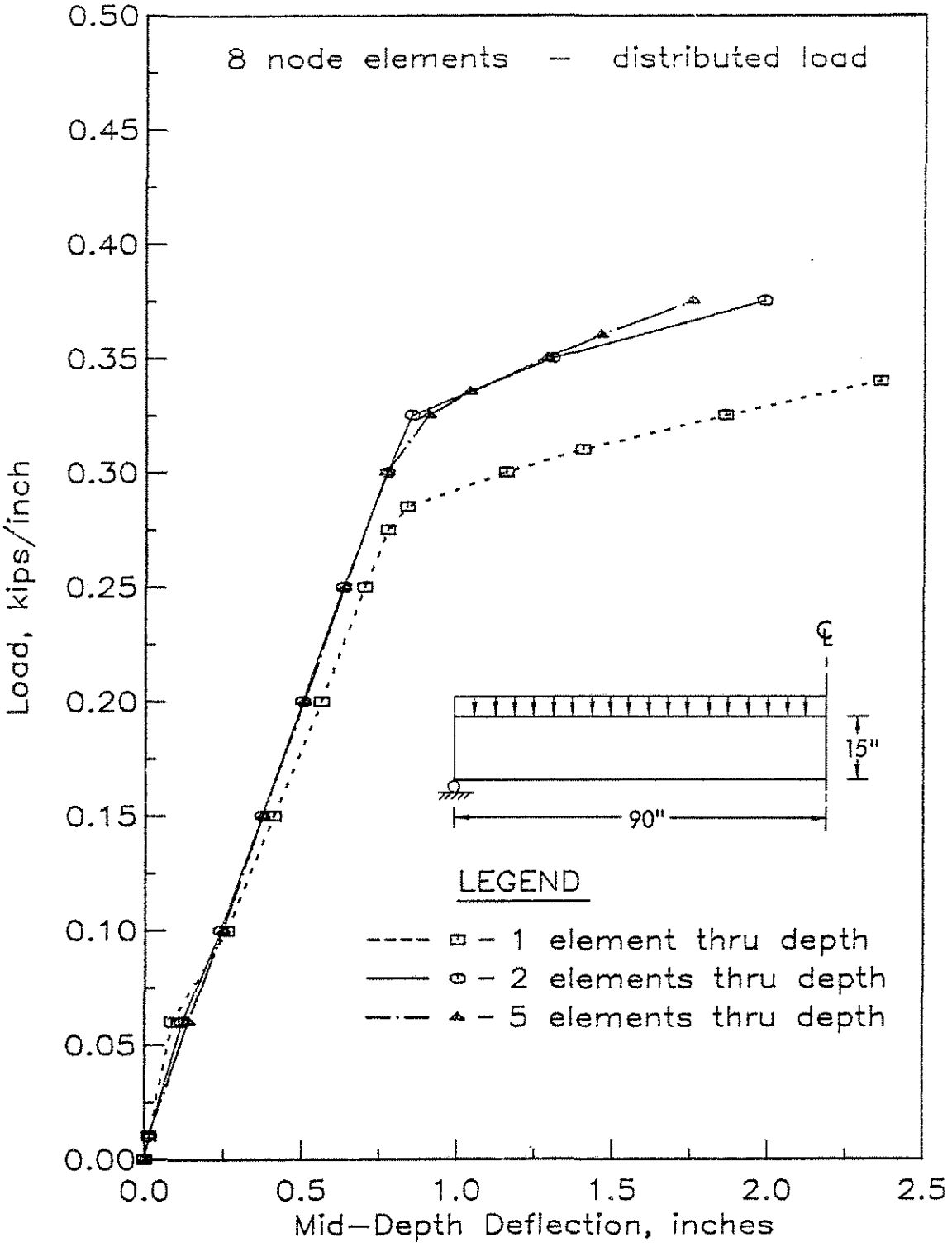

Fig. 3.4 - Load-Deflection Curves for Slender Beam, Distributed Load, Quadratic Elements (Reduced Integration).

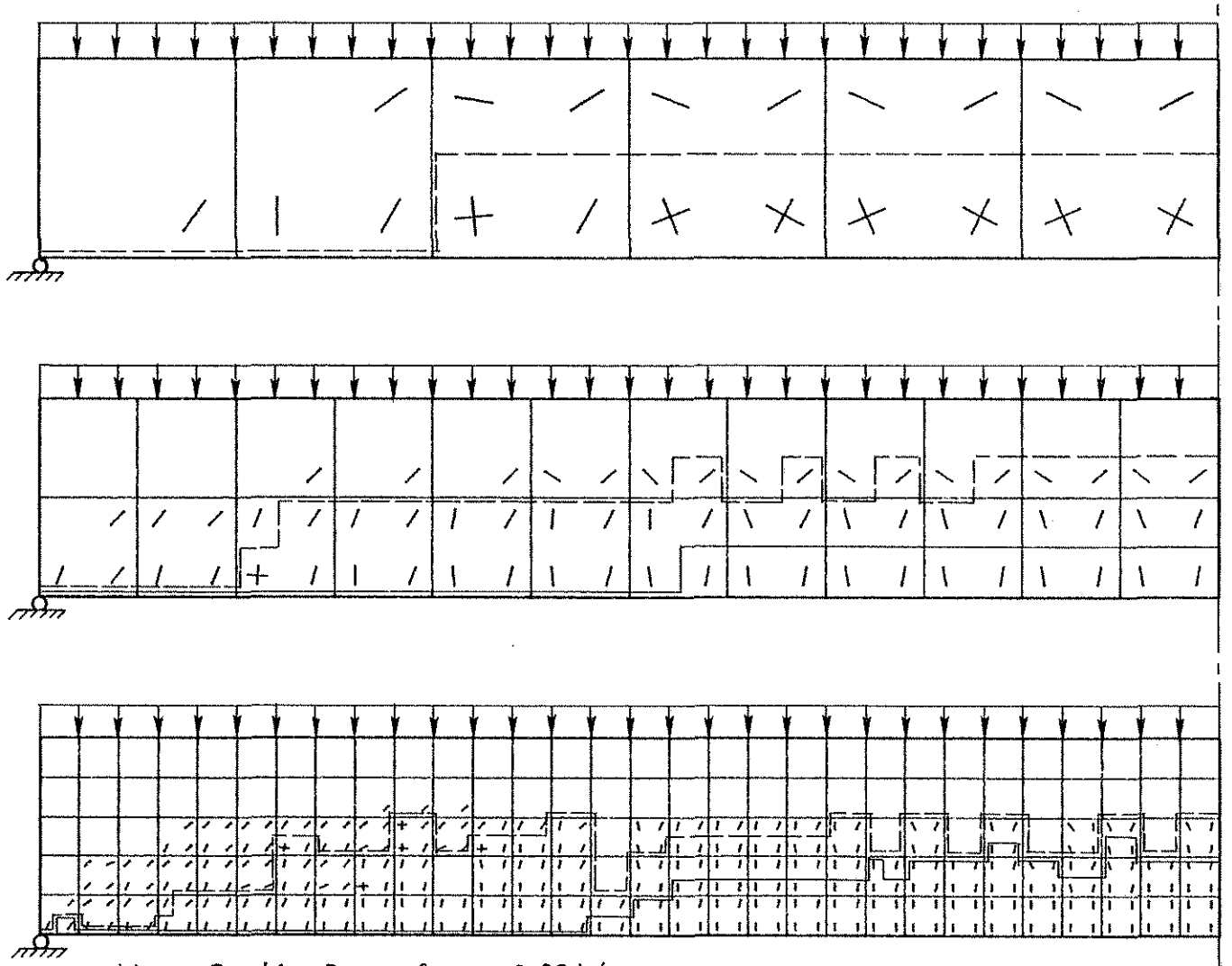

Fig. 3.5 - Crack Patterns for Slender Beam, Distributed Load, Linear Elements.

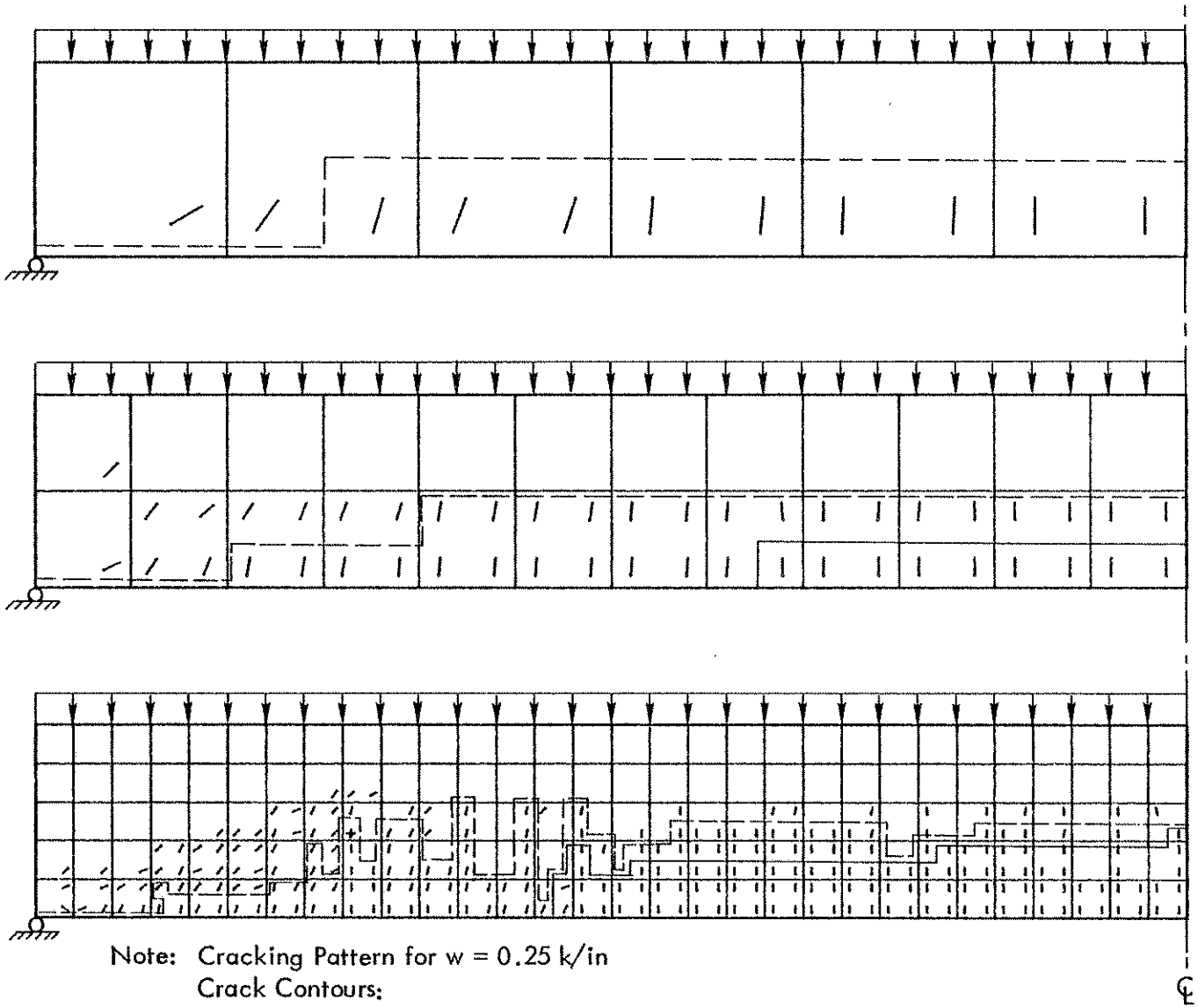

Fig. 3.6 - Crack Patterns for Slender Beam, Distributed Load, Quadratic Elements (Reduced Integration).

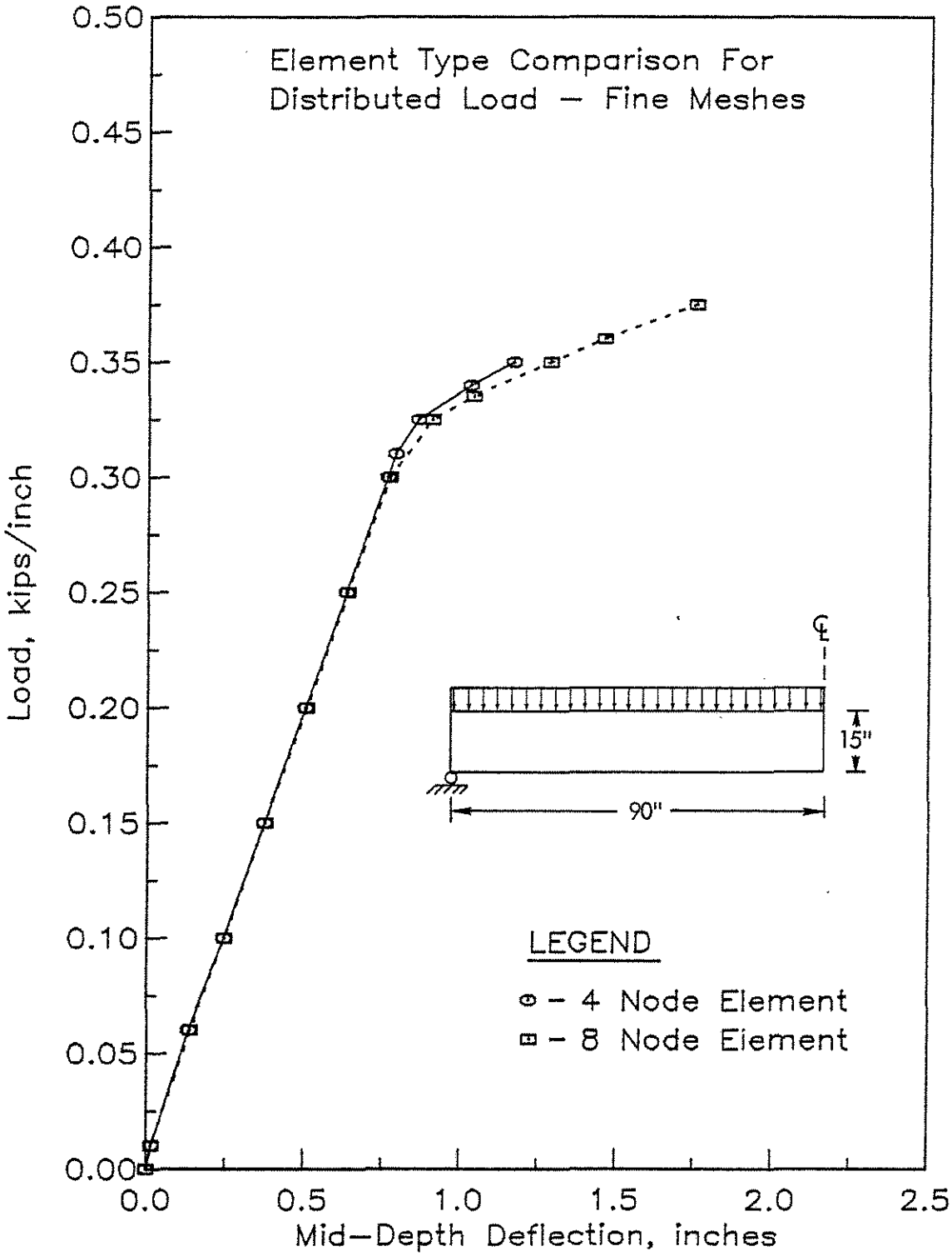

Fig. 3.7 - Comparison of Load-Deflection Curves for Slender Beam, Distributed Load, Linear Elements and Quadratic Elements with Reduced Integration.

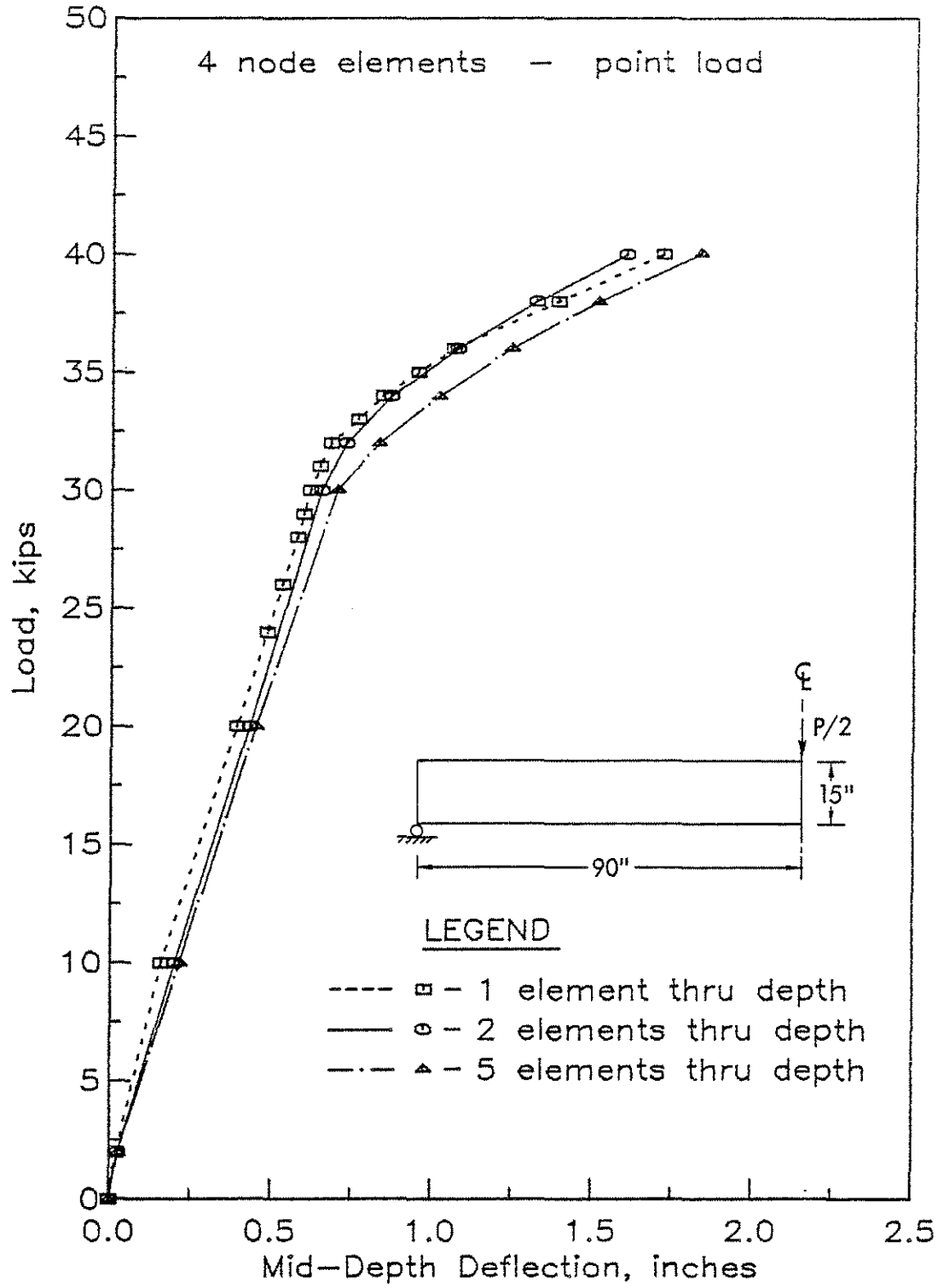

Fig. 3.8 - Load-Deflection Curves for Slender Beam, Concentrated Load, Linear Elements.

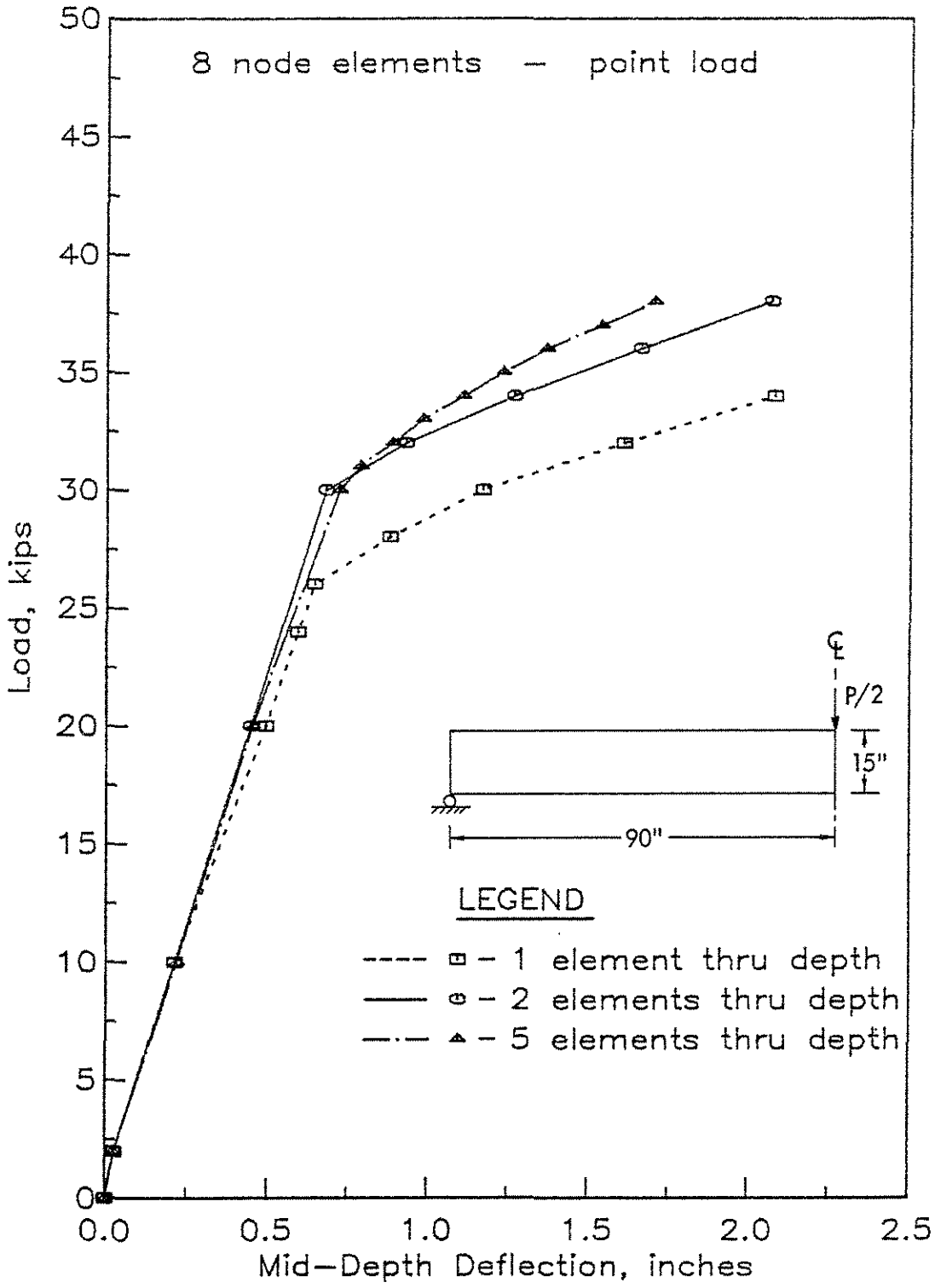

Fig. 3.9 - Load-Deflection Curves for Slender Beam, Concentrated Load, Quadratic Elements (Reduced Integration).

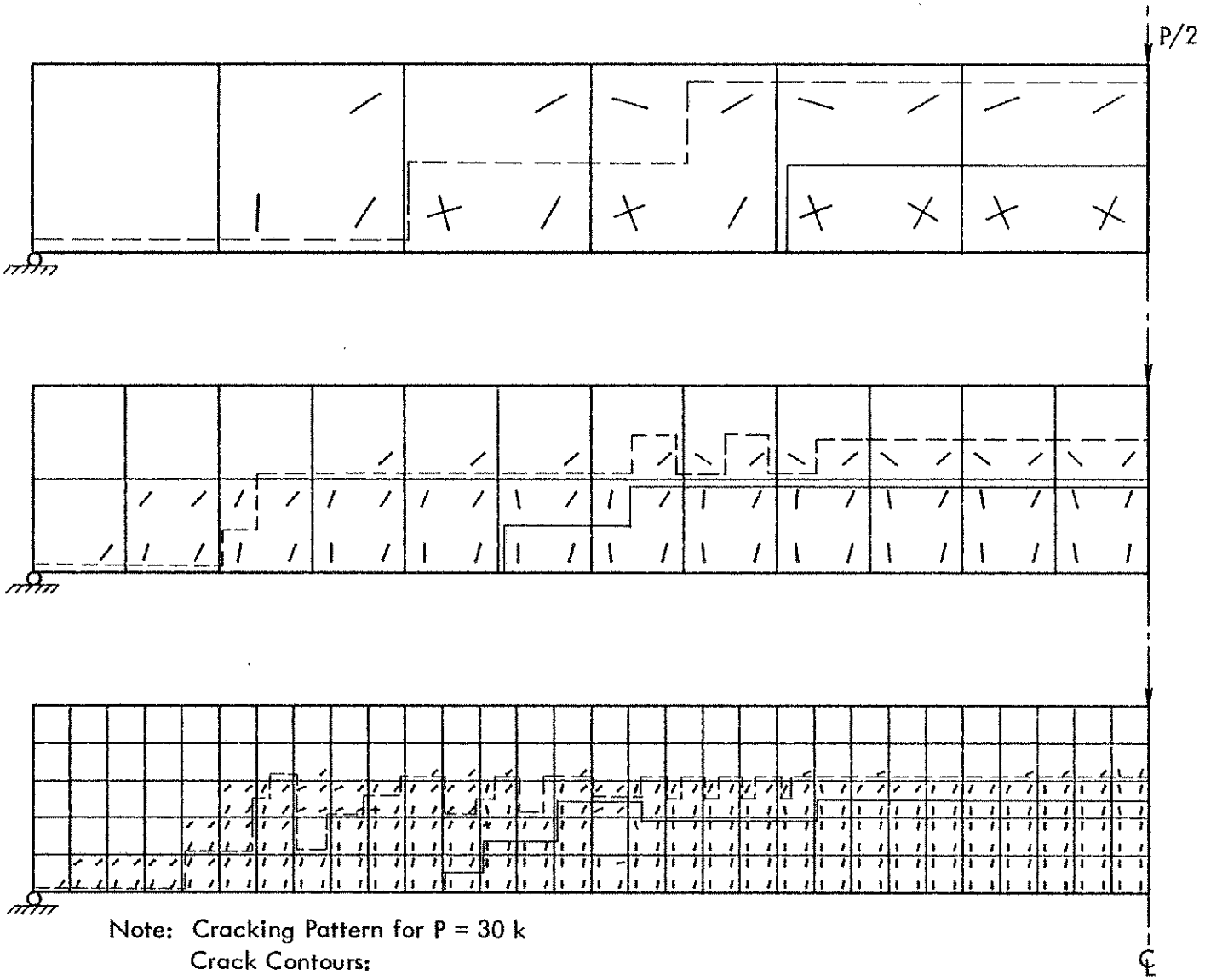

Fig. 3.10 - Crack Patterns for Slender Beam, Concentrated Load, Linear Elements.

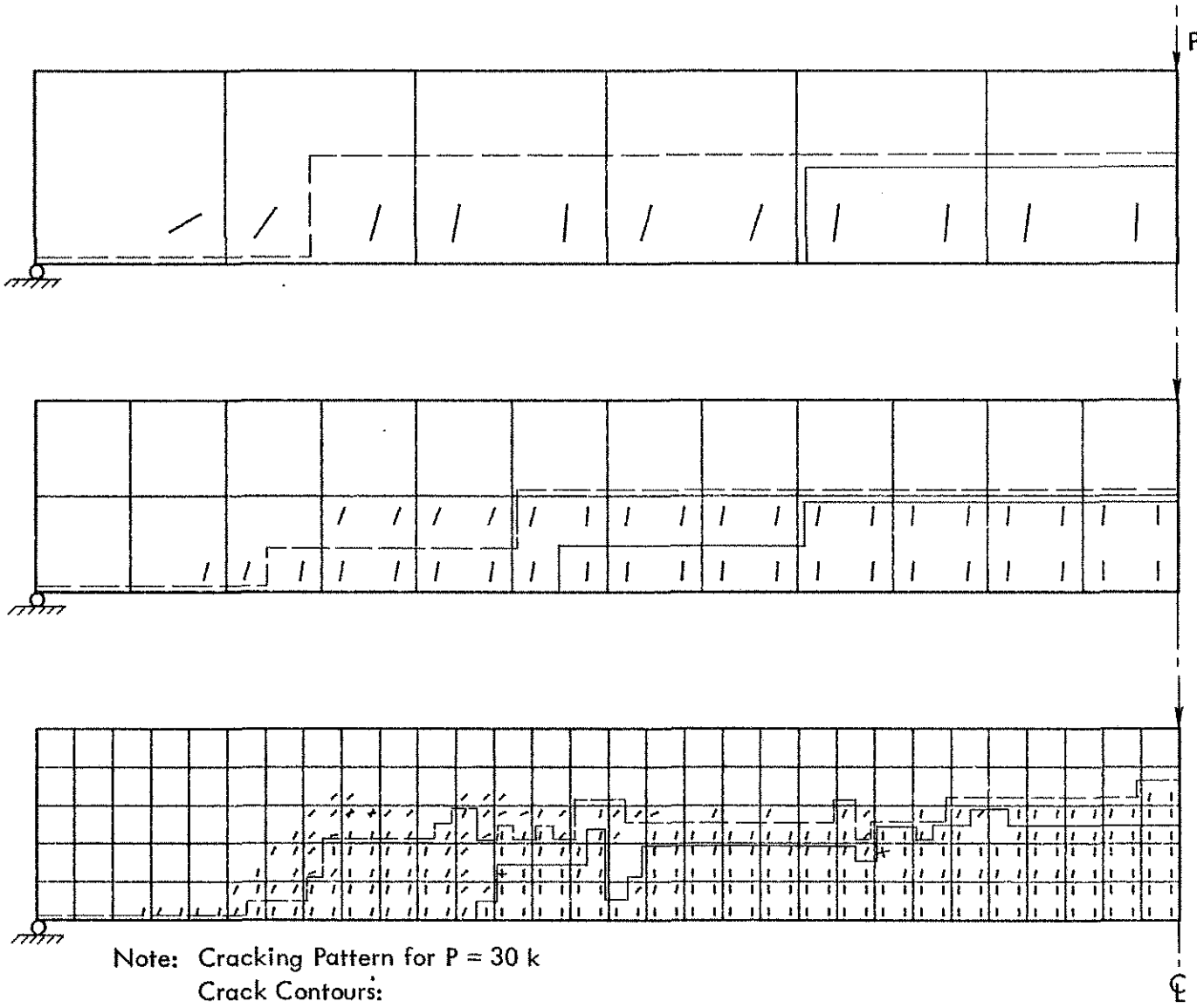

Note: Cracking Pattern for P = 30 k
Crack Contours:
——— P ≤ 10 k
— — P ≤ 20 k

Fig. 3.11 - Crack Patterns for Slender Beam, Concentrated Load, Quadratic Elements (Reduced Integration).

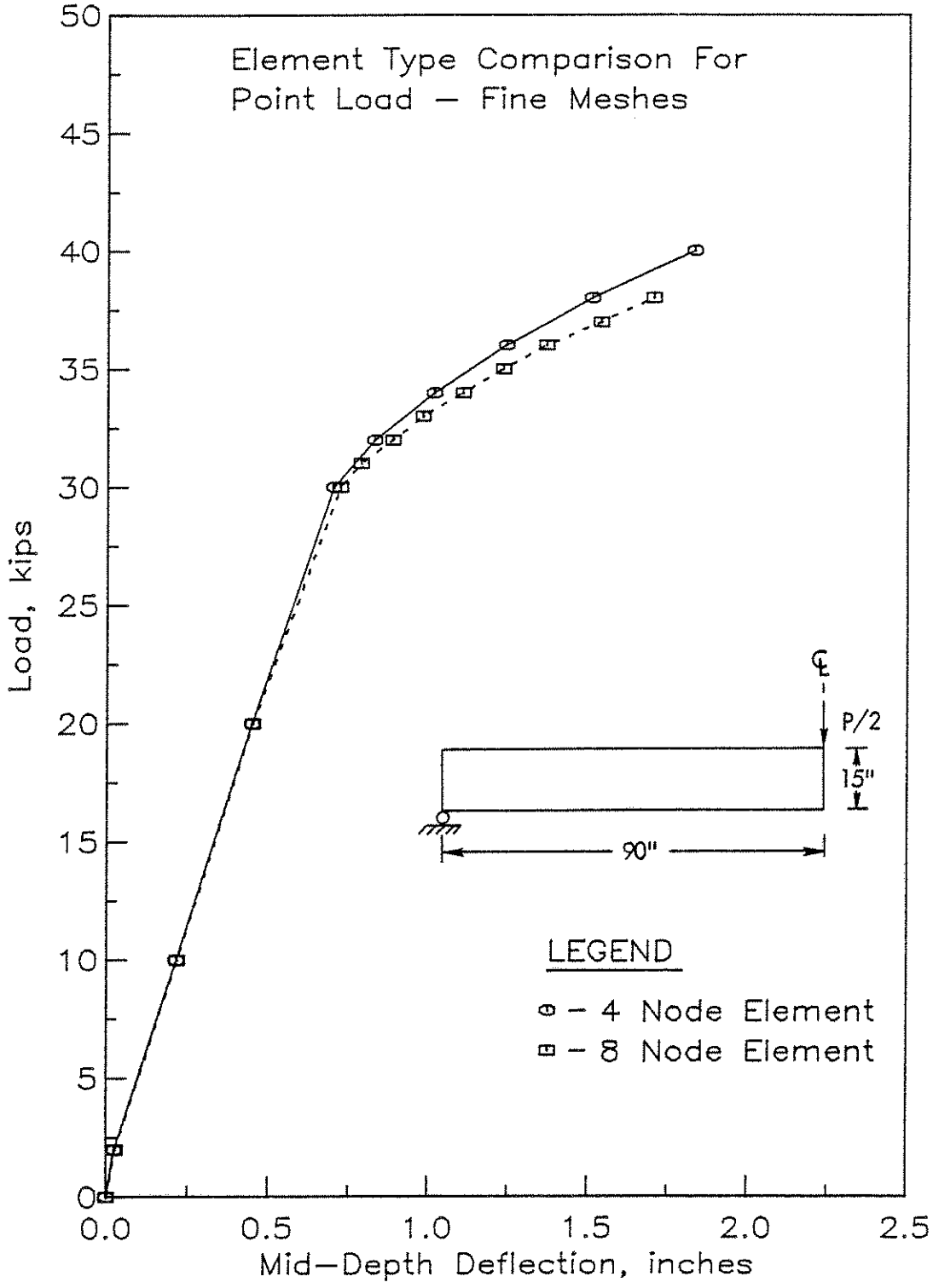

Fig. 3.12 - Comparison of Load-Deflection Curves for Slender Beam, Concentrated Load, Linear Elements and Quadratic Elements with Reduced Integration.

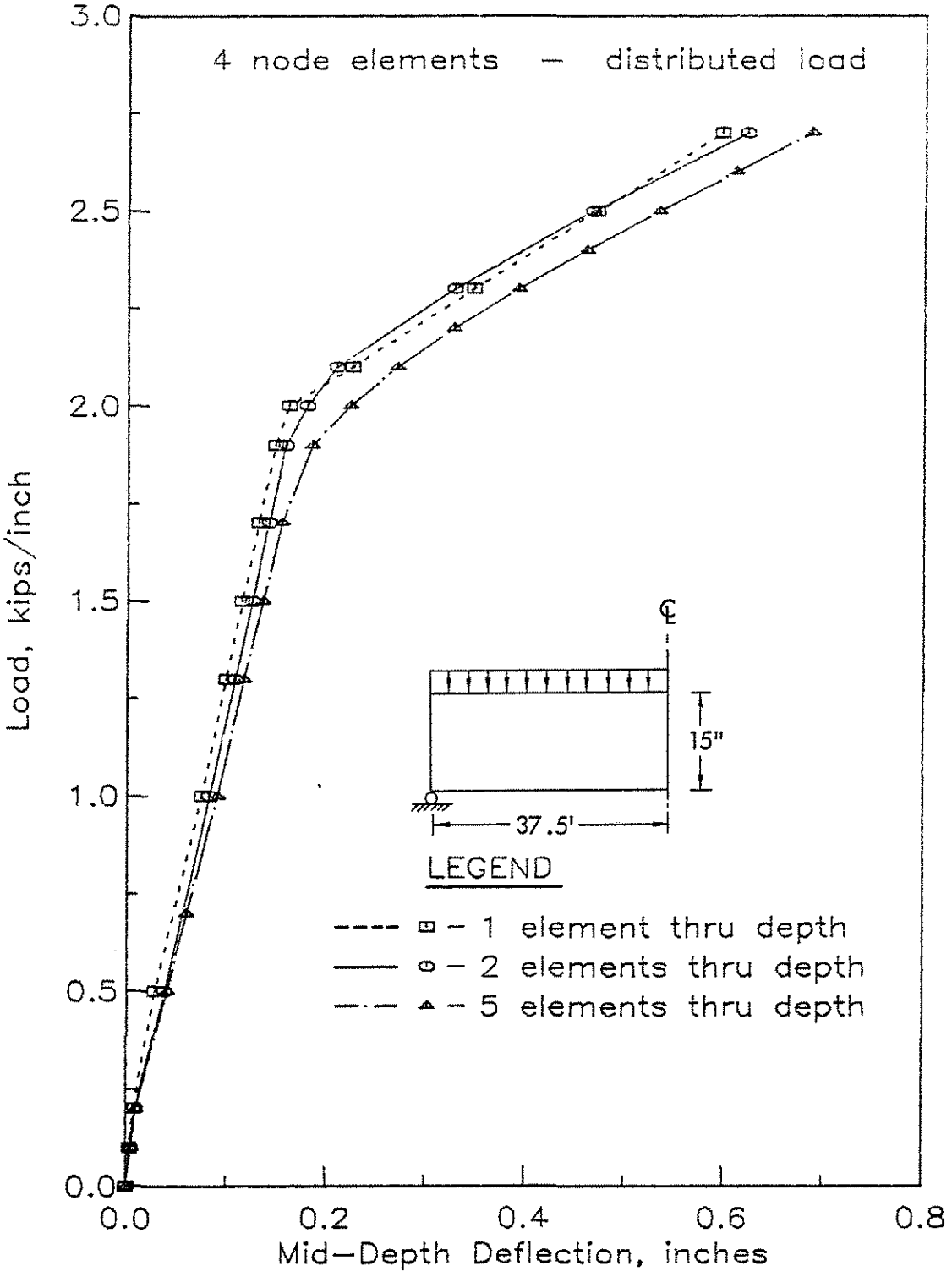

Fig. 3.13 - Load-Deflection Curves for Moderate Beam, Distributed Load, Linear Elements.

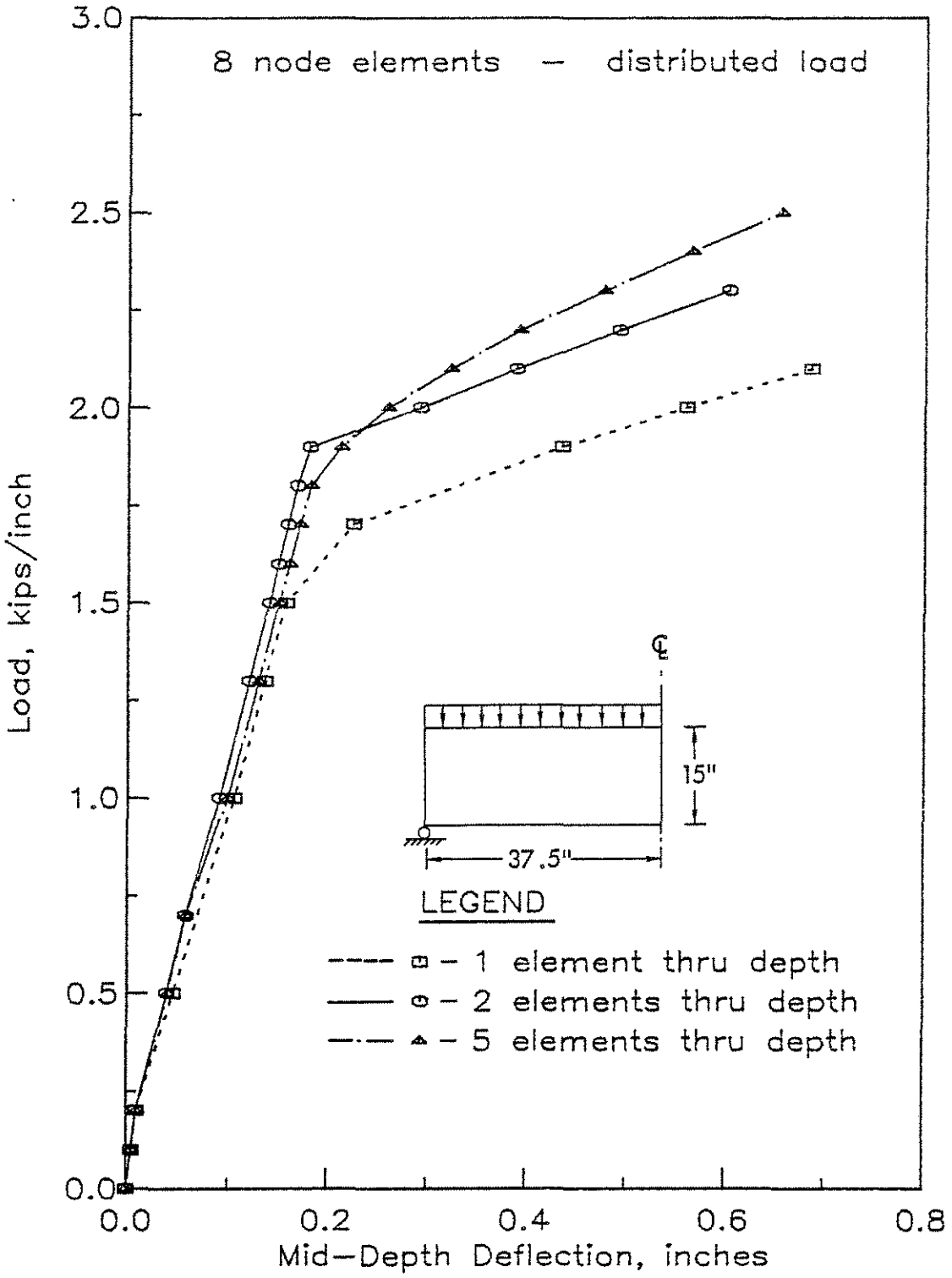

Fig. 3.14 - Load-Deflection Curves for Moderate Beam, Distributed Load, Quadratic Elements (Reduced Integration)

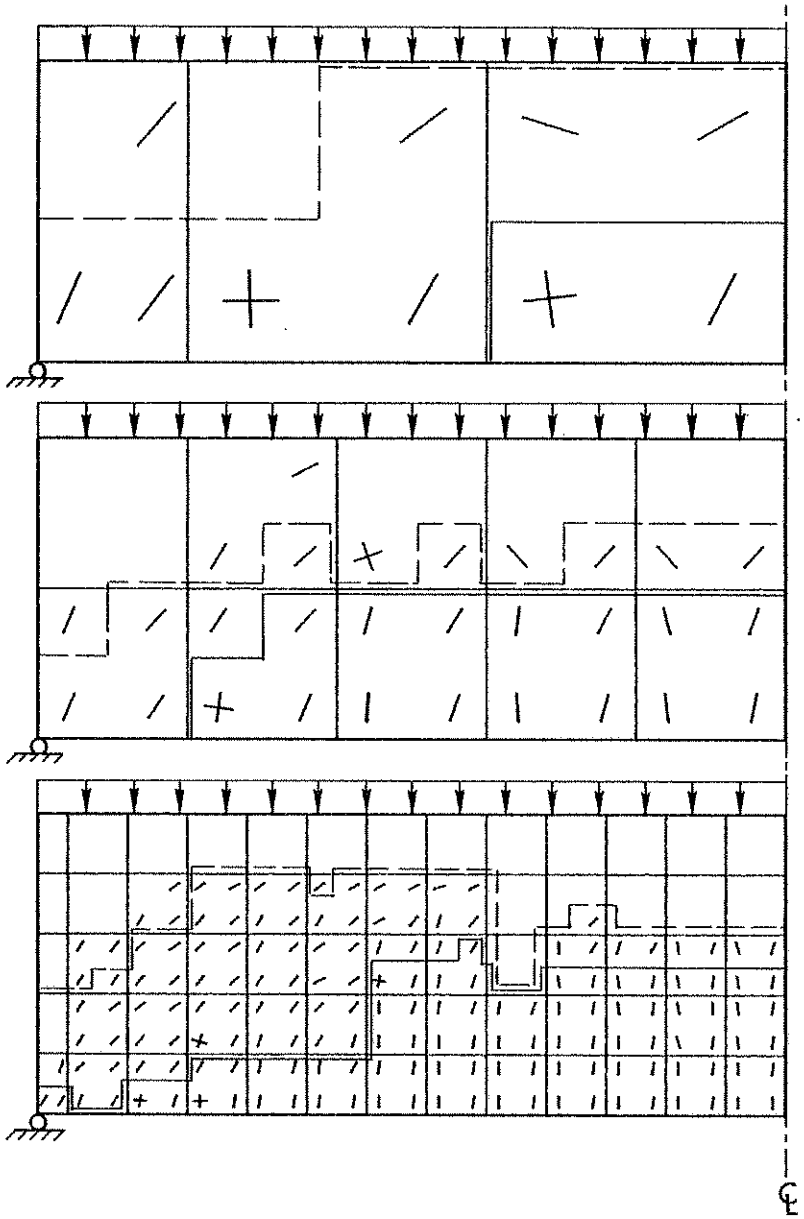

Note: Cracking Pattern for w = 1.7 k/in
Crack Contours:
—— w ≤ 0.5 k/in
— — w ≤ 1.0 k/in

Fig. 3.15 - Crack Patterns for Moderate Beam, Distributed Load, Linear Elements.

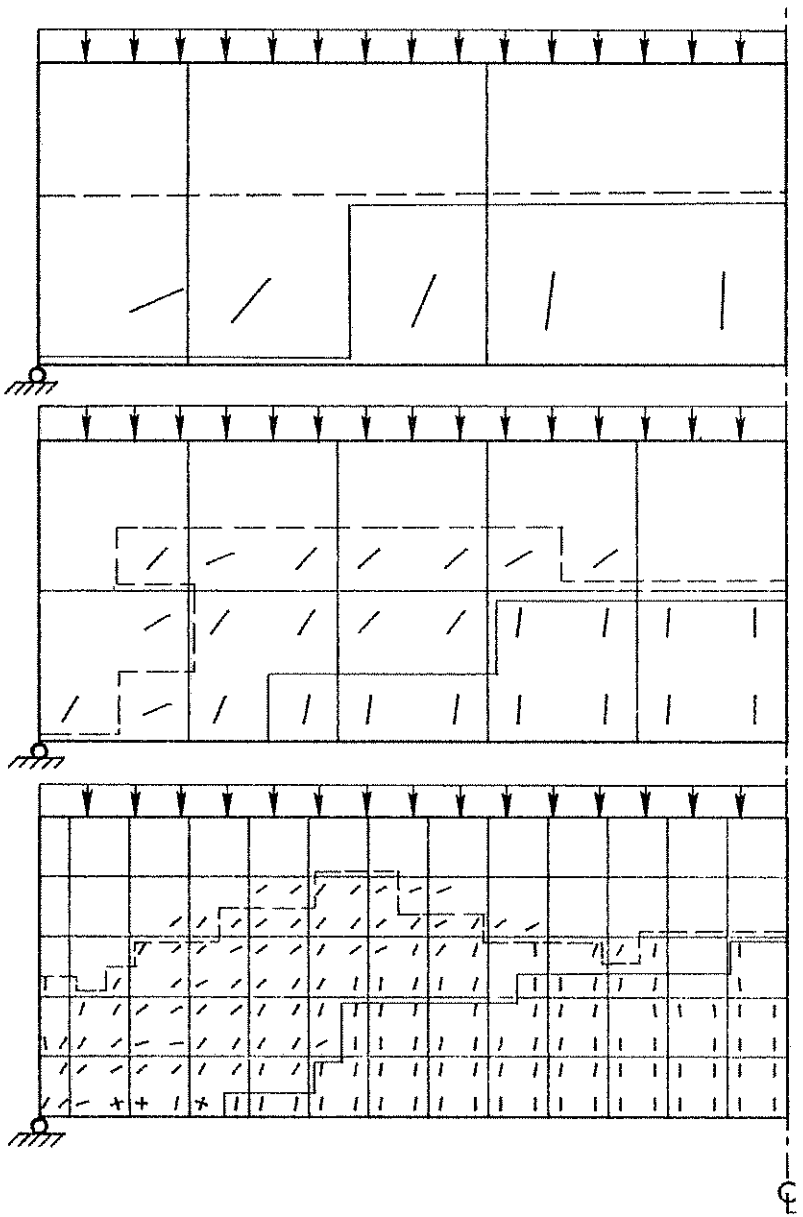

Note: Cracking Pattern for w = 1.7 k/in
Crack Contours:
—— w ≤ 0.5 k/in
—— w ≤ 1.0 k/in

Fig. 3.16 - Crack Patterns for Moderate Beam, Distributed Load, Quadratic Elements (Reduced Integration).

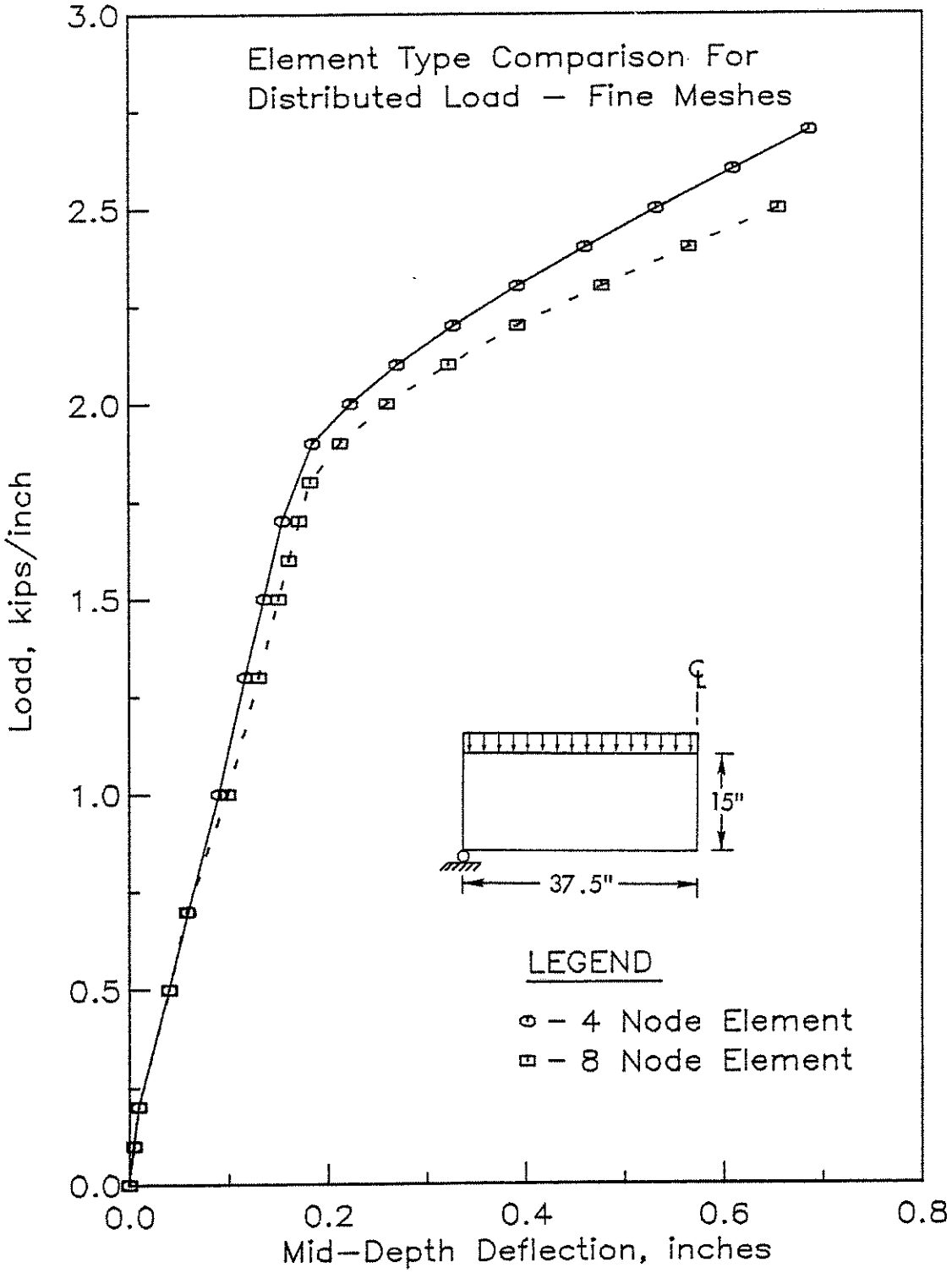

Fig. 3.17 - Comparison of Load-Deflection Curves for Moderate Beam, Distributed Load, Linear Elements and Quadratic Elements with Reduced Integration.

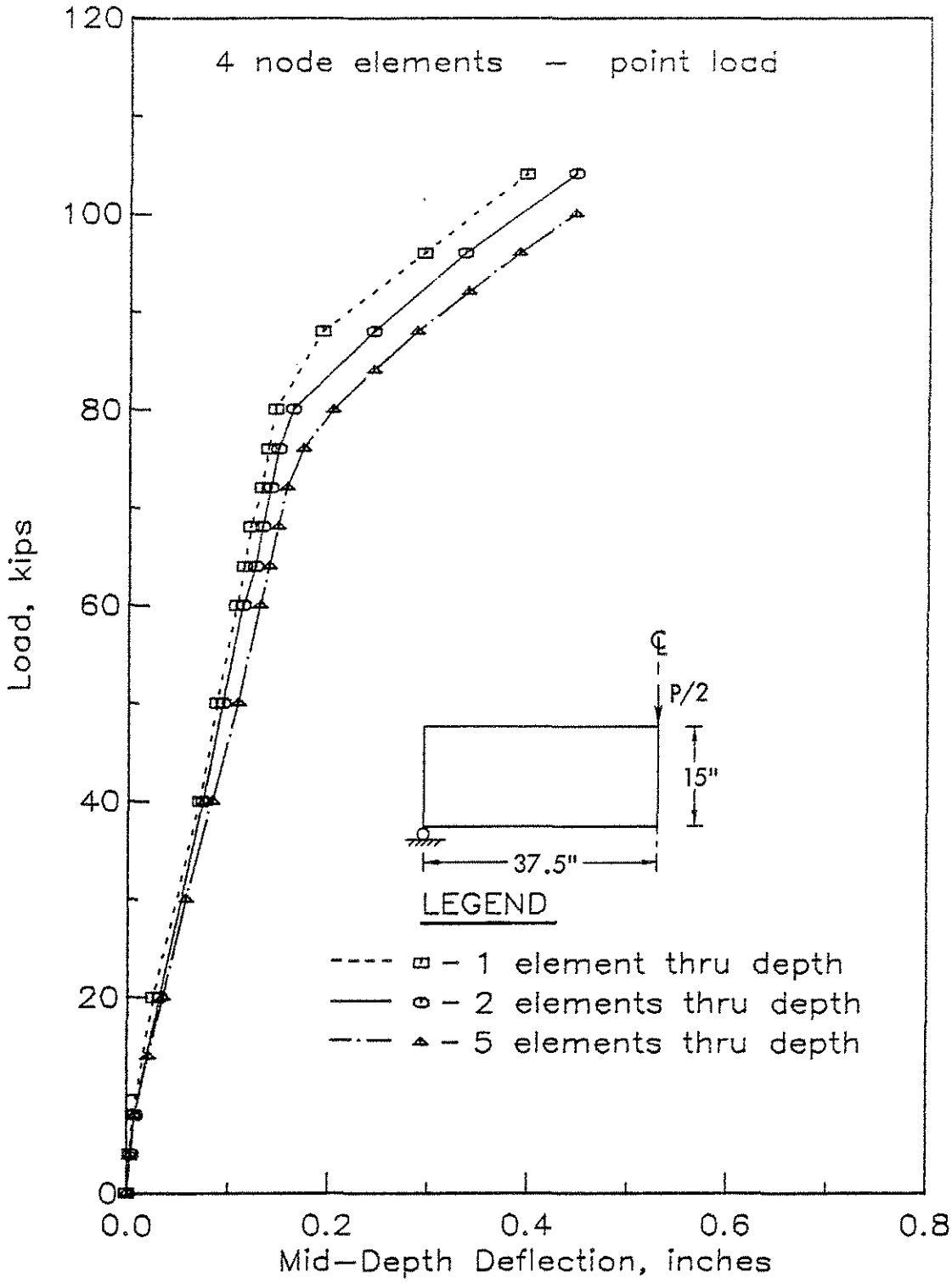

Fig. 3.18 - Load-Deflection Curves for Moderate Beam, Concentrated Load, Linear Elements.

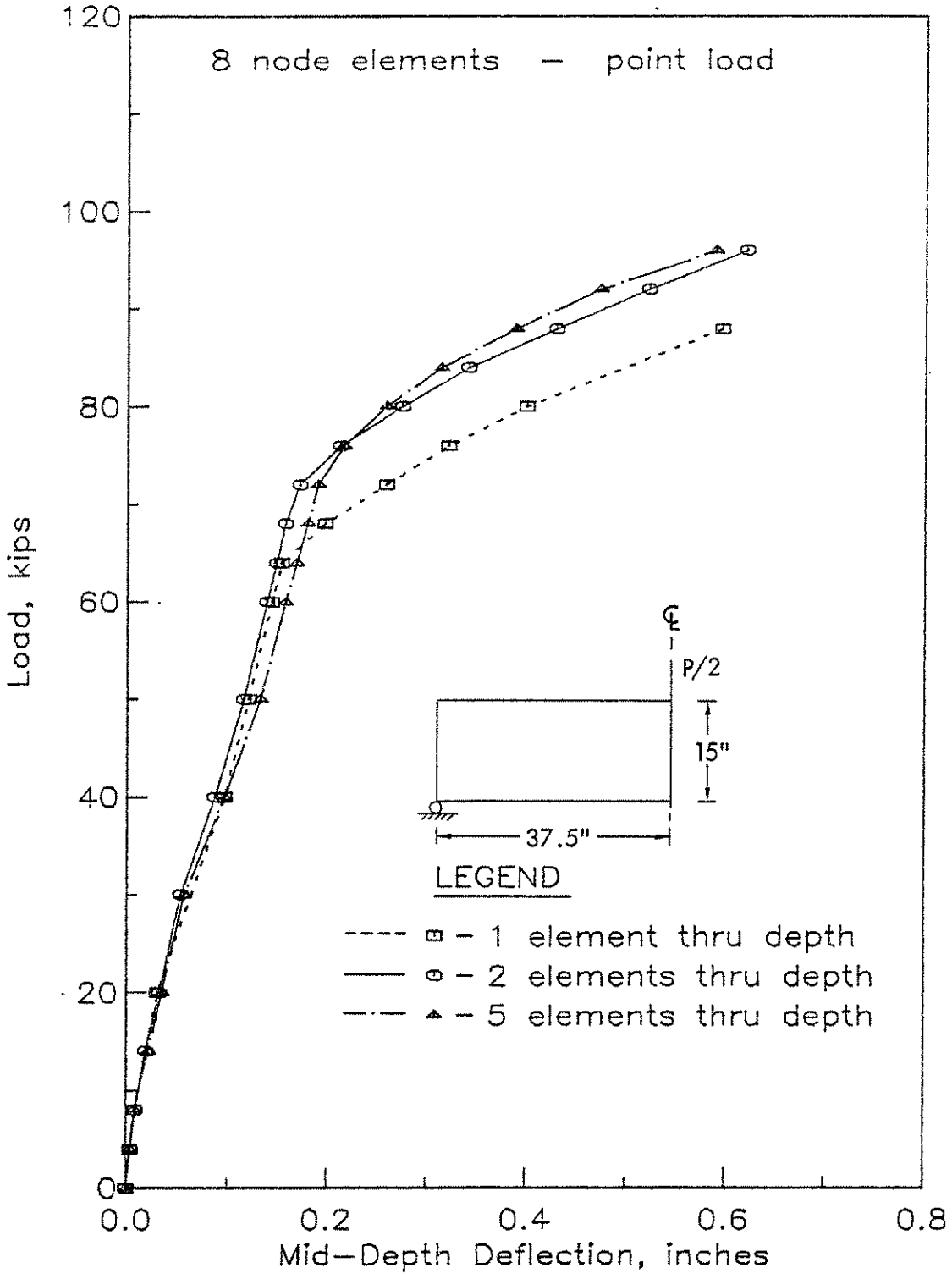

Fig. 3.19 - Load-Deflection Curves for Moderate Beam, Concentrated Load, Quadratic Elements (Reduced Integration).

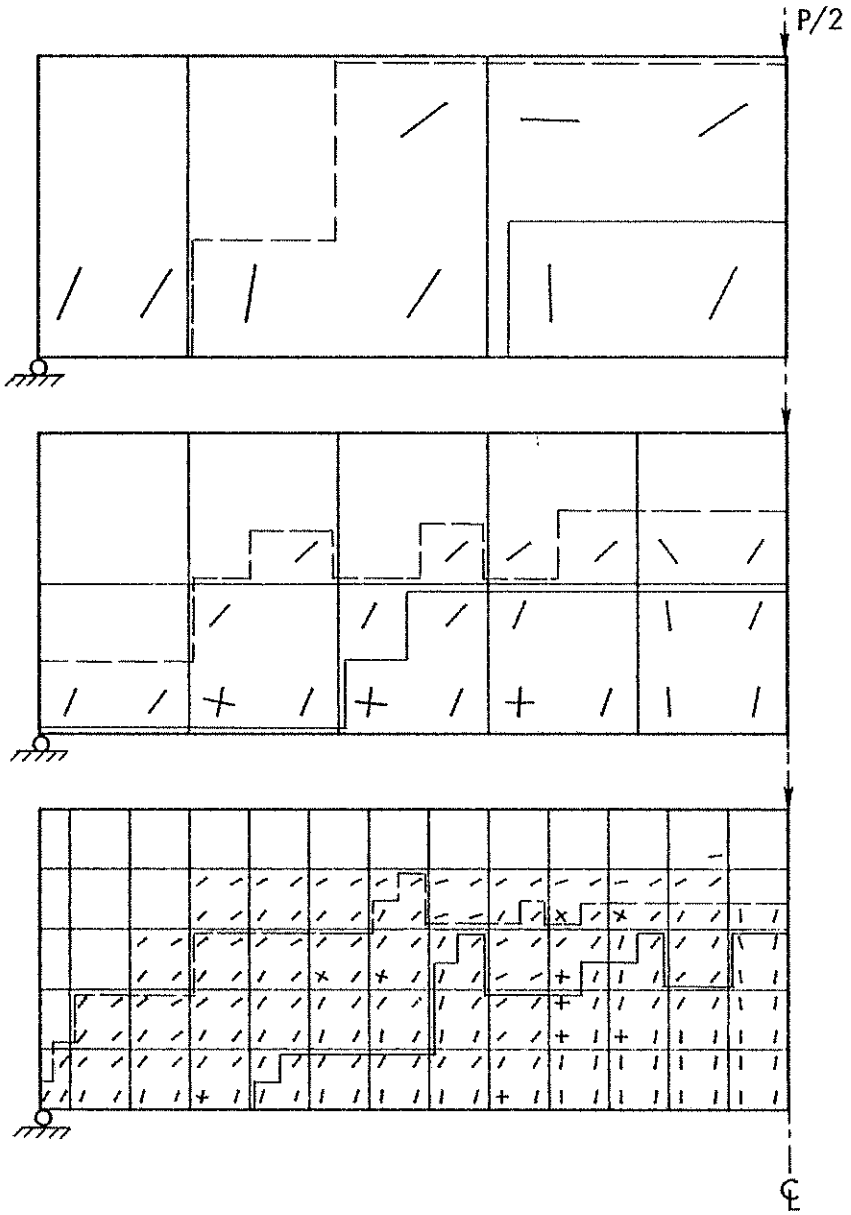

Note: Cracking Pattern for P = 60 k
Crack Contours:
——— P ≤ 20 k
— — P ≤ 40 k

Fig. 3.20 - Crack Patterns for Moderate Beam, Concentrated Load, Linear Elements.

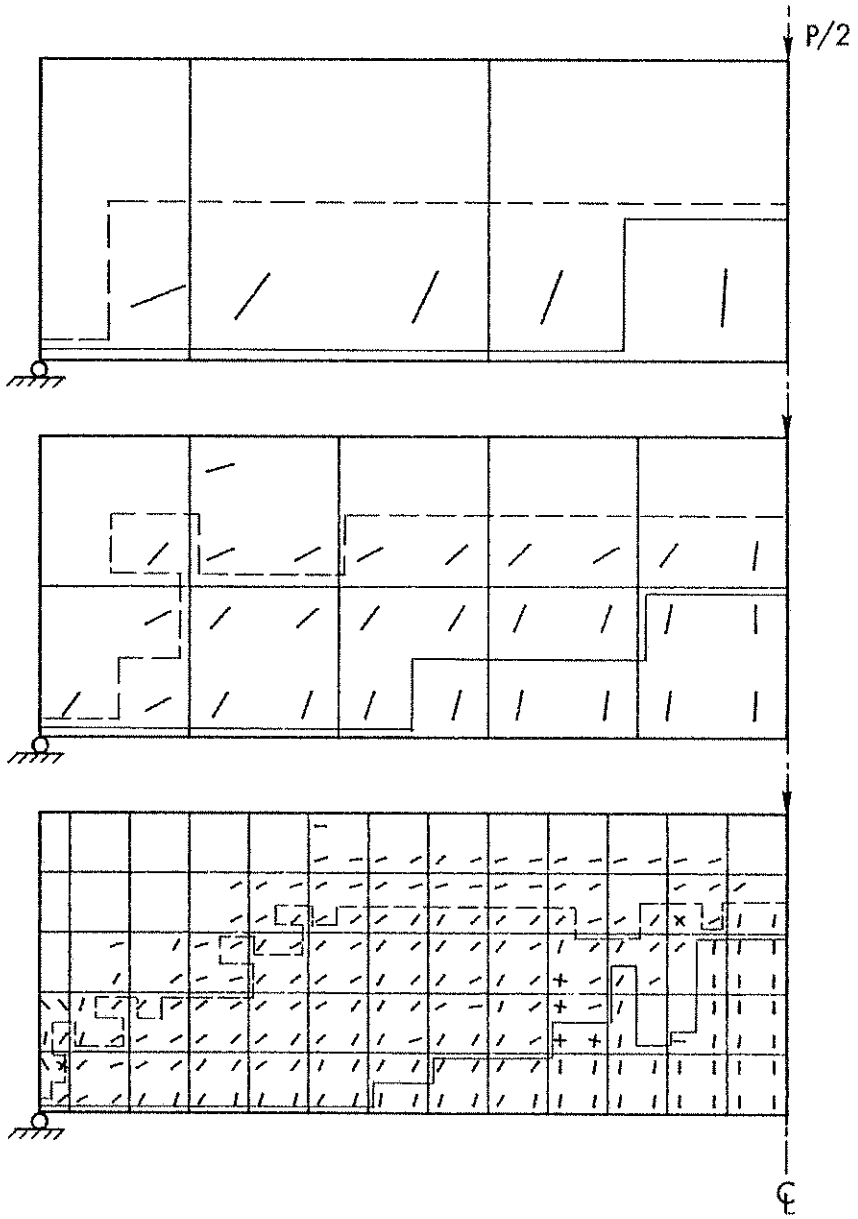

Note: Cracking Pattern for P = 60 k
Crack Contours:
—— P ≤ 20 k
—— P ≤ 40 k

Fig. 3.21 - Crack Patterns for Moderate Beam, Concentrated Load, Quadratic Elements (Reduced Integration).

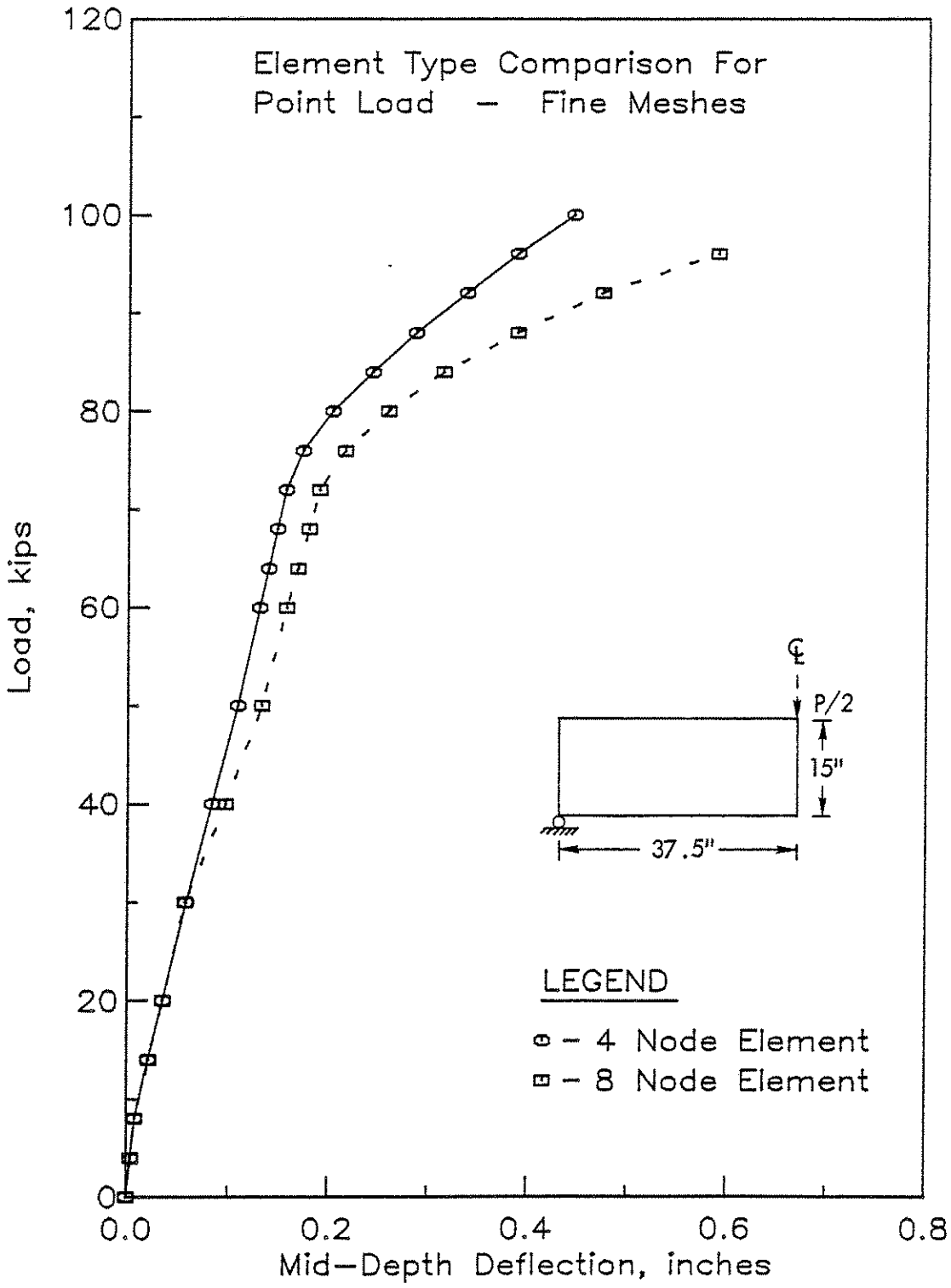

Fig. 3.22 - Comparison of Load-Deflection Curves for the Moderate Beam, Concentrated Load, Linear Elements and Quadratic Elements with Reduced Integration.

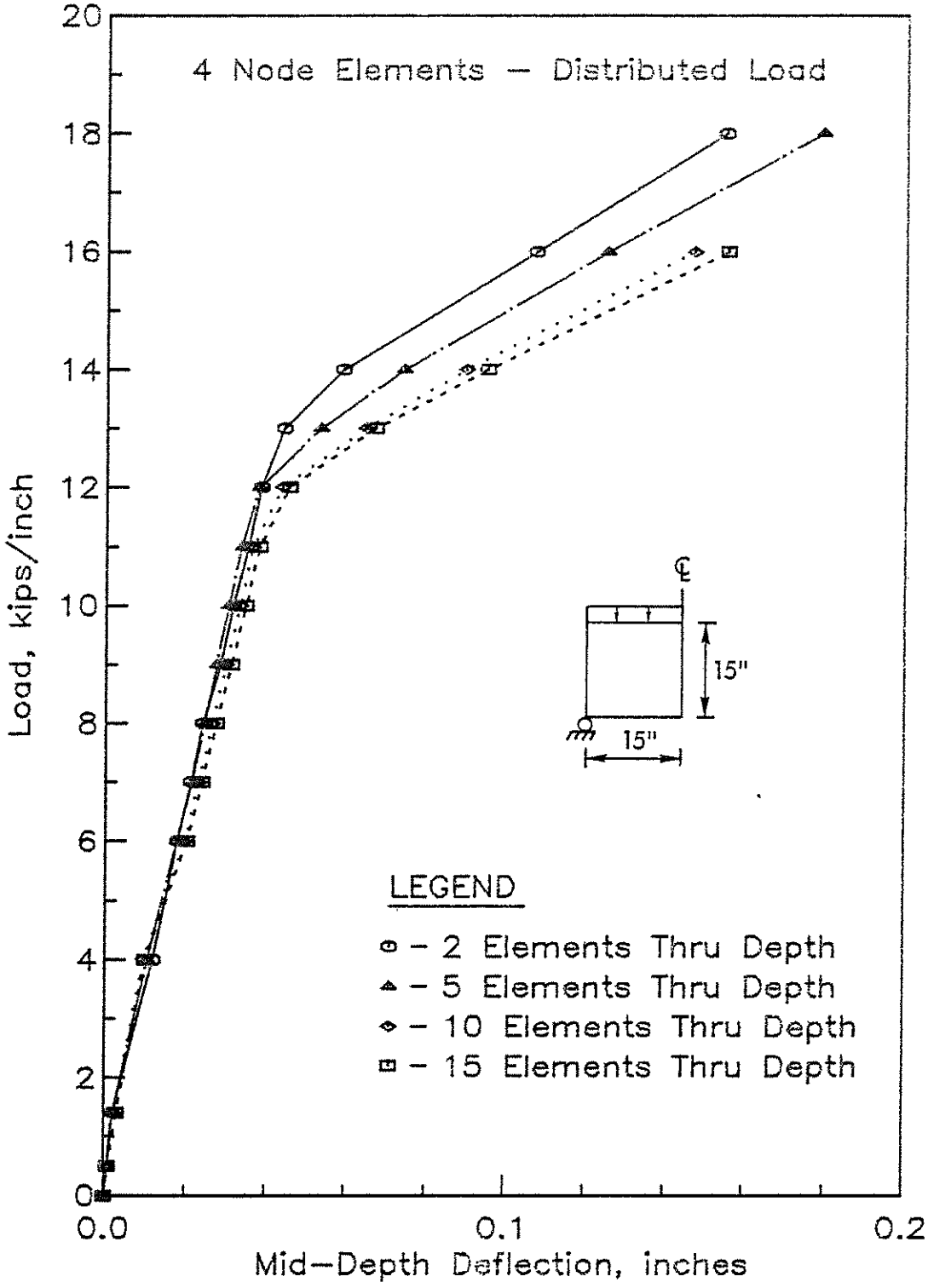

Fig. 3.23 – Load-Deflection Curves for Deep Beam, Distributed Load, Linear Elements

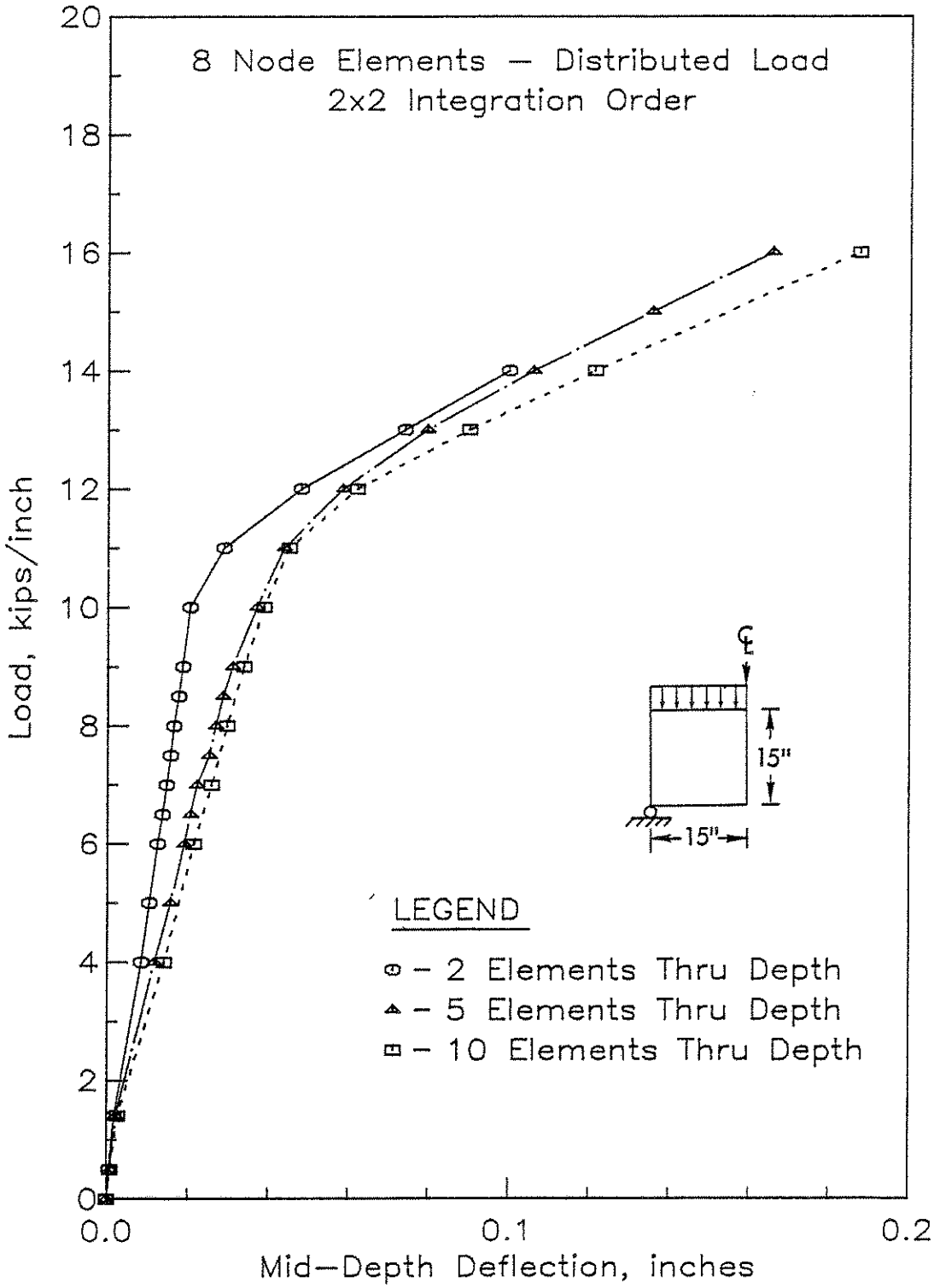

Fig. 3.24 - Load-Deflection Curves for the Deep Beam, Distributed Load, Quadratic Elements (Reduced Integration).

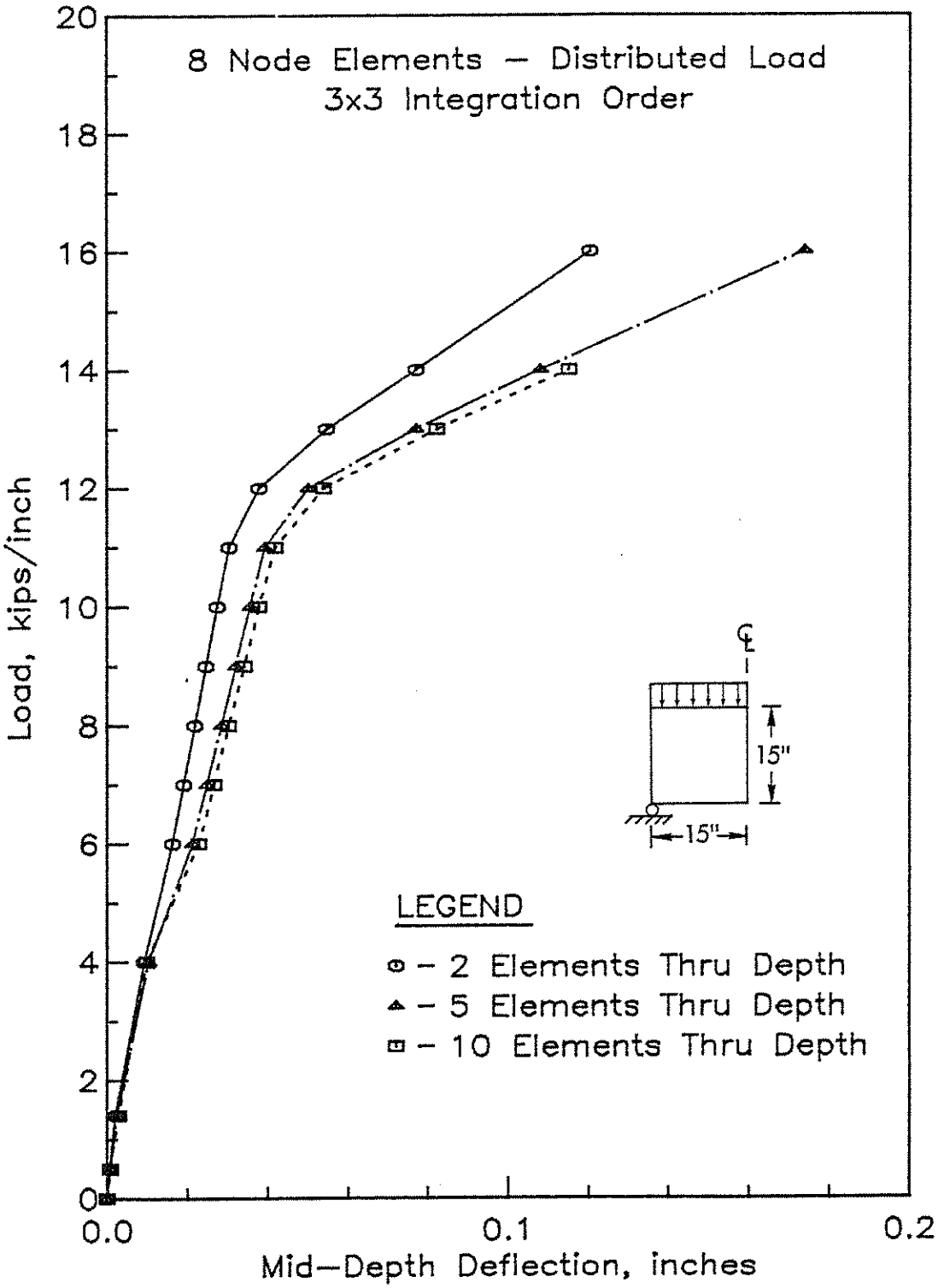

Fig. 3.25 - Load-Deflection Curves for the Deep Beam, Distributed Load, Quadratic Elements (Full Integration).

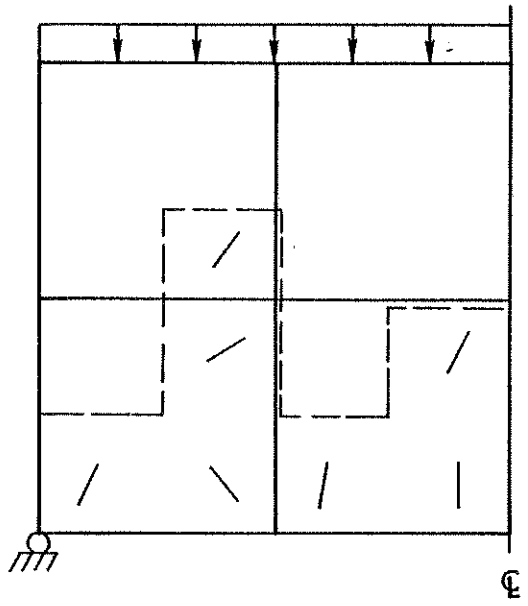

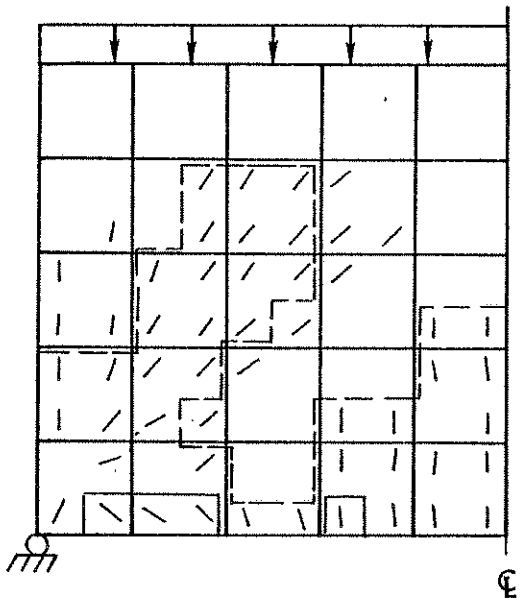

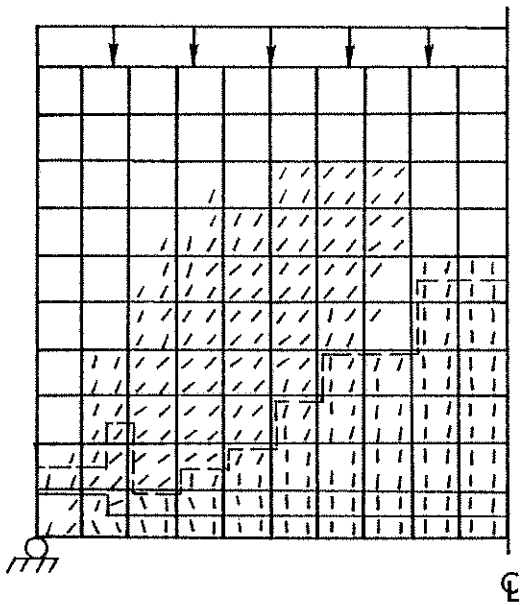

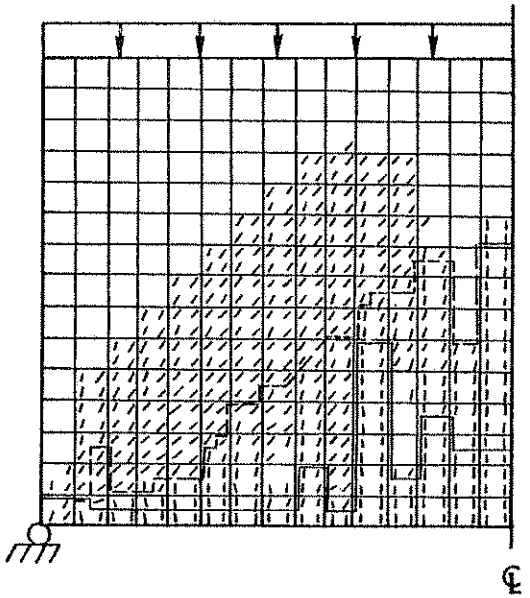

Note: Cracking Pattern for W = 8 k/in

Crack Contours:

——— W ≤ 1.4 k/in

— — — W ≤ 4.0 k/in

Fig. 3.26 - Crack Patterns for Deep Beam, Distributed Load, Linear Elements.

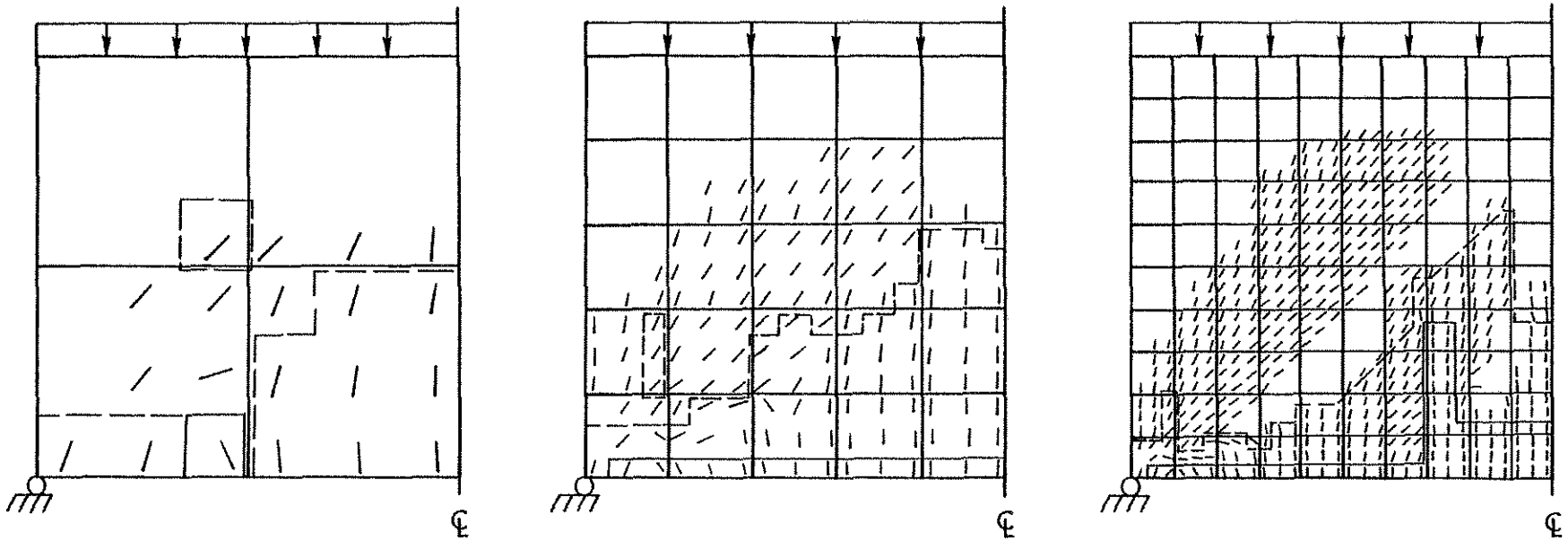

Note: Cracking Pattern for W = 8 k/in

Crack Contours:

——— W ≤ 1.4 k/in

— — — W ≤ 4.0 k/in

Fig. 3.27 - Crack Patterns for Deep Beam, Distributed Load, Quadratic Elements (Full Integration).

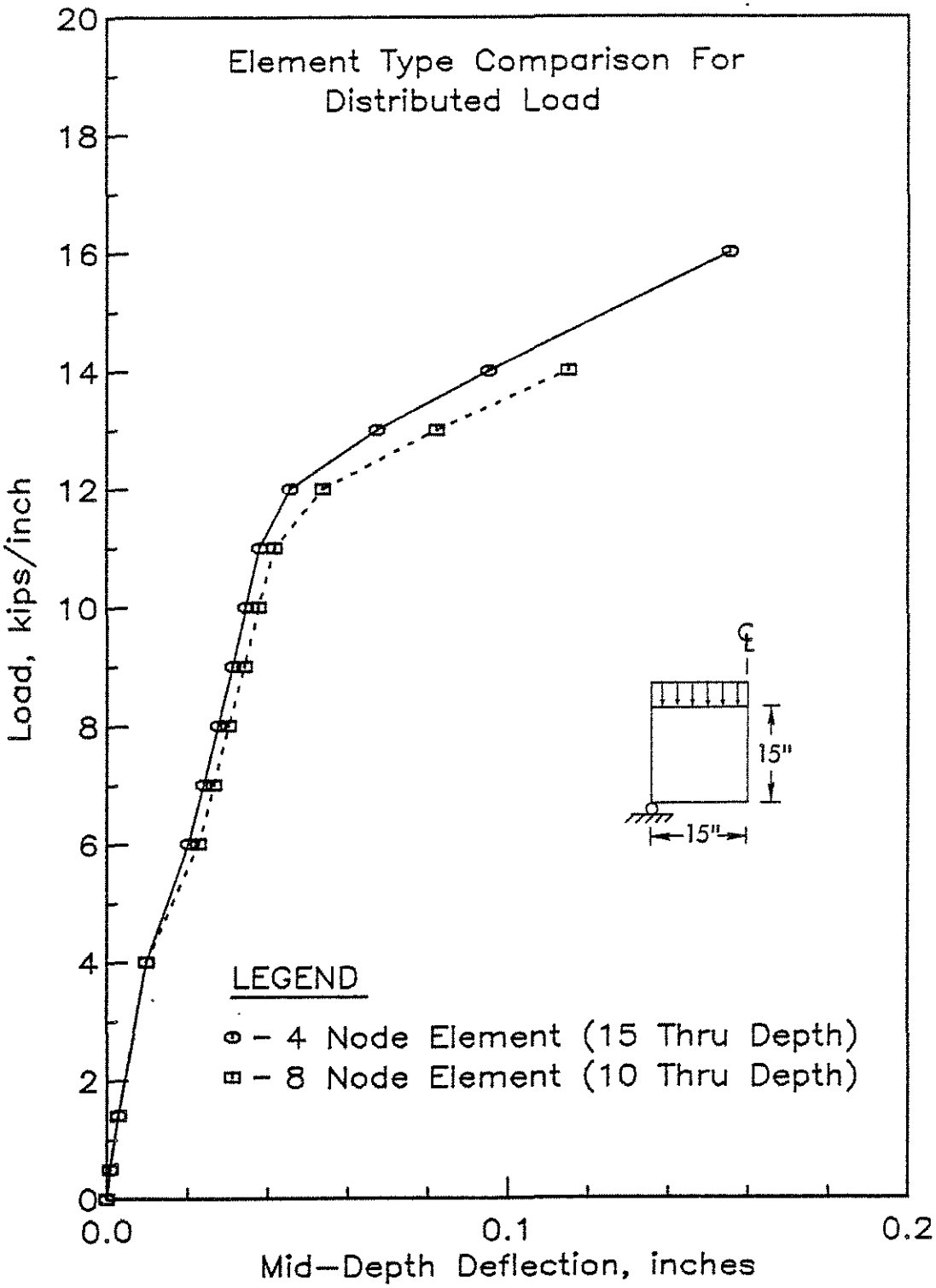

Fig. 3.28 - Comparison of Load-Deflection Curves for the Deep Beam, Distributed Load, Linear Elements and Quadratic Elements With Full Integration .

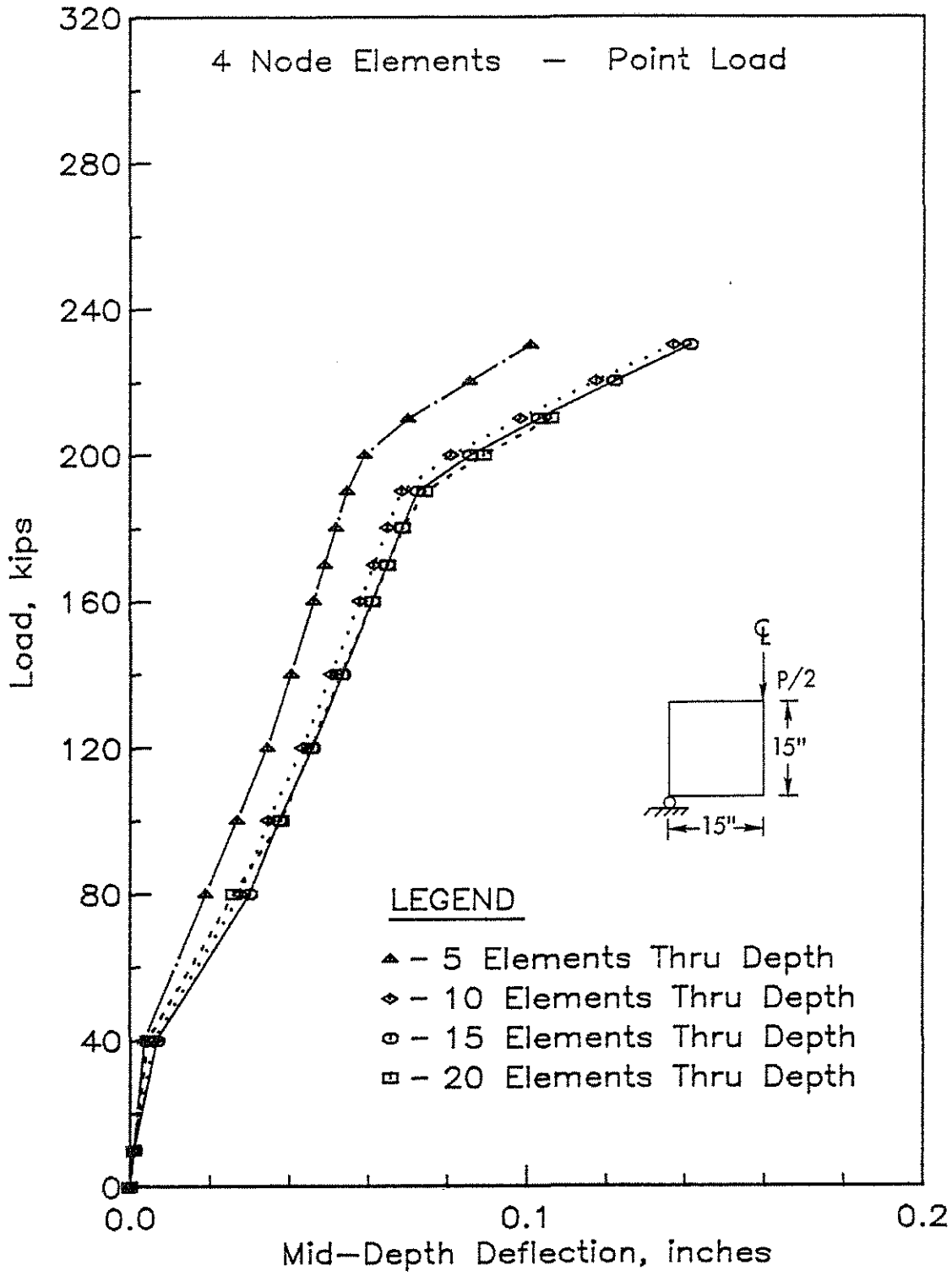

Fig. 3.29 - Load-Deflection Curves for the Deep Beam, Concentrated Load, Linear Elements.

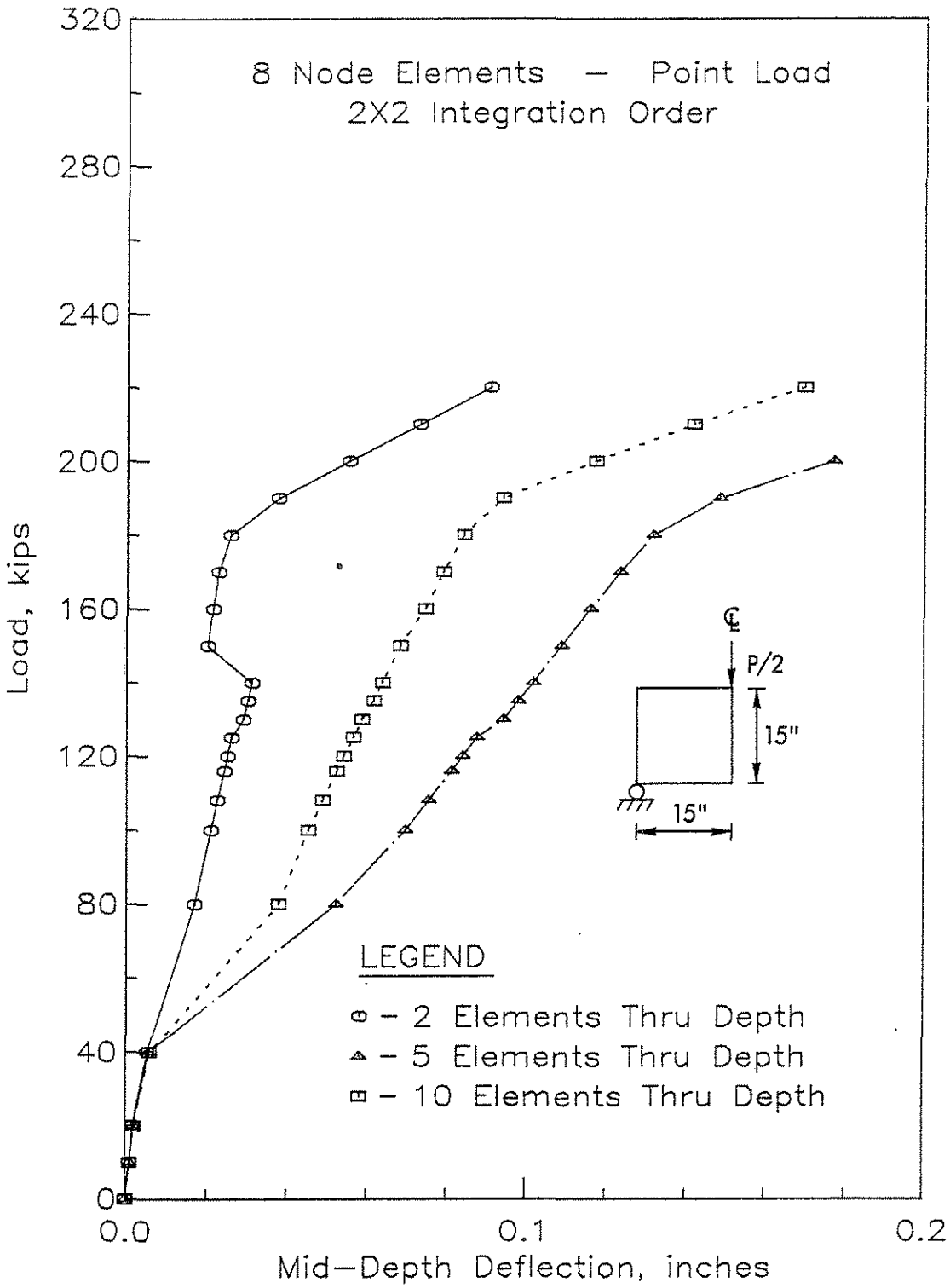

Fig. 3.30 - Load-Deflection Curves for the Deep Beam, Concentrated Load, Quadratic Elements (Reduced Integration).

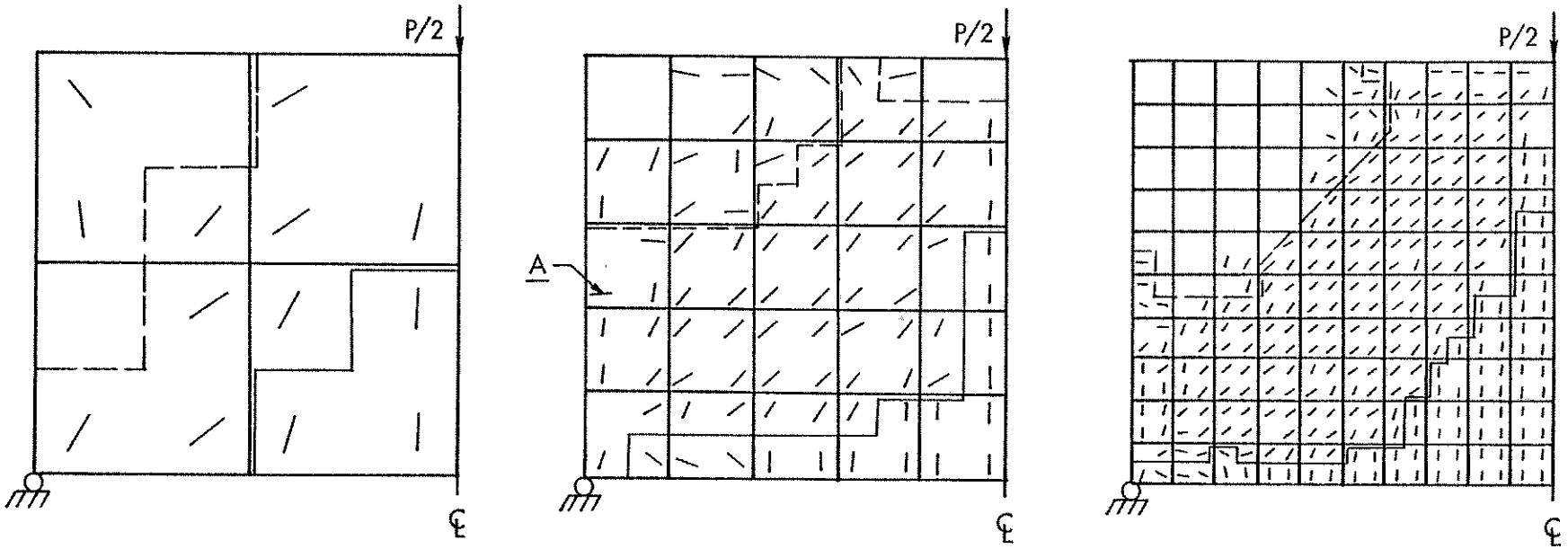

Fig. 3.31 - Crack Patterns for Deep Beam, Concentrated Load, Quadratic Elements (Reduced Integration).

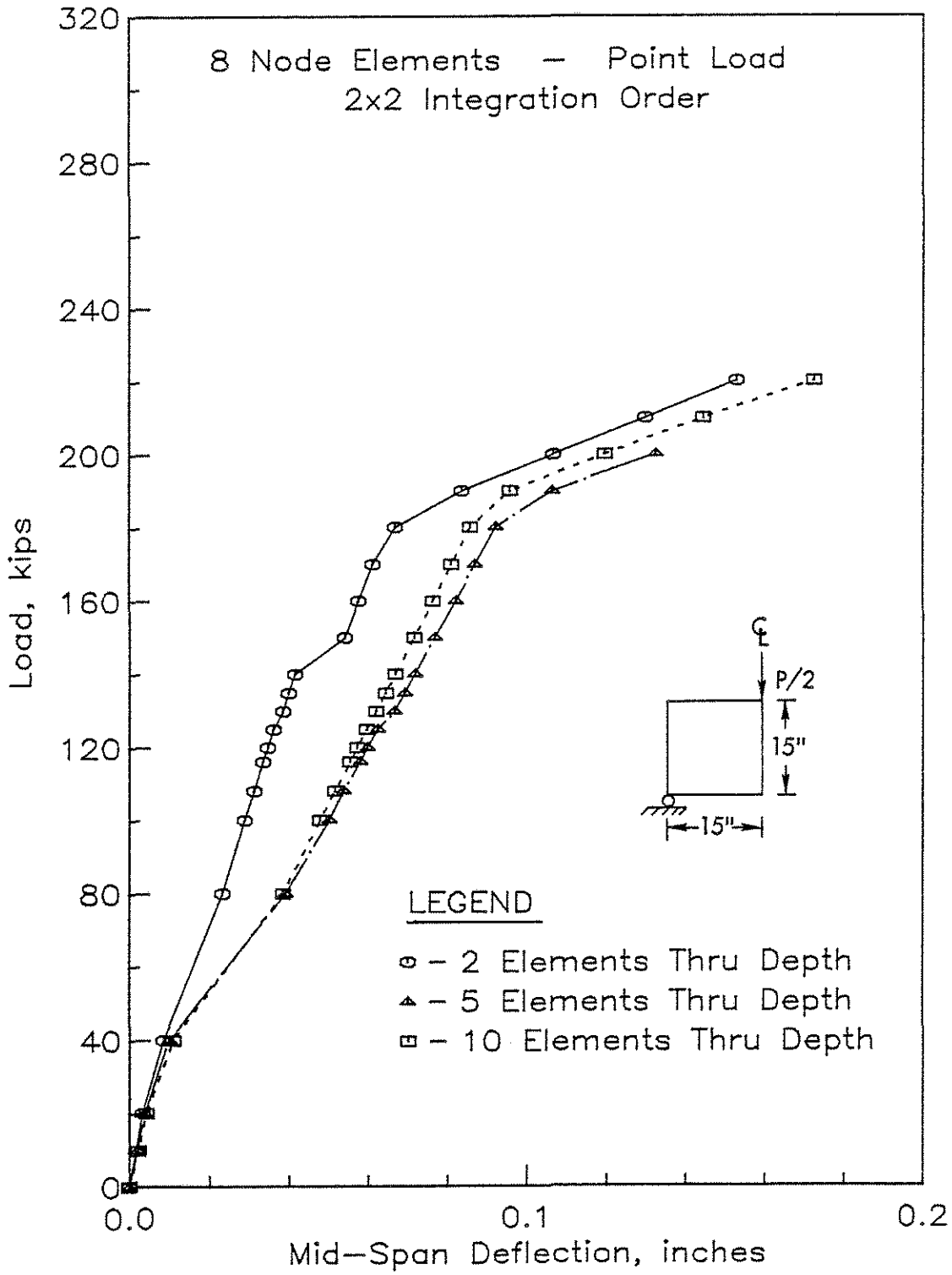

Fig. 3.32 - Load-Deflection Curves for the Deep Beam, Concentrated Load, Quadratic Elements with Reduced Integration, Mid-Span Only Deflection.

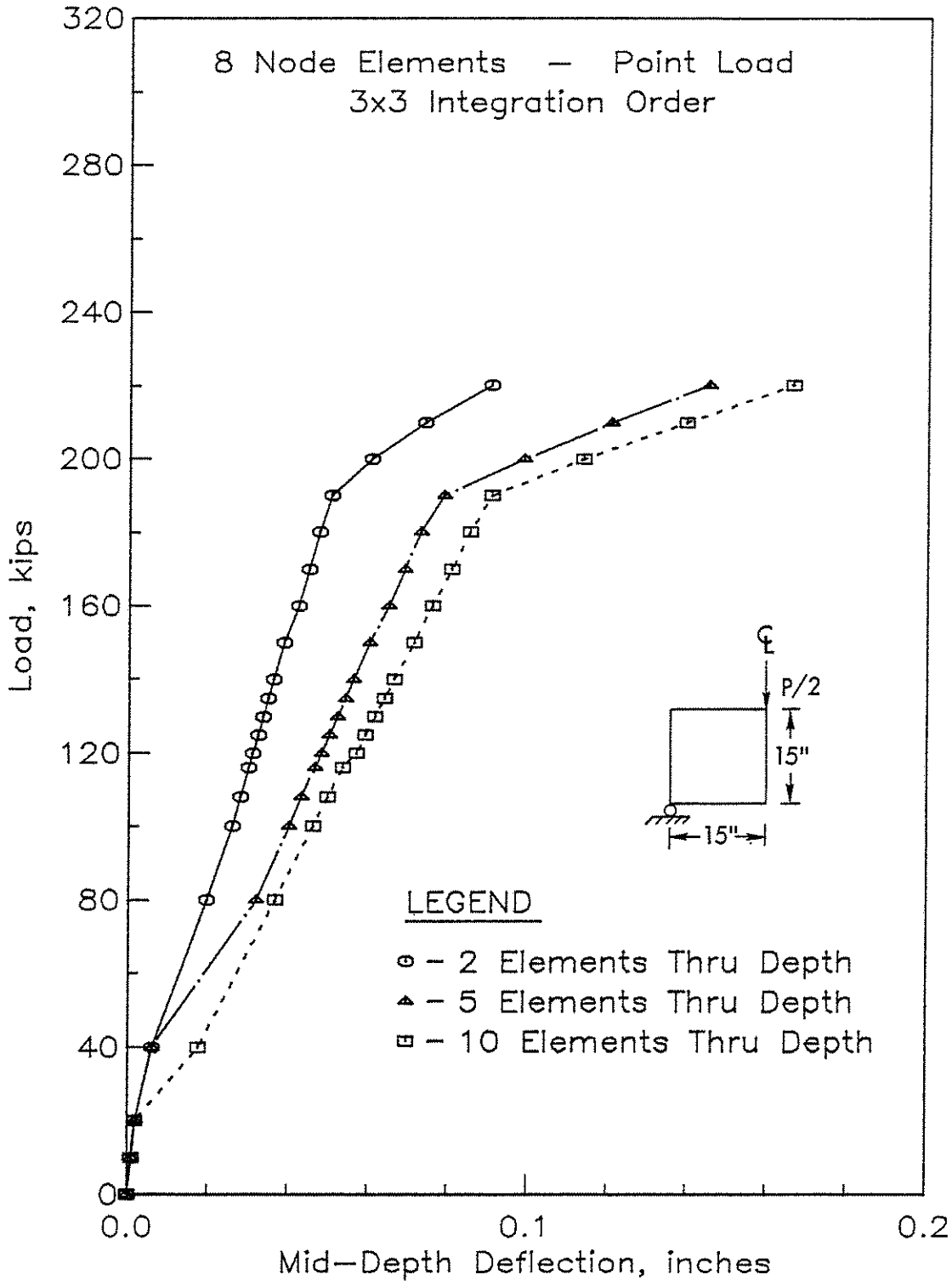

Fig. 3.33 - Load-Deflection Curves for the Deep Beam, Concentrated Load, Quadratic Elements, (Full Integration).

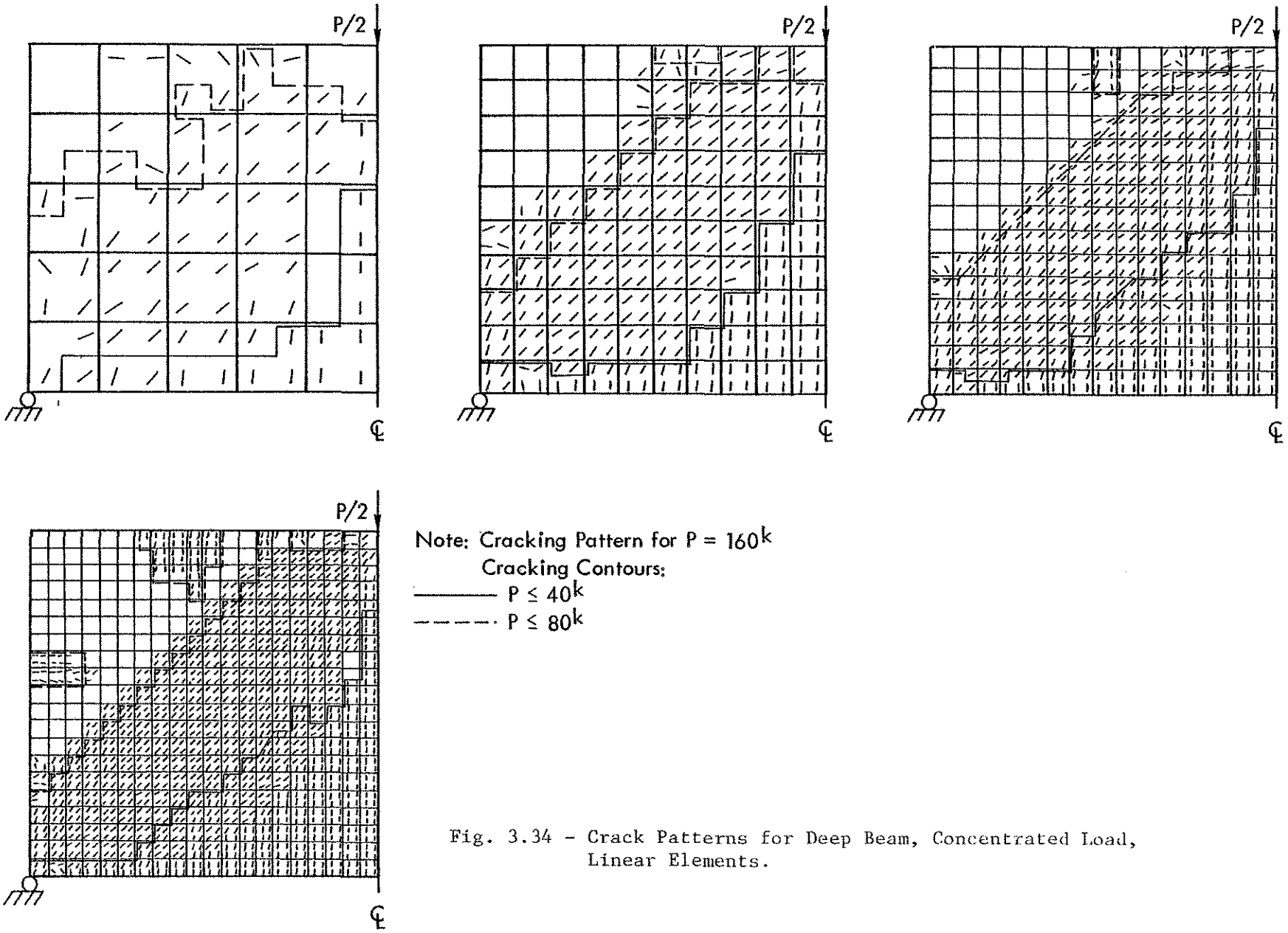

Note: Cracking Pattern for P = 160^k

Cracking Contours:

——— P ≤ 40^k

– – – – P ≤ 80^k

Fig. 3.34 - Crack Patterns for Deep Beam, Concentrated Load, Linear Elements.

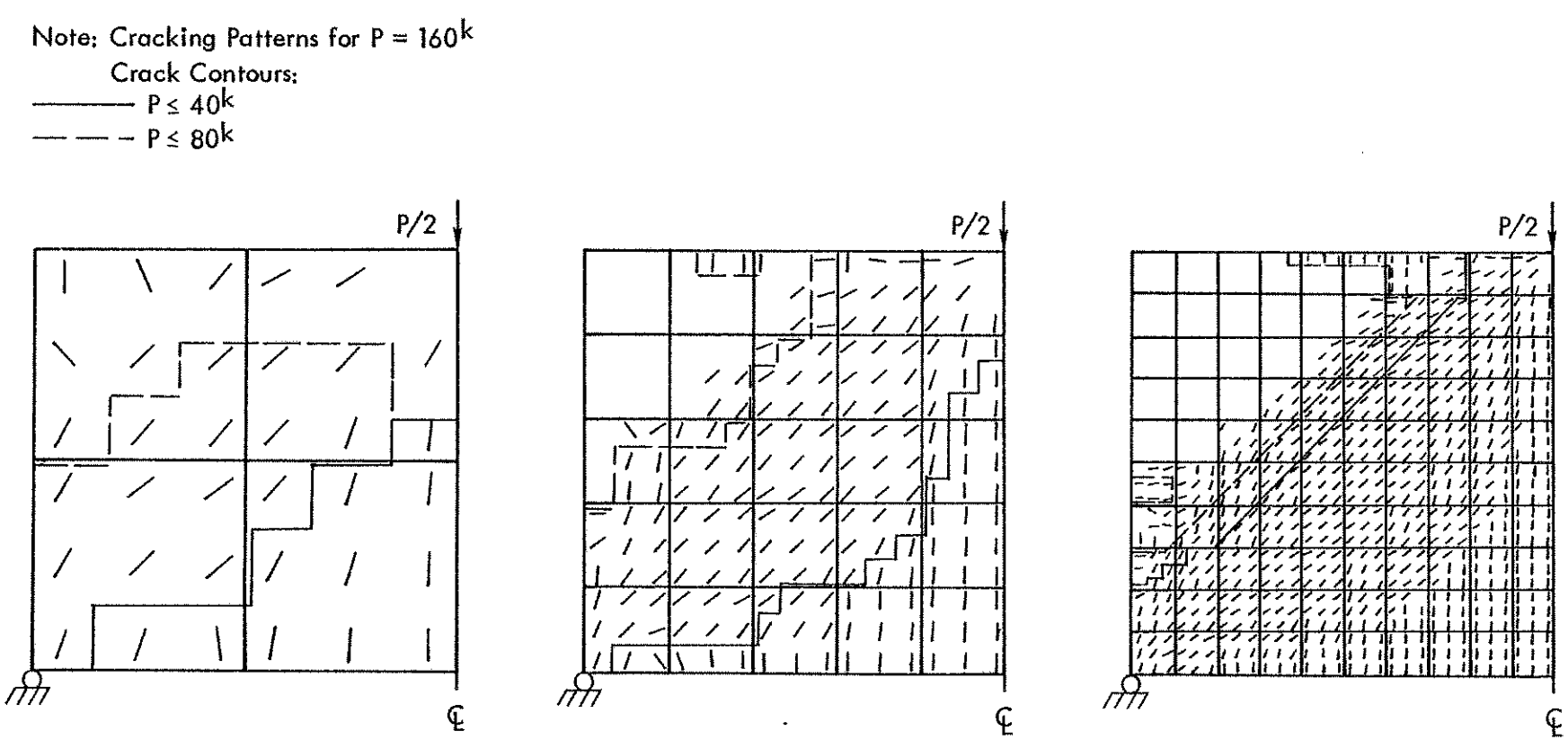

Fig. 3.35 - Crack Patterns for Deep Beam, Concentrated Load, Quadratic Elements (Full Integration).

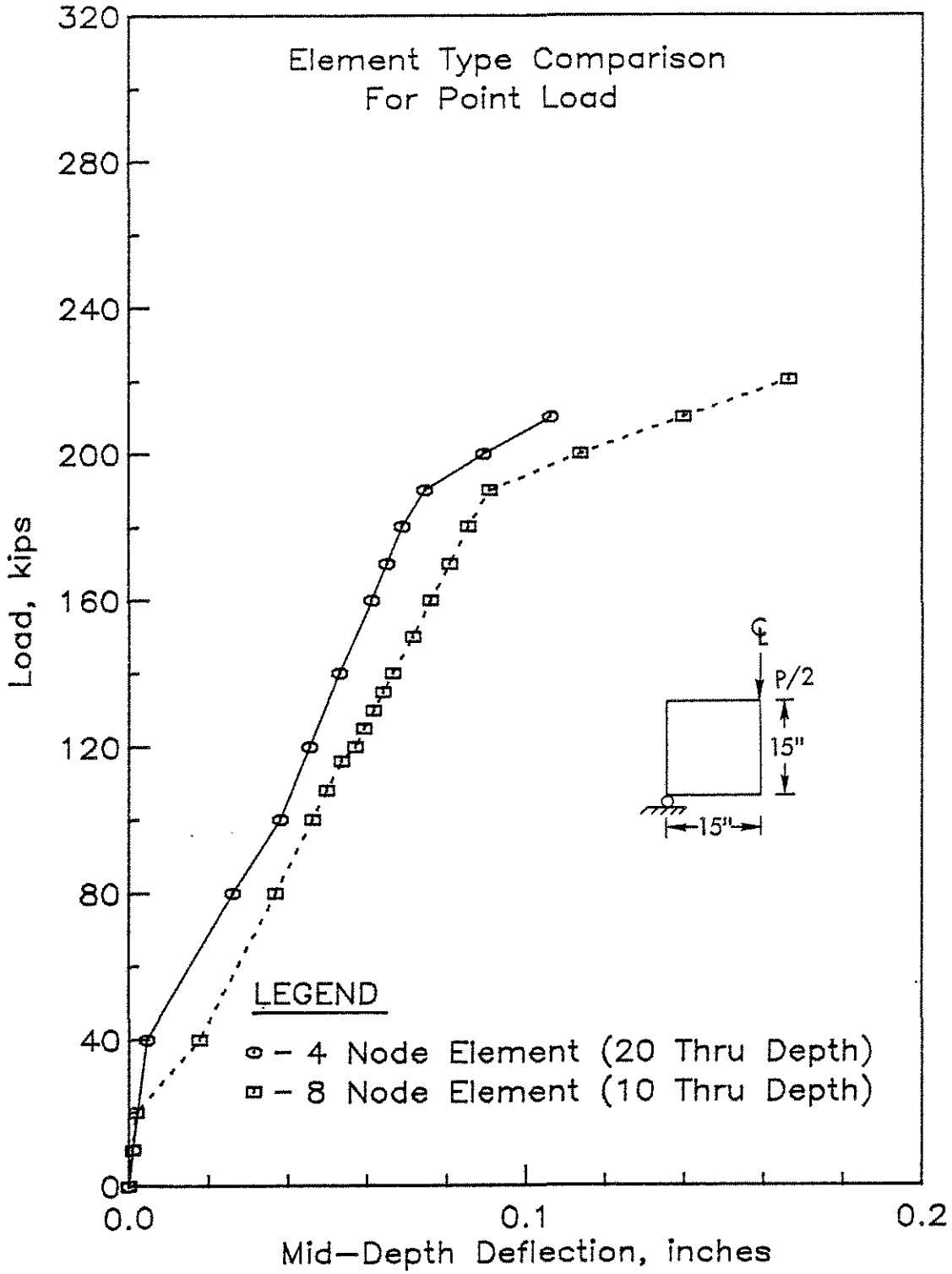

Fig. 3.36 - Comparison of Load-Deflection Curves for Deep Beam, Concentrated Load, Linear Elements and Quadratic Elements with Full Integration.

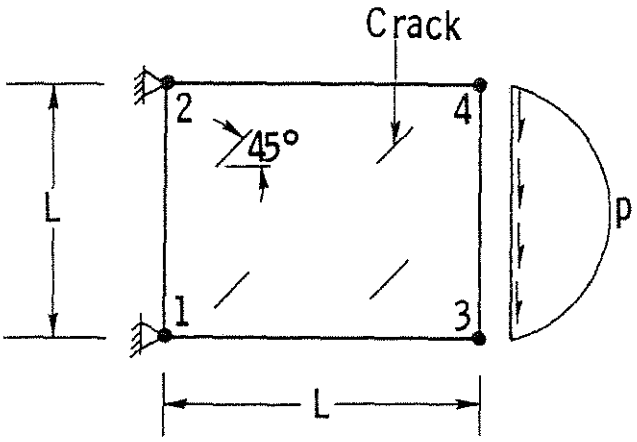

(a) Linear, Four Node Element (2x2 Integration)

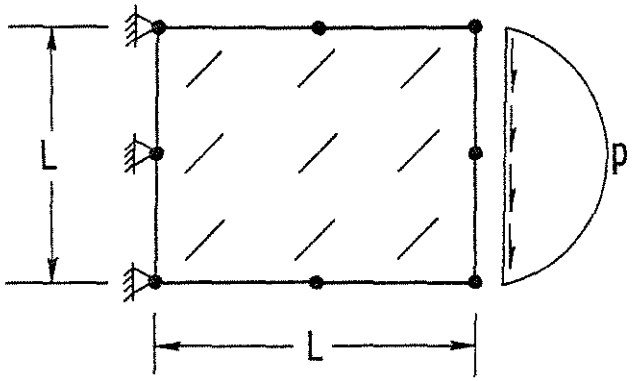

(b) Quadratic Element (3x3 Integration)

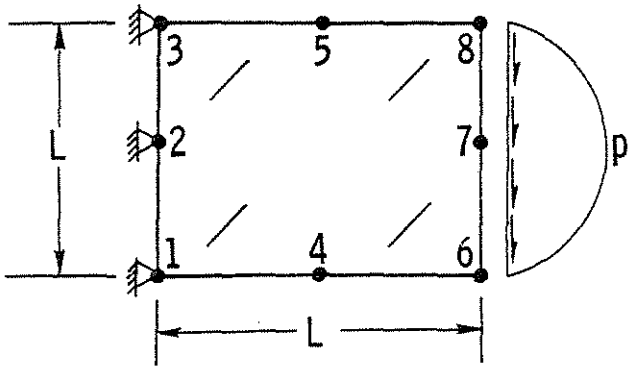

(c) Quadratic Element (2x2 Integration)

Fig. 3.37 - Test Problem for Determination of Cracked Element Stiffness Characteristics.

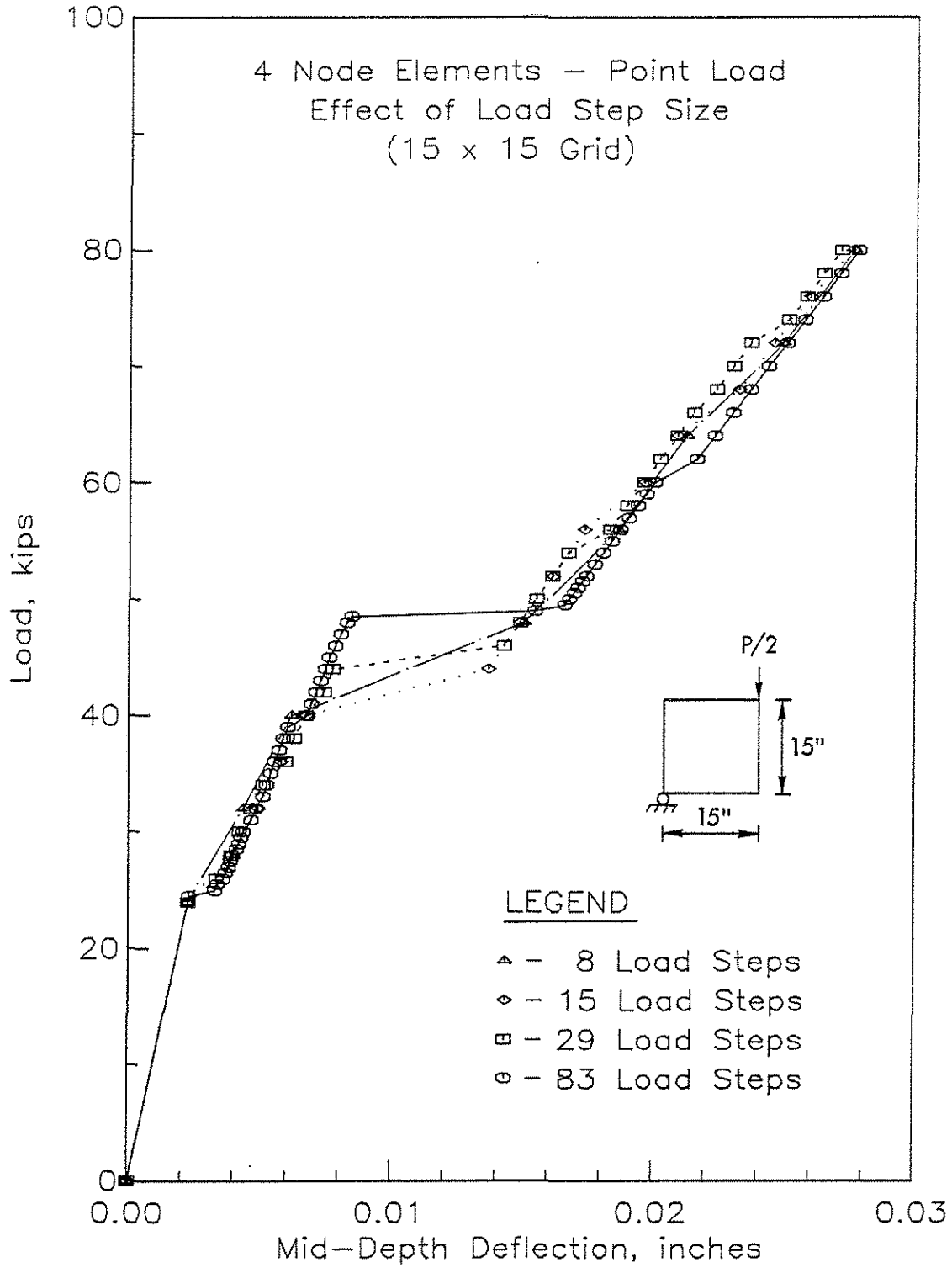

Fig. 3.38 - Effect of Load Increment Size on Load-Deflection Curves.

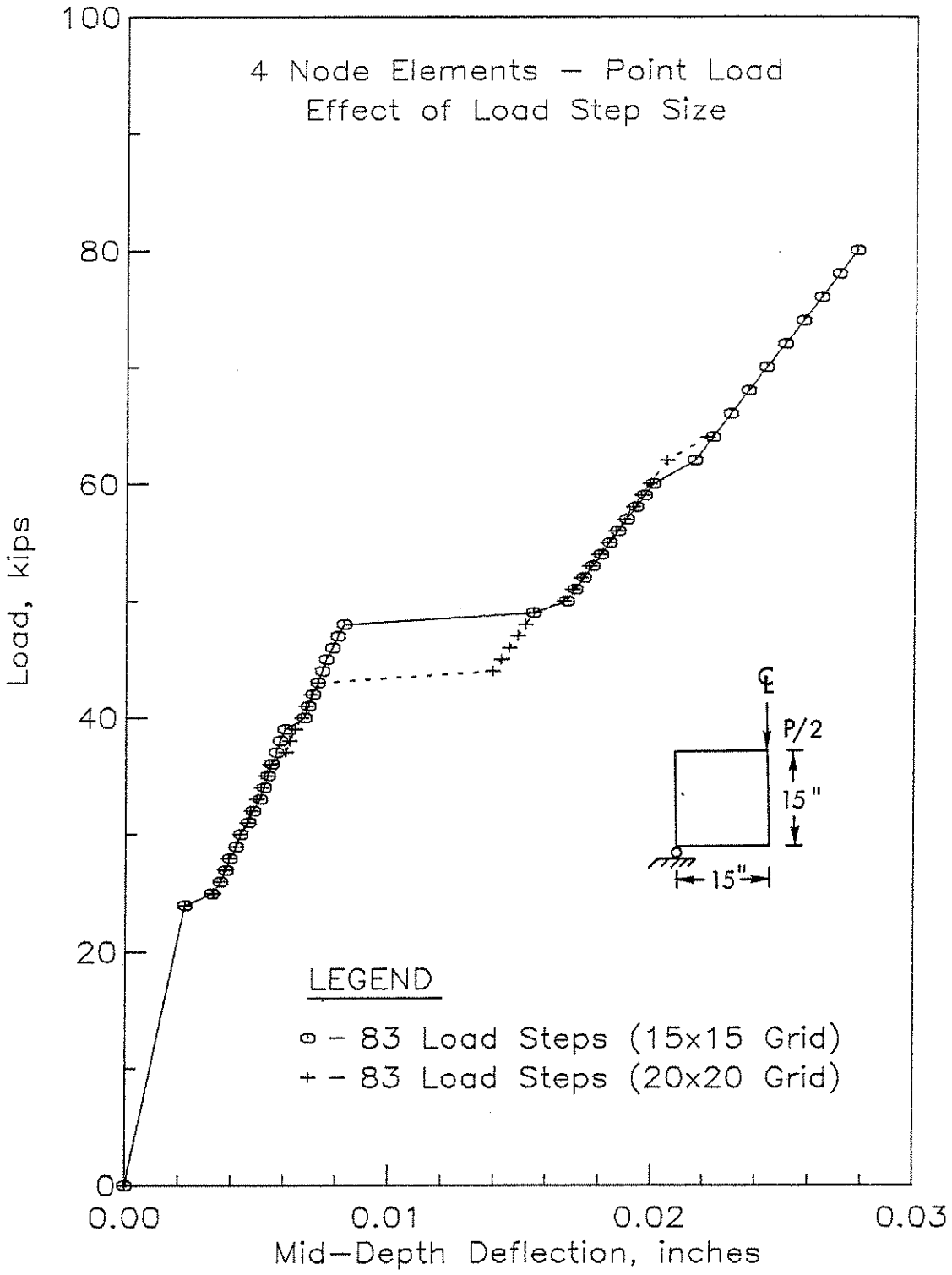

Fig. 3.39 - Effect of Load Increment Size and Grid Refinement on Load-Deflection Curves.

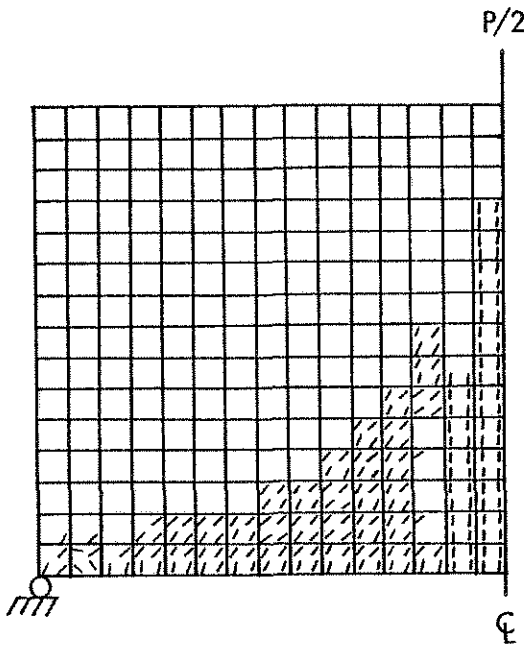

(a) Cracking Pattern for P = 48.5^{k}.
Load Increment No. 50

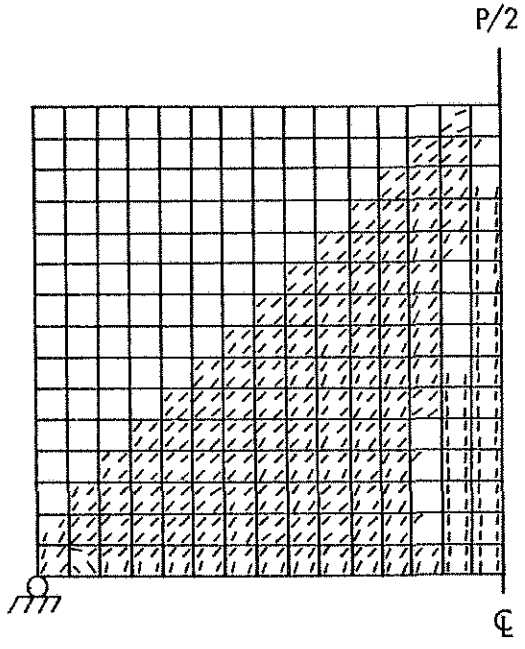

(b) Cracking Pattern for P = 49^{k},
Load Increment No. 51

Fig. 3.40 - Cracking Patterns for Load Increment Size Effects (Linear Element, 15x15 Grid).

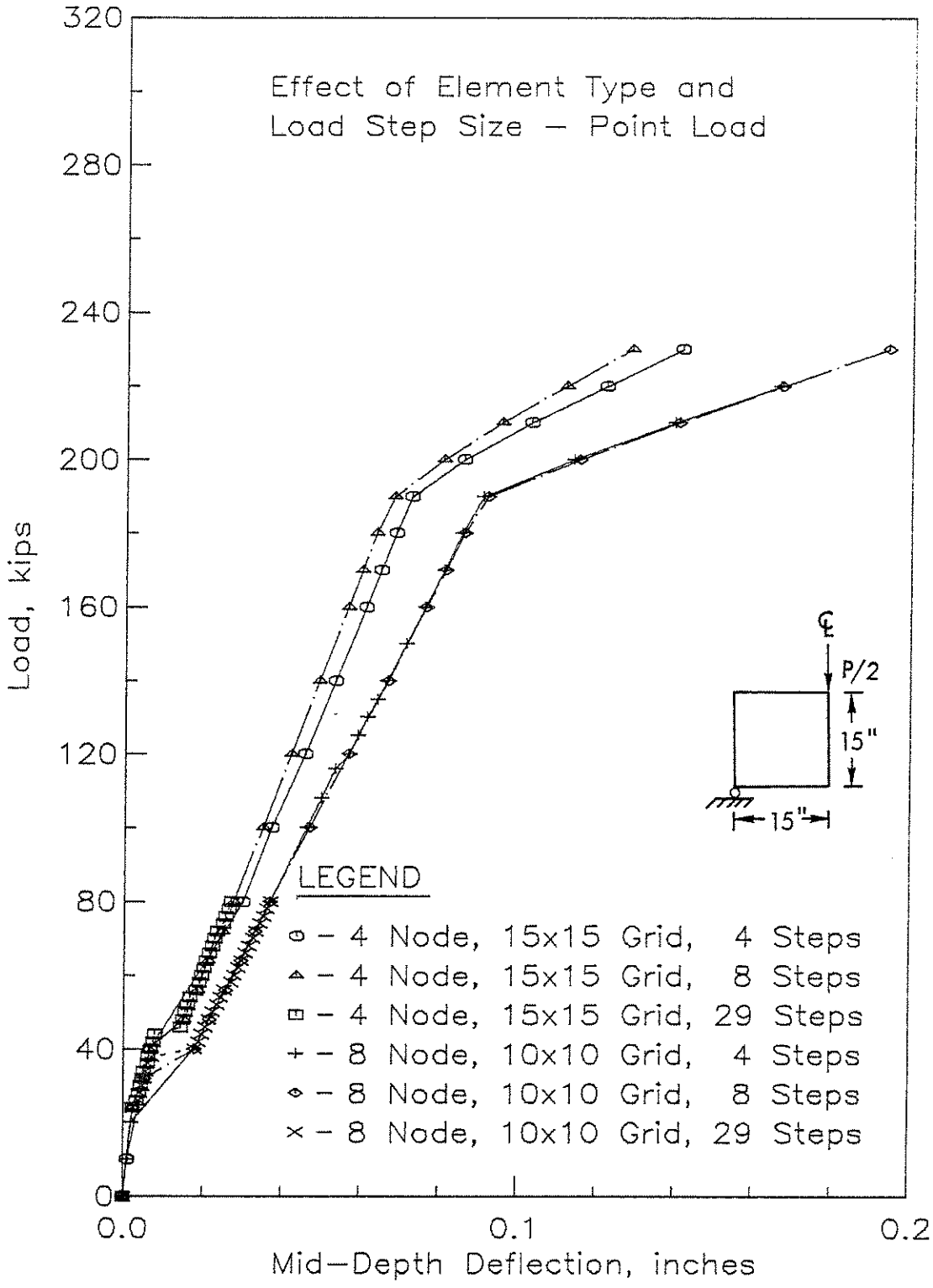

Fig. 3.41a - Effect of Load Increment Size and Element Type on Load-Deflection Curves.

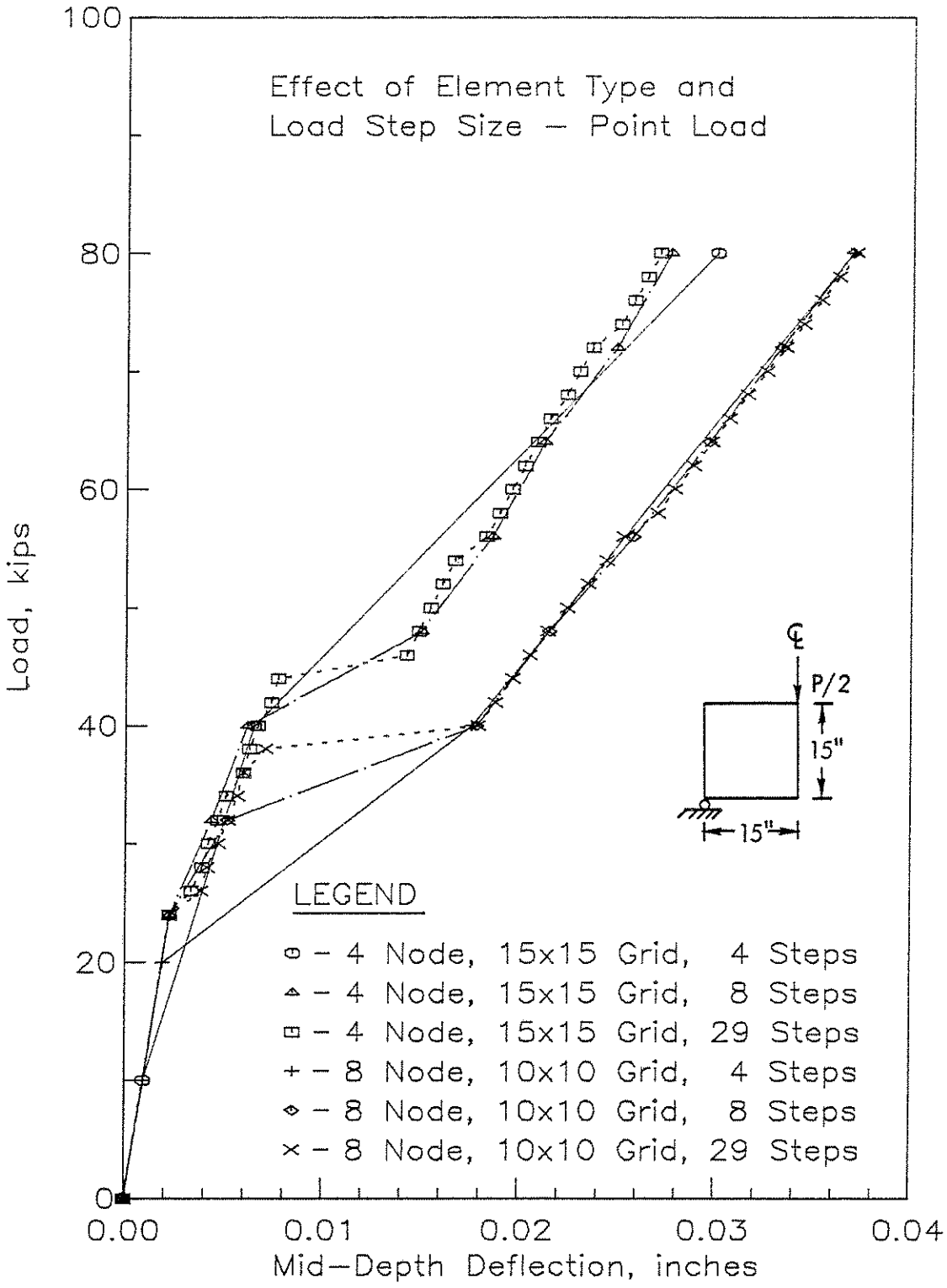

Fig. 3.41b - Effect of Load Increment Size and Element Type, Continued.

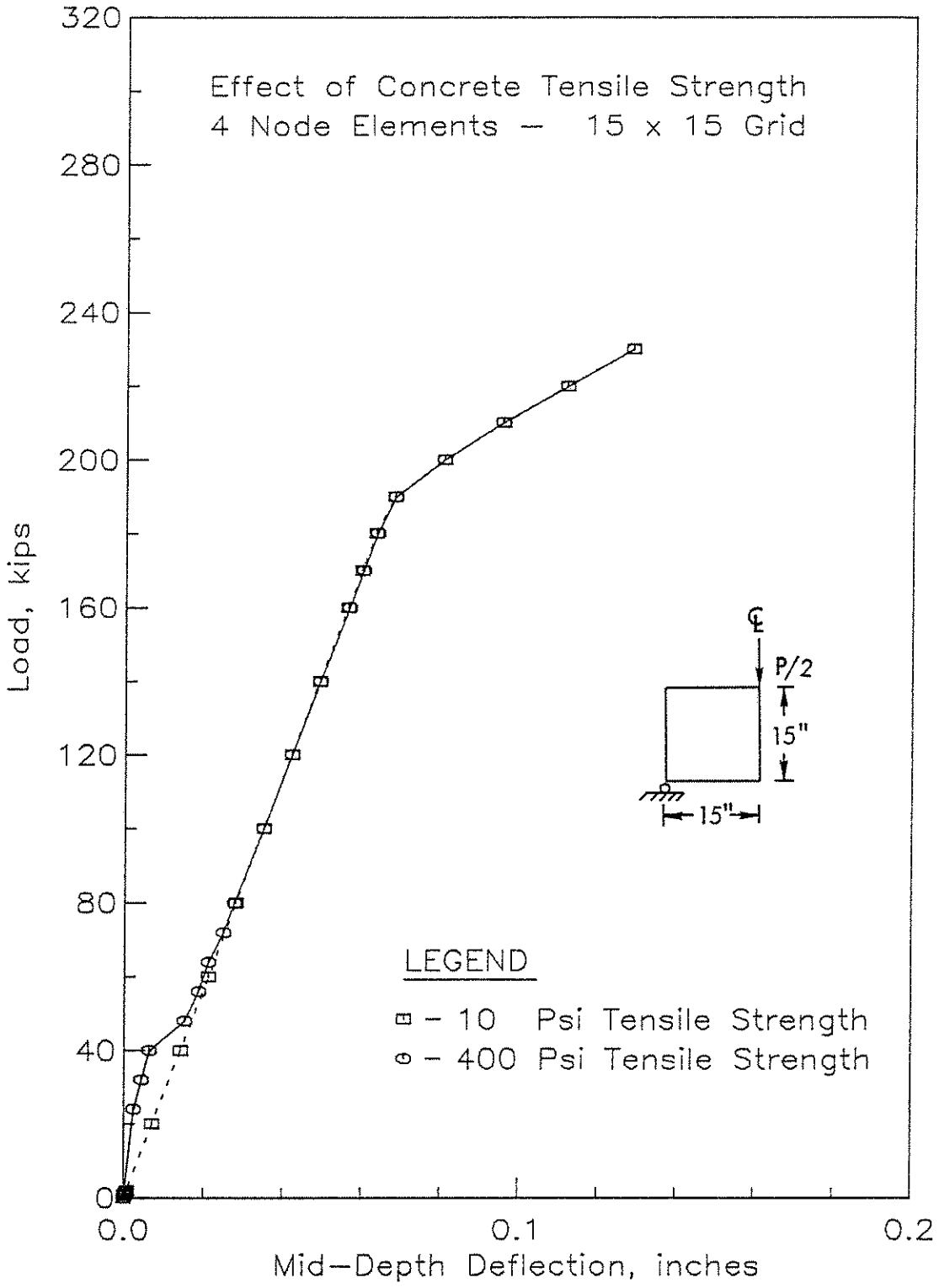

Fig. 3.42 - Effect of Concrete Tensile Strength on Load-Deflection Curves.

APPENDIX A

NOTATION

$[B]$	matrix relating strains at a point to nodal displacements
$\{d\varepsilon\}$	differential strain vector in material coordinates: $d\varepsilon_1$, $d\varepsilon_2$, $d\gamma_{12}$ in local (element) coordinates: $d\varepsilon_x$, $d\varepsilon_y$, $d\gamma_{xy}$
$\{d\sigma\}$	differential stress vector in material coordinates: $d\sigma_1$, $d\sigma_2$, $d\tau_{12}$ in local (element) coordinates: $d\sigma_x$, $d\sigma_y$, $d\tau_{xy}$
$[D_T]$	incremental (tangent) constitutive matrix
E	Young's modulus
f'_t	concrete tensile strength
G	shear modulus
G	energy release rate
G_c	critical energy release rate
$\{IF\}$, $\{IF_S\}$	vector of nodal forces required to maintain an element or structure in its deformed configuration
$[K_T]$	tangent structure stiffness matrix
$\{P\}$	total nodal load vector
$\{R\}$	residual nodal load vector
$\{U\}$	total nodal displacements
α	normal stiffness reduction factor
β	shear stiffness reduction factor
$\{\Delta P\}$	vector of incremental nodal loads
$\{\Delta U\}$	vector of incremental nodal displacements

$\{\varepsilon\}$	vector of strains at a point in material coordinates: ε_1, ε_2, γ_{12} in local (element) coordinates: ε_x, ε_y, γ_{xy}
ν	Poisson's ratio
$\{\sigma\}$	vector of stresses at a point in material coordinates: σ_1, σ_2, τ_{12} in local (element) coordinates: σ_x, σ_y, τ_{xy}